THERMAL CONDUCTIVITY OF MAGNESIA, ALUMINA, AND ZIRCONIA POWDERS IN

AIR AT ATMOSPHERIC PRESSURE FROM 200°F TO 1500°F

A THESIS

Presented to

the Faculty of the Graduate Division

by

Herschel Willcox Godbee

In Partial Fulfillment

of the Requirements for the Degree

Doctor of Philosophy in the School

of Chemical Engineering

Georgia Institute of Technology

July, 1963

THERMAL CONDUCTIVITY OF MAGNESIA, ALUMINA, AND ZIRCONIA POWDERS IN

AIR AT ATMOSPHERIC PRESSURE FROM 200°F TO 1500°F

Approved:

_____

_____

_____

Date approved by Chairman: _11/6/63_

Special permission was obtained from the Graduate Division for placing the page numbers of this thesis at the top center of the page instead of in line with the right hand margin, as required by the thesis instructions issued by the Division. This modification in the format permits the report to be printed on both sides of the paper without altering the pagination of the manuscript.

ACKNOWLEDGMENTS

Finally, special thanks are due Mr. G. D. Davis of the Chemical Technology Division of the Oak Ridge National Laboratory for his valuable aid.

LIST OF SYMBOLS

a	thermal accommodation coefficient.
A	area perpendicular to heat flow.
AC	alternating current.
AWG	American Wire Gage.
A_r	radiating surface area in Equation 69.
B	Boltzmann constant.
Btu	British thermal unit.
BWG	Birmingham Wire Gage.
cm	centimeter.
C_p	heat capacity at constant pressure.
C_v	heat capacity at constant volume.
C_{pg}	heat capacity of gas at constant pressure.
C_{vg}	heat capacity of gas at constant volume.
d	distance between close parallel plates—Equations 62 and 66.
D	particle size.
D.C.	direct current.
DIAM	diameter
D_a	lower point of truncation of a population—page 52.
D_b	upper point of truncation of a population—page 52.
D_m	mean particle size.
D_r	effective inter-particle distance for radiation—Equation 72.
D_s	solid length parallel to heat flow—Figure 32(a).
$D_{50\%}$	median particle size.

e	constant = 2.71828 ...
emf	electromotive force.
E_i	coefficient of linear expansion.
f	semi-principal axis of ellipsoid.
ft	foot.
F	factor defined by Equation 8.
F_a	angle (or "view") factor in Equation 69.
F_ϵ	emissivity factor in Equation 69.
G_s	number of series gas lengths associated with a unit representative length of solid.
h	heat transfer coefficient—Equation 39.
hr	hour.
i	an integer.
in.	inch.
ID	inside diameter.
j	temperature jump distance—Equation 62.
k	thermal conductivity.
kva	kilovolt-ampere.
k_a	thermal conductivity defined by Equation 12.
k_c	thermal conductivity of continuous phase.
k_d	thermal conductivity of discontinuous phase.
k_e	effective thermal conductivity of two-phase body.
k_{esv}	effective thermal conductivity calculated by Equation 11.
k_{fc}	contribution of forced convection to k_e.
k_g	thermal conductivity of bulk gas.
k_g^o	apparent thermal conductivity of gas defined by Equation 66.
k_g^*	modified gas thermal conductivity defined by Equation 68.

k_{gsc} contribution of gas and solid in series and in parallel to k_e—Equation 67.

k_m mean thermal conductivity over a temperature range—Equation 34.

k_{nc} contribution of natural convection to k_e.

k_r contribution of radiation to k_e.

k_{sc} contribution of particle-to-particle contact to k_e.

L   length; in particular the distance between potential taps.

ln   logarithm to base e.

log   logarithm to base 10.

m   empirical constant in Equation 15.

M   empirical constant in Equation 14.

M_s mass of solid.

n   empirical constant in Equation 15.

n_r index of refraction.

N   empirical constant in Equation 14.

N_{Pr} Prandtl number $\equiv \dfrac{\eta C_{pg}}{k_g}$.

OD   outside diameter.

p   a quantity defined by Equation 13.

P   absolute pressure.

P_b breakaway pressure defined by Equation 81.

P_d degree of packing defined by Equation 32.

P_s standard deviation of P_1—Equation 28.

P_1 length occupied by discontinuous phase per unit length.

P_2 area occupied by discontinuous phase per unit area.

P_3 volume occupied by discontinuous phase per unit volume.

q_1 heat flow per unit time.

q_r heat transfer per unit time by radiation—Equation 69.

q^o heat flow per unit time per unit area given by Equation 62.

Q heat flow per unit time.

Q_{gsc} heat flow per unit time through gas and solid in series and in parallel.

R radius.

S solid area perpendicular to heat flow—Figure 32(a).

S_{ln} logarithmic (to base e) standard deviation.

t temperature.

t_{avg} average temperature $= 1/2 \ (t_i + t_{i+1})$.

t_o temperature at zero time.

T absolute temperature.

TC thermocouple.

u function defined by Equation 30.

v function defined by Equation 28.

V volts.

V_d volume fraction discontinuous phase.

$V_{d\ min}$ minimum volume fraction solid—procedure on page 56.

$V_{d\ max}$ maximum volume fraction solid—procedure on page 56.

V_T volume of test cylinder.

W coefficient in Equation 18.

x space coordinate.

X length of representative cell of two-phase body.

y space coordinate; in particular the depth of a thermocouple in the test cylinder.

z space coordinate.

Z constant in Equation 66.

α a shape factor defined by Equation 51.

β an angle defined by Equation 21.

γ ratio of gas heat capacity at constant pressure to gas heat capacity at constant volume.

δ finite difference.

Δ finite difference.

ϵ emissivity.

ζ constant = 1.7811 ...

η viscosity of gas.

θ time.

λ mean free path of gas molecule—Equation 65.

ν quantity defined by Equation 24.

ξ term to indicate order of magnitude—Equations 36 and 39.

π constant = 3.14159 ...

ρ density.

ρ_{PF} density of pore-free solid.

σ Stefan-Boltzmann constant.

τ thermal diffusivity $\equiv \dfrac{k}{\rho C_P}$.

ϕ molecular diameter of gas as determined from viscosity.

ψ sphericity in Equation 86.

ω quantity in Equation 19.

Ω quantity in Equation 19.

LIST OF TABLES

LIST OF FIGURES

SUMMARY

Attempts to understand how heat is transferred through powder-gas systems usually devolve to attempts to determine the systems' thermal conductivities. There are an unlimited number of powder-gas "systems" possible, even for a single solid in a single gas, and appeal is generally made to some theory which predicts thermal conductivity in order to reduce the number of experimental measurements required. Reliable thermal conductivity measurements on sufficiently well characterized powder-gas systems over a wide range of conditions are needed for an understanding of the basic phenomena governing heat transfer in these systems. Also, such measurements permit meaningful evaluations of theories proposed to predict thermal conductivity of two phase systems from more easily measured properties and existing tabulated properties of the pure constituents.

This study presents measured thermal conductivities for extensively characterized magnesia, alumina, and zirconia powders. Thermal conductivities of the powders in dry air at atmospheric pressure were determined at volume fractions solid varying from 0.49 to 0.70 as a function of temperature from about $200^{\circ}F$ to about $1500^{\circ}F$. Particle-size distribution (by several techniques), chemical composition, x-ray diffraction pattern, weight loss on heating, pore-free density, and surface area of each powder were measured. Mean particle sizes of the powders varied from about 211 to 1023 microns.

The thermal conductivities of the various powders were determined by a steady-state method employing radial heat flow in a hollow cylinder and by an unsteady-state method based on the model of heating a cylinder of a perfect conductor surrounded by an infinite amount of the material whose thermal conductivity is being measured. The unsteady-state method was used to corroborate a few of the results obtained by the steady-state method; it provided an independent check on the results. The uncertainty of the steady-state measurements was estimated to be about ± 10 per cent; and the uncertainty of the unsteady-state method, about ± 11 per cent. Reproducibility of the observations was about ± 3 per cent. These measurements are the basis for the following conclusions: (a) the conductivity of the powder in air at atmospheric pressure increases with temperature for each material; (b) the thermal conductivity increases with increasing volume fraction solid for a given powder at a fixed temperature; (c) the thermal conductivity is critically dependent on volume fraction solid near the maximum volume fraction solid obtainable with a powder; (d) a sorbed film increases the conductivity of the powder above that of the powder after it has been treated to remove the film below about $850^{\circ}F$ for magnesia and alumina and below about $1050^{\circ}F$ for zirconia; (e) mechanical pressure (as distinguished from gas pressure) on the powder enhanced the conductivity of the powder; (f) an alumina powder had a slightly lower conductivity than a magnesia powder at the same volume fraction solid with essentially the same shape factor in accord with predictions of the theory proposed in this work; (g) two magnesia powders having the same volume fraction solid and close to the same shape factor but different particle-size distributions, mean particle sizes, and points of

truncation had the same effective thermal conductivity, in accord with predictions of the theory proposed in this work.

Prediction of the thermal conductivity of a powder-gas system is possible in principle for single-sized particles of known shape in a fixed spatial arrangement if the thermal conductivities of the constituents are known. However, for most real powders the particles are not single sized, the shape is not known, and the spatial arrangement is not fixed. Theoretical relations based on idealized models of these real powders generally relate the thermal conductivity of a powder-gas system to the volume concentrations of the constituents and their thermal conductivities. Implicit in the derivations are assumptions of particle shape and spatial arrangement. Ofttimes to force these relations to fit a broad spectrum of experimental data recourse has been made to empirical constants. Too much reliance on empirical and semi-empirical relations leads away from an understanding of the fundamental heat transfer processes taking place in powders, and often leads to the conclusions that heat transfer through powders is hopelessly complicated and not amenable to sound mathematical treatment. Too little use appears to have been made of the well-established small particle technology and firm mathematics describing small particle relationships.

In view of the foregoing, a theoretical expression is presented to relate the effective thermal conductivity of statistically describable two-phase systems to the conductivities of the pure phases, the volume concentrations of the phases, and a shape factor. Auxiliary equations to relate bulk gas conductivity and small inter-particle distance and

to predict a radiation heat transfer contribution to effective thermal conductivity are derived. The shape factor is a property of the discontinuous phase and is related to the two-phase body only through the volume balance. In the derivation of the expression no assumptions are made concerning particle shape, size, or spatial arrangement. However, the derivation is based on a simplified model in that the isotherms in the model are assumed to be planes perpendicular to the heat flow. In exact solutions of the heat flow equation, no assumptions are made regarding the heat flow or temperature pattern. On the other hand, exact solutions have been effected only for simple shapes in fixed arrangements that seem to fall far short of describing actual powder-gas systems.

The shape factor required for solution of the equation proposed in this study was obtained from the particle-size distribution of the powders. Results calculated by the proposed equation agree well with the measured effective thermal conductivities. Predicted and experimental conductivities generally agreed within ±5 per cent.

Comparison of the experimental conductivities with an exact solution of the heat flow equation in which the particles are assumed to be ellipsoids far enough apart so as not to interact showed that this exact solution underestimates the measured effective thermal conductivities. Comparison of the experimental conductivities with a simplified solution in which the particles are assumed to be spheres and the heat flow lines are assumed to be straight parallel lines showed that the simplified solution gave fair agreement depending upon the value of a constant set by the geometry of the model.

The results of this investigation suggest that the effect of particle parameters, the effect of mechanical (not gas) pressure, the effect of sorbed films, and the effect of radiation heat transfer on the thermal conductivity of powders are interesting areas for further work. Powders having known particle-size distributions, surface areas, shape factors, etc. should be synthesized or blended so that the influence of these parameters may be investigated systematically. Better control of particle parameters will permit more meaningful intercomparisons between different investigations of heterogeneous systems.

TABLE OF CONTENTS

TABLE OF CONTENTS
(Continued)

TABLE OF CONTENTS

(Continued)

CHAPTER I

INTRODUCTION

Knowledge of the facility with which heat is transported through matter and through a vacuum is important in the consideration of many applied and theoretical problems. Perhaps the transport of heat through porous media is the least amenable to mathematical analysis. Certainly the literature of the field is large and difficult to interpret. To reconcile the results of different investigators and to find an accord in the various proposed models and analyses is even more difficult. This study presents experimental heat transfer data on a variety of porous materials which have been extensively characterized, and success-fully correlates these data as well as all the literature data that are adequately characterized in terms of a proposed model for heat transfer through porous media.

Heat transfer is conventionally described in terms of the "co-efficient of thermal conductivity" or more commonly, the "thermal con-ductivity." It is that property of a material which determines the temperature gradient under fixed heat flow. The definition of thermal conductivity, k, is contained in the generalized statement of experience with heat flow called Fourier's law or equation

$$Q = -kA \frac{dt}{dx} \tag{1}$$

where the heat flow per unit time, Q, and the temperature gradient, dt/dx, are perpendicular to the area A.

Thermal conductivity may be measured by either static or dynamic methods. In static methods the sample is allowed to come to steady-state conditions; i.e., the temperature is a function of a space coordinate only, and the temperature at two or more positions is measured. The thermal conductivity is then determined from an integration of Equation 1. In dynamic methods the sample is in an unsteady-state; i.e., temperature is a function of a time coordinate as well as a space coordinate, and the temperature change with time at one or more positions is measured. The thermal diffusivity, τ, is then usually determined from an appropriate (though approximate) solution of the equation which relates thermal conduction to temperature history. For a homogeneous isotropic material, containing no heat sources or sinks, if thermal conductivity is constant and if the small difference between C_v and C_p is negligible

$$\frac{dt}{d\theta} = \tau \left(\frac{\partial^2 t}{\partial x^2} + \frac{\partial^2 t}{\partial y^2} + \frac{\partial^2 t}{\partial z^2} \right), \tag{2}$$

where θ = time,

$\tau = \dfrac{k}{\rho C_p} \equiv$ thermal diffusivity,

ρ = density, and

C_p = heat capacity at constant pressure.

Although most unsteady-state methods determine k indirectly from τ, some offer the possibility of determining both k and τ from a single experiment.

Thermal conductivity depends on the chemical composition, physical structure, and the state of a substance. It is not a constant for any one material, but may be a function of a number of variables. Factors

which may influence the thermal conductivity of nonmetallic solids have been very well summarized by Austin (1)[*] as follows:

(a) chemical composition, molecular structure in pure compounds, and impurities in solid solutions;

(b) physical texture: (1) porosity, total void space and size and shape of pores with solid phase continuous, size and shape of grains with gas phase continuous; (2) presence of a vitreous or liquid phase, total amount and distribution of phase; (3) development of ceramic bond and sintering, time at temperature level; and (4) anisotropy and directional effects;

(c) temperature;

(d) pressure, stress or strain; and

(e) heat flow.

The thermal conductivities of most metals, at ordinary temperatures, show a small and nearly linear decrease with increase of temperature, but a few (e.g., aluminum and platinum) show the opposite effect, as do also many alloys. The thermal conductivity of most nonmetallic materials varies considerably with temperature (see for example Kingery (2) and Figure 1). The thermal conductivity of many crystalline materials decreases with increasing temperature, being in general proportional to the reciprocal of the absolute temperature. The thermal conductivity of an amorphous body, such as fused silica, increases with increasing temperature (Figure 1). However, the temperature dependence of k cannot be predicted with certainty, and thermal conductivity data cannot be reliably extrapolated to higher or lower temperatures.

---

[*] Numbers in parentheses refer to references listed in the Bibliography.
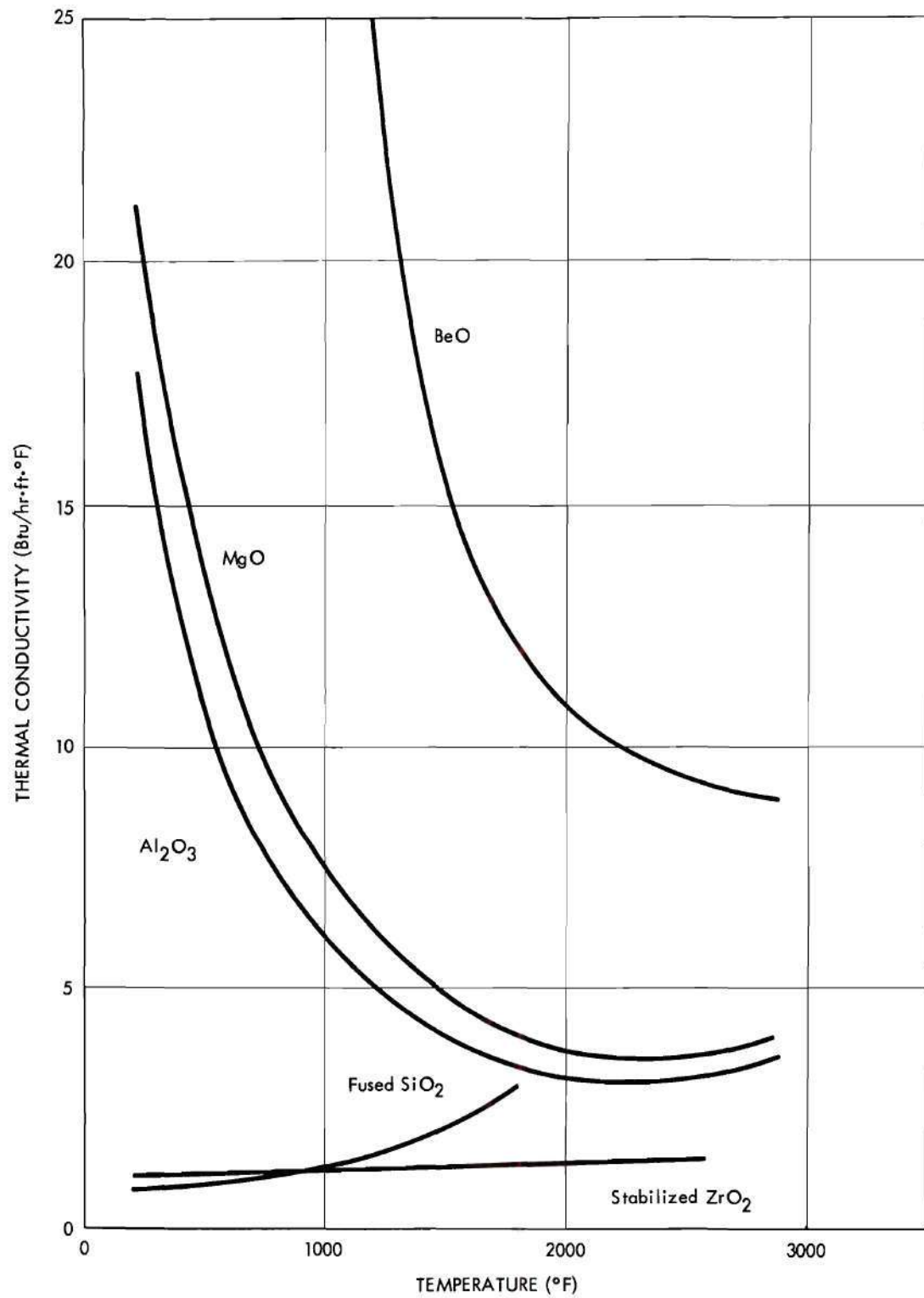
Fig. 1. Variation of Thermal Conductivity of Dense Solids with Temperature (2).

Among the many factors that influence thermal conductivity of nonmetallic solids, physical texture causes great variation. Speaking broadly, there are two types of porous materials, cellular and granular. A cellular material is a two-phase system in which the solid phase is continuous and the gas phase is dispersed. A refractory in which voids (cells) are formed by the volatilization or combustion of some ingredient during firing is representative of this type of substance. A granular material is a two-phase system in which the gas phase is continuous and the solid phase is dispersed. Snow, sands, wools, and dusts are representative of this type of substance. In general, a granular material has a lower conductivity than a cellular one of the same material and porosity.

Factors influencing thermal conductivity are treated in more detail by Austin (1), Barrett (3), Kingery and McQuarrie (4), and Powers (5) as well as most standard texts on heat transfer.

A survey of the literature on thermal conductivity reveals that steady-state methods of measuring k are more widely used than unsteady-state methods; however, unsteady-state methods have become more widely used since instruments for accurately recording rapidly changing temperatures as well as computers for handling the more complex solutions of Equation 2 have become available. Steady-state methods determine thermal conductivity directly while unsteady-state methods generally determine thermal diffusivity so that a knowledge of density and heat capacity is required before thermal conductivity can be determined. The so-called "thermal conductivity probe" is an unsteady-state method that permits direct measurement of k. It is based on the heating of a cylinder of

perfect conductor surrounded by an infinite amount of the material whose conductivity is being measured. Other unsteady-state methods permitting direct measurement of k, as well as τ, are discussed by Carslaw and Jaeger (6). Since confidence in unsteady-state methods is usually based on agreement with steady-state methods, the use of steady-state methods appears to be desirable until a fairly comprehensive collection of reliable data has been acquired.

In steady-state methods for measuring thermal conductivity the principal problem is achieving a heat flow pattern which corresponds to that assumed in solving Equation 1. Test specimens may take a shape for which an exact solution of Equation 1 is possible. These shapes are a plane plate (slab), a sphere, a cylinder, and a prolate spheroid. In flat plate arrangements heat flows through a sample of constant cross section whose lateral surfaces are, ideally, covered with a nonconductor of heat. Since there is no perfect thermal insulator, a technique frequently used to reduce lateral heat flow to negligible values is to provide heat guards (separately heated portions of the test material) whose temperature profile matches as closely as is practical the temperature profile of the test sample. To obtain adequate guarding for accurate determinations of k, quite large samples are required in this arrangement. Radial flow through a hollow sphere or prolate spheroid is an attractive arrangement since no heat losses occur except through the leads to the heater and thermocouples, but the forming of uniform heat sources and fabricating of hollow samples is frequently a difficult requirement. Cylindrical arrangements lose heat at their ends. A technique to reduce axial heat flow in a cylinder to negligible values

is to provide end heat guards. Another technique to reduce axial heat flow in a cylinder is to use a sample which is long compared with its diameter and to work only in the center section where the isothermal surfaces are essentially cylindrical.

In unsteady-state methods the principal problem is knowing how nearly the boundary conditions in an experiment match those postulated in solving Equation 2. Boundary conditions in unsteady-state methods are achieved by guard methods and/or sample configuration. Advantages of unsteady-state methods are that some permit very rapid measurements and that some may be used *in situ* which is a distinct advantage for materials such as snow, rocks, and moist soils. Accurate temperature measurement, especially at very high temperatures, is a problem common to both methods. Standard texts such as Jakob (7), Carslaw and Jaeger (8), and Kingery (9) present some of the advantages, disadvantages, and mathematics of established steady-state and unsteady-state methods of measuring thermal conductivity. Ross (10) presents an excellent survey on methods of measuring thermal conductivity.

Each method and arrangement of apparatus indicated above has certain limitations and the choice of one over another is governed by physical structure, temperature, and conductivity. However, thermal conductivity can be measured with equivalent results by both steady-state and unsteady-state methods, by different arrangements of apparatus, and by different investigators. This fact is indicated by the results of Woodside (11) on silica aerogel using both steady-state and unsteady-state methods and by Powell's comparison of the thermal conductivity of iron measured by several investigators (12). It is further indicated by

the results of Adams (13) and of Kingery (14) on the determination of k for aluminum oxide using steady-state radial heat flow in a hollow prolate spheroid, sphere, and cylinder.

From a consideration of the advantages and limitations of the various satisfactory arrangements outlined above, an apparatus utilizing radial flow in a hollow-cylinder was chosen to measure the thermal conductivity of various porous materials as a function of temperature and volume fraction solid under steady-state and unsteady-state conditions. To reduce heat flow out the ends of the cylinder, both a sample long compared with its diameter and heat guards were used.

CHAPTER II

REVIEW OF THE LITERATURE ON THEORETICAL EQUATIONS FOR THERMAL CONDUCTIVITY OF MIXTURES

A powder may be defined as a heterogeneous system in which solid particles are surrounded by a fluid or, in the case of a vacuum, by empty space. In the limits the solid and surrounding fluid may be considered to be either in series or in parallel with each other. Surely in a real porous body part of the fluid is effectively in series and part in parallel with the solid, so the true effective conductivity may be assumed to be between these limits. Assuming no convection in the pores and no radiation between solid surfaces, the effective thermal conductivities for these limiting distributions of material are

$$k_e = (1 - V_d) \, k_c + V_d k_d \, , \tag{3}$$

for parallel layers or laminae and

$$\frac{1}{k_e} = \frac{(1 - V_d)}{k_c} + \frac{V_d}{k_d} \, , \tag{4}$$

for series layers or laminae where

k_e = effective thermal conductivity of the two-phase body,

k_c = thermal conductivity of the continuous phase,

k_d = thermal conductivity of the discontinuous phase, and

V_d = volume fraction of the discontinuous phase.

For a given V_d, if k_c and k_d are approximately equal, Equations 3 and 4 show that the distribution of material makes little difference in the effective thermal conductivity. However, for most powders k_d is large compared to k_c, so that some account must be taken of the ratio of series to parallel laminae. For example, a porous material with a V_d of 0.58 and a k_d/k_c of 1000 has a k_e for parallel laminae of 580 k_c and a k_e for series laminae of 2.4 k_c. For the same V_d with k_d/k_c equal 50, k_e for parallel laminae is 29 k_c and k_e for series laminae is 2.3 k_c. This may be contrasted with the case, again with $V_d = 0.58$, which for k_d/k_c equal 2, k_e for parallel laminae is 1.6 k_c and k_e for series laminae is 1.4 k_c.

Equation 3 may be viewed as a volume fraction-weighted arithmetic mean of the separately determined k_d and k_c, and Equation 4 may be viewed as a volume fraction-weighted harmonic mean of the separately determined k_d and k_c. Since the effective thermal conductivity of a powder, assuming negligible radiation and convection, should be found between the upper limiting value, Equation 3, and the lower limiting value, Equation 4, several investigators have considered the intermediate weighted geometric mean to describe the effective conductivity of a powder. Lichtenecker (15) presented such an empirical relation as follows

$$k_e = k_d^{V_d} \cdot k_c^{(1 - V_d)} . \tag{5}$$

Woodside and Messmer (16) found that for packed beds of quartz sand, glass beads, and lead shot ($V_d = 0.41$ to $V_d = 0.81$) in various fluids (ranging from Freon-12 to water) Equation 5 overestimated k_e when k_d/k_c exceeded 20.

Numerous theoretical expressions have been derived for evaluating the effective thermal conductivity of a heterogeneous body. These derivations seem to fall into two categories: the first of which contains no assumptions about the heat flow and temperature patterns and the second of which contains an assumption about either the heat flow or the temperature pattern. Expressions in the first category are sometimes referred to as accurate, rigorous, or exact solutions. Expressions in the second category are referred to as "simplified" or approximate solutions. The words accurate, approximate, etc. refer to the mathematics of the solution and not necessarily to the effective conductivity predicted by the solution. In an excellent survey of theoretical relations for determining the effective conductivity of heterogeneous substances, Powers (17) classifies theoretical relations as equations based on flux laws (the first category above) and as equations based on Ohms law (the second category above). Babanov (18), Gorring and Churchill (19), Laubitz (20), and Woodside and Messmer (16) review some of the schemes used in deriving relations to predict k_e.

Exact Solutions

Although many of the exact solutions have evolved from work in electricity, magnetism, hydrodynamics, etc. they apply equally well to any case of mass or energy flow under a potential difference or driving force.

Maxwell (21) derived an expression for the effective conductivity of a heterogeneous body composed of spheres of one conductivity embedded in a matrix of another conductivity. His equation is

$$k_e = k_c \left[\frac{k_d + 2k_c - 2V_d (k_c - k_d)}{k_d + 2k_c + V_d (k_c - k_d)} \right]. \tag{6}$$

It is assumed that the spheres are so far apart that they have no influence on one another. Lord Rayleigh (22) considered the interactions between particles for the cases of uniform spheres and cylinders in "rectangular order" (spheres in a cubic array and cylinders in a square array). For small values of V_d the Rayleigh equation for spheres is identical to Equation 6 (Maxwell's equation).

Many expressions have been derived based on modifications and extensions of the Maxwell and Rayleigh equations (23, 24, 25, 26, and 27). Burgers (23) and Fricke (24) developed more general solutions for particles embedded in a matrix by assuming the particles to be ellipsoids. With the assumption also that the particles are far enough apart so as not to interact, Fricke obtained

$$k_e = k_c \left[\frac{1 + V_d (F \frac{k_d}{k_c} - 1)}{1 + V_d (F - 1)} \right]; \tag{7}$$

for spheroids $(f_1 = f_2 \neq f_3)$

$$F = 1/3 \sum_{i=1}^{3} \left[1 + \left(\frac{k_d}{k_c} - 1 \right) f_i \right]^{-1} \tag{8}$$

and

$$\sum_{i=1}^{3} f_i = 1 . \tag{9}$$

The factor F represents the ratio of the overall average temperature gradients in the two phases. The factors f_i are the semi-

principal axes of the ellipsoid. If $f_1 = f_2 = f_3$, i.e., the particles are spheres and Equation 7 reduces to Maxwell's equation. In calculating the thermal conductivity of soil, de Vries (28) took $f_1 = f_2 = 1/8$ and $f_3 = 3/4$. Woodside and Messmer (16) found that Equation 7 with de Vries' values for f_i gave fair agreement with their experimental conductivities for beds of quartz sand, glass beads, and lead shot in various fluids at about $86^\circ F$. They concluded that Equation 7 with de Vries' values of f_i underestimates k_e when k_d/k_c is very large (from their data, "very large" k_d/k_c appears to be about 100).

Equations of the Maxwell-Rayleigh type usually yield results that correspond fairly well with experimental results for cellular material and emulsions. Gorring and Churchill (19) compared a large body (99 systems) of literature data with equations of this type and found good agreement between experimental and calculated results. However, exact solutions have usually not yielded good agreement when compared with experimental results on powders. Perhaps the difficulty is, as pointed out by Laubitz (20), that although the mathematics is exact the model is so artificial that it radically departs from real powders.

Simplified Solutions

Assumptions about the heat flow or temperature pattern, i.e., the assumption of a more restricted model, can reduce the problem of calculating the effective thermal conductivity of a hetergeneous system from that of solving a partial differential equation to that of solving an ordinary differential equation (Fourier's law). Simplified solutions are generally of two types: in the first the heat flow lines are assumed to be straight and parallel, and in the second the isotherms are

assumed to be planes perpendicular to the heat flow. Solutions of the first type are sometimes said to be based on the assumption of linear heat flow, the assumption of zero sidewise conductivity, or the assumption that the conductivity of the components is vanishingly small in directions perpendicular to the heat flow. Solutions of the second type are said to be based on the assumption of linear isotherms, the assumption of infinite sidewise conductivity, or the assumption that the conductivity of the components is infinite in directions perpendicular to the heat flow. Lichtenecker (29 and 30) derived expressions for the electrical conductivity and the dielectric constant of aggregates for several models (squares, triangles, circles, and ellipses in a square) using both of the above assumptions. His solutions were two dimensional, i.e., independent of the third dimension.

Linear Heat Flow

For cubes in a cubic array with the assumption of linear heat flow, the expression for effective thermal conductivity is

$$k_e = k_c \left[\frac{(1 - v_d^{1/3} + v_d) + \dfrac{k_c}{k_d}(v_d^{1/3} - v_d)}{(1 - v_d^{1/3}) + \dfrac{k_c}{k_d} v_d^{1/3}} \right]. \qquad (10)$$

This expression was derived by G. S. son Frey (31) to describe the electrical conductivity of binary aggregates. Lichtenecker's (29) two-dimensional model corresponding to this case gives an equation which is easily converted to the above equation, showing that the model is independent of the third dimension. For most powders encountered in practice, Equation 10 gives results which are factors of 2 to 3 lower

than experimental results. Tsao (32) presents a more general form of this equation assuming the particles to be parallelepipeds.

Schumann and Voss (33) derived an equation based on a two-dimensional model in which the solid is bounded by a rectangular hyperbola. The expression they obtained is

$$k_e = k_c (1 - V_d)^3 + \left[1 - (1 - V_d)^3 \right] k_a \tag{11}$$

where

$$k_a = \frac{k_c k_d}{k_c + p (k_c - k_d)} \left[1 + \frac{p (1 + p) (k_c - k_d)}{k_c + p (k_c - k_d)} \ln \frac{k_c (1 + p)}{p k_d} \right] \tag{12}$$

and

$$(1 - V_d) = (p^2 + p) \ln \frac{p + 1}{p} - p . \tag{13}$$

Since the calculation of k_e from k_c, k_d, and V_d is somewhat involved, Schuman and Voss presented a graph of k_e/k_c versus k_d/k_c with $(1 - V_d)$ as a parameter to permit rapid estimation of k_e.

Wilhelm et al. (34) observed that, on the average, experimental conductivities were larger than those computed by Equation 11. They hypothesized that this difference in calculated and experimental conductivities could be explained by the neglect of solid-to-solid contact. They deduced an expression to correct the effective conductivity as calculated by Equation 11.

Their suggested correction is

$$\log (k_e - k_{esv}) = M + N \frac{k_d}{1 - V_d} \tag{14}$$

where k_{esv} = effective thermal conductivity calculated by Equation 11 and M and N = constants obtained empirically from experimental measurements. For k_e in Btu/hr·ft·$^{\circ}$F, M = -1.759 and N = 0.0129.

Preston (35), from a study of his data plus the data used by Wilhelm et al., suggests the following modification of the Schumann and Voss equation:

$$k_e = m\,(k_{esv})^n,\qquad(15)$$

where for k_e in Btu/hr·ft·$^{\circ}$F, m = 1.536 and n = 0.959.

Deissler and Eian (36) derived the following expression, valid for $V_d = \pi/6$, for the effective thermal conductivity of spherical particles in a cubic array:

$$k_e = k_c \left\{ \frac{\pi}{2\left(\frac{k_c}{k_d} - 1\right)^2}\left[\left(\frac{k_c}{k_d} - 1\right) - \ln \frac{k_c}{k_d}\right] + 1 - \frac{\pi}{4}\right\}.\qquad(16)$$

They also derived an expression for cylinders in a square array, valid for $V_d = \pi/4$, with heat flow perpendicular to the longitudinal axis:

$$k_e = k_c \left\{ \frac{\pi}{2\left(\frac{k_c}{k_d} - 1\right)} - \frac{\frac{\pi}{2} - \sin^{-1}\left(\frac{k_c}{k_d} - 1\right)}{\left(\frac{k_c}{k_d} - 1\right)\left[2\frac{k_c}{k_d} - \left(\frac{k_c}{k_d}\right)^2\right]^{1/2}}\right\}.\qquad(17)$$

Since this is a two-dimensional model, Lichtenecker's (30) equation corresponding to this case can be converted to Equation 17.

Using the two Equations, 16 and 17, above plus the fact that at $V_d = 1$, $k_e = k_d$ and at $V_d = 0$, $k_e = k_c$, Deissler and Eian constructed

a log-log plot of k_e/k_c versus k_d/k_c with $(1 - V_d)$ as a parameter. Values of $(1 - V_d)$ intermediate to the four known values are determined by interpolation. They found good agreement between conductivities estimated by their analysis and experimental data from both their studies and the data compiled by Wilhelm et al. Laubitz (20) generalized Equation 16 for V_d equal to or less than $\pi/6$. Equation 17 may be easily generalized for V_d equal to or less than $\pi/4$ in similar manner.

Gorring and Churchill (19) developed an expression for effective thermal conductivity for a cubic array of particles bounded by paraboloids of revolution. They obtained fair to excellent agreement with experimental data (56 systems) on packed beds and powders. The form of their equation which they used in these comparisons is

$$k_e = k_c \left[\frac{1.92}{W^{2/3}} \left(\frac{k_d}{k_c} \right)^{1/3} \right] \tag{18}$$

where W is a coefficient obtained through a volume balance of the phases.

Willhite, Kunii, and Smith (37) derived an equation based on a two-dimensional model which is a modification of the one used by Kunii and Smith (38) which, in turn, is similar to the model used by Yagi and Kunii (39) for uniform spherical particles. The relationship for effective conductivity proposed by Willhite, Kunii, and Smith is

$$k_e = k_c \left[1 + V_d \left(1 - \frac{k_c}{k_d} \right) + V_d \left(\frac{\Omega}{\omega} \right) \left(1 - \frac{k_c}{k_d} \right)^2 \right] \tag{19}$$

where

$$\omega = \frac{1}{2} \left[\frac{\left(1 - \frac{k_c}{k_d} \right)^2 \sin^2 \beta}{\ln \left\{ \frac{k_d}{k_c} - \left(\frac{k_d}{k_c} - 1 \right) \cos \beta \right\} - \left(1 - \frac{k_c}{k_d} \right) \left(1 - \cos \beta \right)} \right], \tag{20}$$

$$\sin^2 \beta = \frac{V_d}{13.23\ V_d - 5.36}\ , \tag{21}$$

and the quantity Ω is proportional to the equivalent length of the path for heat transfer through a given spherical particle by conduction. They took Ω equal 2/3 for spherical particles of low conductivity. For nonspherical particles and spherical particles of high conductivities they found that using Ω equal 1/2 improved agreement between calculated and experimental conductivities. The number of points of contact in beds of spherical particles, $(\sin^2 \beta)^{-1}$, is taken from the experimental work of Smith, Foote, and Busang (40). Willhite, Kunii and Smith found good agreement between predicted and experimental results for a large body of data in the literature (33, 35, 41, 42, 43, and 44). Masamune and Smith (45) present a further variation of this model with terms to predict the effect of pressure on bulk gas conductivity and to evaluate a solid-to-solid heat transfer contribution to effective thermal conductivity.

Linear Isotherms

For cubes in a cubic array with the assumption of linear isotherms, the expression for effective thermal conductivity is

$$k_e = k_c \left[\frac{(1 - V_d^{2/3}) + \frac{k_d}{k_c} V_d^{2/3}}{(1 - V_d^{2/3} + V_d) + \frac{k_d}{k_c}(V_d^{2/3} - V_d)} \right]. \tag{22}$$

This expression was first derived by G. S. son Frey (31) to describe the electrical conductivity of binary aggregates. Russell (46) later obtained

the same result for thermal conductivity and it is referred to in the literature — as well as in this study — as Russell's equation. Lichtenecker's (30) two-dimensional model corresponding to this case gives an equation which is easily converted to Equation 22 above. Russell's equation yields results that correspond fairly well with experimental results for cellular materials and emulsions, but generally yields results for powders that are about a factor of two low. Laubitz (20) found that he could explain his experimental results on powders, $V_d = 0.290$ to $V_d = 0.475$, of magnesia, alumina, and zirconia in air satisfactorily by doubling k_e predicted by Russell's equation and adding a term to account for radiation. Austin (1) concludes that Russell's equation and Maxwell's equation give substantially identical results for the same system (see Appendix I).

Topper (47) derived an expression, valid for $V_d = 0$ to $V_d = \pi/6$, for the effective conductivity of uniform spherical particles in a cubic array. Webb (48) derived an expression, valid for $V_d = \pi/6$, using this model also. Woodside (49) obtained an expression, equivalent to Topper's, for this model which is

$$k_e = k_c \left[1 - \left(\frac{6V_d}{\pi}\right)^{1/3} \left\{ 1 - \left(\frac{v^2 - 1}{v}\right) \ln \left(\frac{v + 1}{v - 1}\right) \right\} \right]^{-1} \tag{23}$$

where

$$v = \left[1 + \frac{4}{\pi \left(\frac{k_d}{k_c} - 1\right)\left(\frac{6V_d}{\pi}\right)^{2/3}} \right]^{1/2} . \tag{24}$$

Woodside found that values for the effective thermal conductivity of snow, calculated using Equation 23, agreed fairly well with experimental values.

Laubitz (20) compared his results for magnesia, alumina, and zirconia powders with Equation 23 and concluded that the calculated results were larger than his experimental ones.

Shimokawa (50) derived an equation for an orthorombic packing ($V_d = \pi/3 \sqrt{3}$) of uniformly sized spheres. His relation for effective thermal conductivity is

$$k_e = k_c \left[\frac{\pi}{\sqrt{3}} \left\{ \left(\frac{k_d}{k_d - k_c}\right)^2 \left(\ln \frac{k_d}{k_c}\right) - \frac{k_d}{k_d - k_c} \right\} + 1 - \frac{\pi}{2\sqrt{3}} \right]. \tag{25}$$

He found that his measured electrical conductivities (of ion exchange beds) compared favorably with a modified Maxwell equation; however, he found the comparison even better with his equation. This expression may be generalized for V_d equal to or less than $\pi/3 \sqrt{3}$.

Deissler and Boegli (51) suggested that it might be possible to obtain an expression for effective thermal conductivity and account for the irregular arrangement and shape of the particles by using the heat conduction equation in conjunction with statistical methods. They did not apply their suggestion to a model. Tsao (32) derived an equation for randomly sized and distributed particles using a statistical approach. His expression for effective thermal conductivity is

$$k_e = k_c \left[\int_o^1 \frac{dP_1}{1 + \left(\frac{k_d}{k_c} - 1\right) P_2} \right]^{-1} \tag{26}$$

where

$$P_2 = \int_{P_1}^1 \frac{e^{-v^2/2}}{\sqrt{2\pi}} \, dv, \tag{27}$$

$$v = \frac{P_1 - P_3}{P_s} , \qquad (28)$$

$P_1 \equiv \dfrac{\text{length occupied by phase d}}{\text{unit length}} ,$

$P_2 \equiv \dfrac{\text{area occupied by phase d}}{\text{unit area}} ,$

$P_3 \equiv \dfrac{\text{volume occupied by phase d}}{\text{unit volume}} ,$ and

$P_s \equiv$ standard deviation of P_1.

Warren and Messmer (52) question the validity of Tsao's mathematics. Aside from the doubt cast upon Tsao's mathematics, the fact remains that P_s is probably as difficult to obtain experimentally as is k_e itself. Nevertheless, Tsao's approach to calculating the effective thermal conductivity of heterogeneous media by applying statistical theory seems valid, and a variation of his approach is presented in Chapter IX.

Comparison of Linear Heat Flow and Linear Isotherms Solutions

A discussion of simplified expressions for predicting effective thermal conductivity would be incomplete without a comparison of "linear heat flow" and "linear isotherms" solutions for a given geometrical model under similar conditions. Consider, for example, cubes in a cubic array with linear heat flow (Equation 10) and with linear isotherms (Equation 22) at $k_d/k_c = 1000$ and $V_d = \pi/6$. The linear heat flow solution predicts that $k_e = 3.69\ k_c$ and the linear isotherms solution predicts that $k_e = 5.12\ k_c$ under these conditions. This may be contrasted with spheres in a cubic array, again with $k_d/k_c = 1000$ and $V_d = \pi/6$, for which the linear heat flow solution (Equation 16) gives $k_e = 9.51\ k_c$ and the linear isotherm solution (Equation 23) gives $k_e = 97.5\ k_c$. Comparisons such as these

lead to the conclusion that, all other conditions being equal, a simplified expression to predict k_e based on linear heat flow gives lower results than one based on linear isotherms for the same geometrical arrangement of particles. The magnitude of the difference depends on k_d/k_c and V_d since obviously as k_d/k_c approaches unity and V_d approaches zero any theoretically sound expression considering heat transfer by conduction only predicts that k_e approaches k_c.

CHAPTER III

EXPERIMENTAL METHODS AND APPARATUS

Experimental Methods

Radial heat flow in a hollow-cylinder was chosen with which to measure thermal conductivity under steady-state and unsteady-state conditions. Much more work was done in this study with the steady-state method of operation than with the unsteady-state. The unsteady-state method was used to corroborate a few of the results obtained by the steady-state method and to provide an independent check on the results. The principles of each method are briefly reviewed below.

Steady-State Method

The steady-state method is based on a model having radial heat flow outward through a cylinder of material whose thermal conductivity is the unknown. For materials that are not rigid, e.g., powders, the sample is held between two concentric tubes or cylinders to achieve and maintain the desired sample shape. Heat, usually produced by an axially located electrical resistance heater, is conducted radially outward through the sample. It is generally considered advisable to cover the heater with another tube of a good thermal conductor to equalize the temperature over the heater surface. Use of a thin wire as the central heater—Schleiermacher's method (53)—has not been successful with powders at high temperatures because of bowing of the wire caused by thermal expansion (54). In determining the thermal conductivities of

alumina and glass powders, Weininger and Schneider (55) used a glass tube wound with platinum wire inside a Monel tube as a central heater. For their work on uranium oxide powder, Deissler and Boegli (51) used a carbon rod inside a ceramic tube as a central heater. Measurement of heat input per unit length in both cases was accomplished by connecting leads for voltage measurement across a known length of heater.

The temperature at two or more known radial distances must be determined in order to evaluate thermal conductivity. Weininger and Schneider (55) silver soldered thermocouples to the inner Monel and outer steel tubes which confined their powder samples. Deissler and Eian (36) in determining the thermal conductivity of a magnesia powder used four groups (90° apart) of five radially positioned thermocouples located in a plane across the center of their test section. Mica spacers located on either side of the thermocouple junctions aided in maintaining the distance between thermocouples.

Cylindrical arrangements lose heat at their ends and some means must be provided to minimize longitudinal heat flow. One way to compensate for longitudinal heat loss is to make the cylinder long and measure only in the central portion where the isotherms approximate those of an infinite cylinder. This is the approach used by Weininger and Schneider (55). Another way to reduce longitudinal heat flow to negligible proportions is to use "heat guarding". Heat guarding may be accomplished by nonuniform heater winding; i.e., the windings on the ends of the heater are more closely spaced than those in the middle so that a region with negligible axial temperature drop may be achieved in the sample. Heat guarding may also be accomplished by placing auxiliary coils above and

below the main cylindrical arrangement to produce temperatures in a central zone which approximate those which would result from radial heat flow alone. Deissler and Eian (36) used end guard heaters on their central heater in order to achieve essentially radial heat flow.

To achieve high mean temperatures without severe temperature gradients between thermocouples in the same plane but at different radial distances, the entire cylindrical assembly may be covered with insulation or may be placed in a furnace. Laubitz (20), in measuring the thermal conductivity of magnesia, alumina, and zirconia powders at temperatures up to about $1800^\circ F$, used what amounted to a long cylindrical furnace as his outer container.

To summarize, use of a system having radial heat flow outward through a cylinder of powder is a straight-forward method of measuring thermal conductivity. Operated in a steady-state mode it is simple in principle, and it has the advantage for powders that the cylindrical sample shape is easy to achieve. However, it does require care to ensure that the heat flow approximates radial flow in an infinite cylinder. The mathematics of the method are treated later in Chapter VI.

Unsteady-State Method

The unsteady-state method is based on the assumption of a model which employs heating a cylinder of a perfect conductor surrounded by an infinite homogeneous medium whose thermal conductivity is the unknown. From suitable solution of the heat flow equation, the thermal conductivity of the medium (sample) is deduced from a record of the temperature change of the perfect conductor (heater) as a function of

time. This method is variously referred to as the "transient line heat source," "thermal conductivity probe," or "transient needle" method. A heater made of a good thermal conductor is generally treated to a first approximation as a perfect conductor, although sometimes corrections are devised to correct for the fact that the heater has a finite conductivity (56).

When the system, comprised of heater, sample, and container, is at uniform and steady temperature, a constant, known power is supplied to the heater, and the temperature rise of the heater is recorded. Thermal conductivity is calculated from the power input and the time-temperature record.

Since only radial heat flow is assumed in this method, longitudinal heat flow must be reduced to a negligible value. Techniques to achieve radial heat flow are the same as those used in the steady-state method above; viz., samples with very large length-to-diameter ratios (57), or heat guards are used.

While the theory applies to an infinite medium, the method is applied to finite samples by using only that portion of the heating time during which the heat front does not "see", i.e., is unaffected by, the extent of the sample. Errors introduced by supplying varying power to the heater (caused by change in heater resistance with temperature) can be made negligible by using resistance wire with a low temperature coefficient of resistance, or by using a constant-power power supply.

This unsteady-state method has been used fairly extensively for powders at temperatures close to ambient (11, 16, 56, 58, and 59). However, it has been used by DeNee (60) to determine the thermal conductivity

of quartz sand packs at liquid nitrogen temperatures, but it does not appear to have been used much at temperatures above ambient. The development of the method is reviewed by Woodside (11). Sources of error in the method are treated in detail by Blackwell (57). The theory of the method is presented by Blackwell (57) and by Carslaw and Jaeger (61). An abbreviated mathematical treatment is presented later in Chapter VI.

Experimental Apparatus

The experimental apparatus consisted basically of an upright cylindrical sample container with a central heater to provide a radial temperature gradient and a furnace to maintain temperature level. The central heater was either a platinum-wound resistance heater for steady-state measurements or a stainless steel tube resistance heater for un-steady-state measurements. An isometric drawing of the sample container and steady-state central heater is given in Figure 2. A schematic diagram of the sample container in place in the controlled-temperature furnace is given in Figure 3. The principal components of the sample container and associated equipment used in carrying out the conductivity measurements (viz., the central heater, central heater power supply, power measuring equipment, and temperature measuring equipment) are shown schematically in Appendix II (Figure 47) for the steady-state mode of operation. The equipment set-up was the same for the unsteady-state mode of operation with the substitution of the stainless steel tube resistance heater for the platinum-wound heater and a recording potentiometer for the manual potentiometer.

A basic requirement of the apparatus used in both modes of operation was that it include a centrally-located test zone having isotherms

CERAMIC SPACER

SAMPLE

INNER INCONEL TUBE

THERMOCOUPLE

OUTER INCONEL PIPE

INNER HEATER
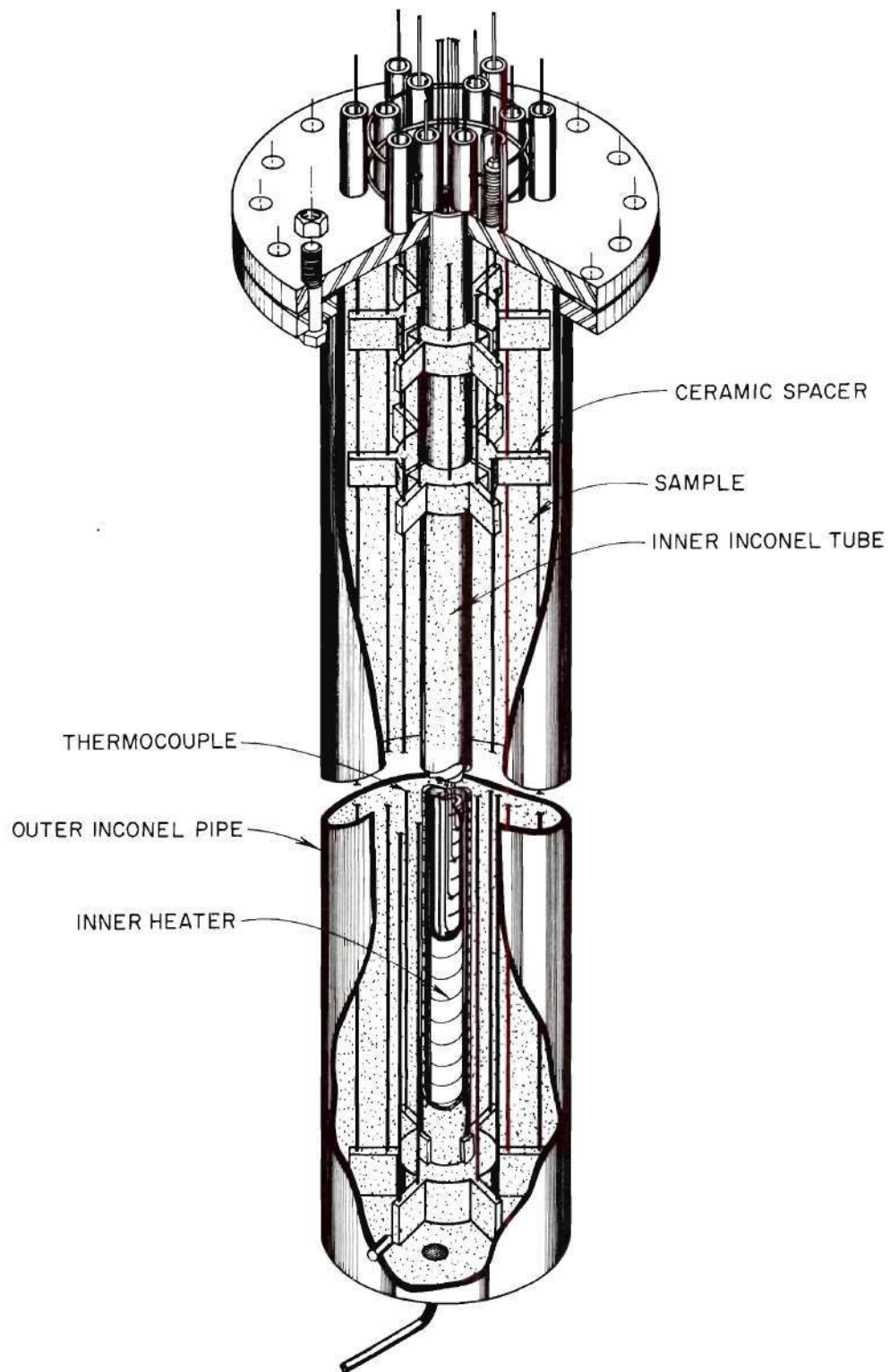
Fig. 2.   Sample Container.
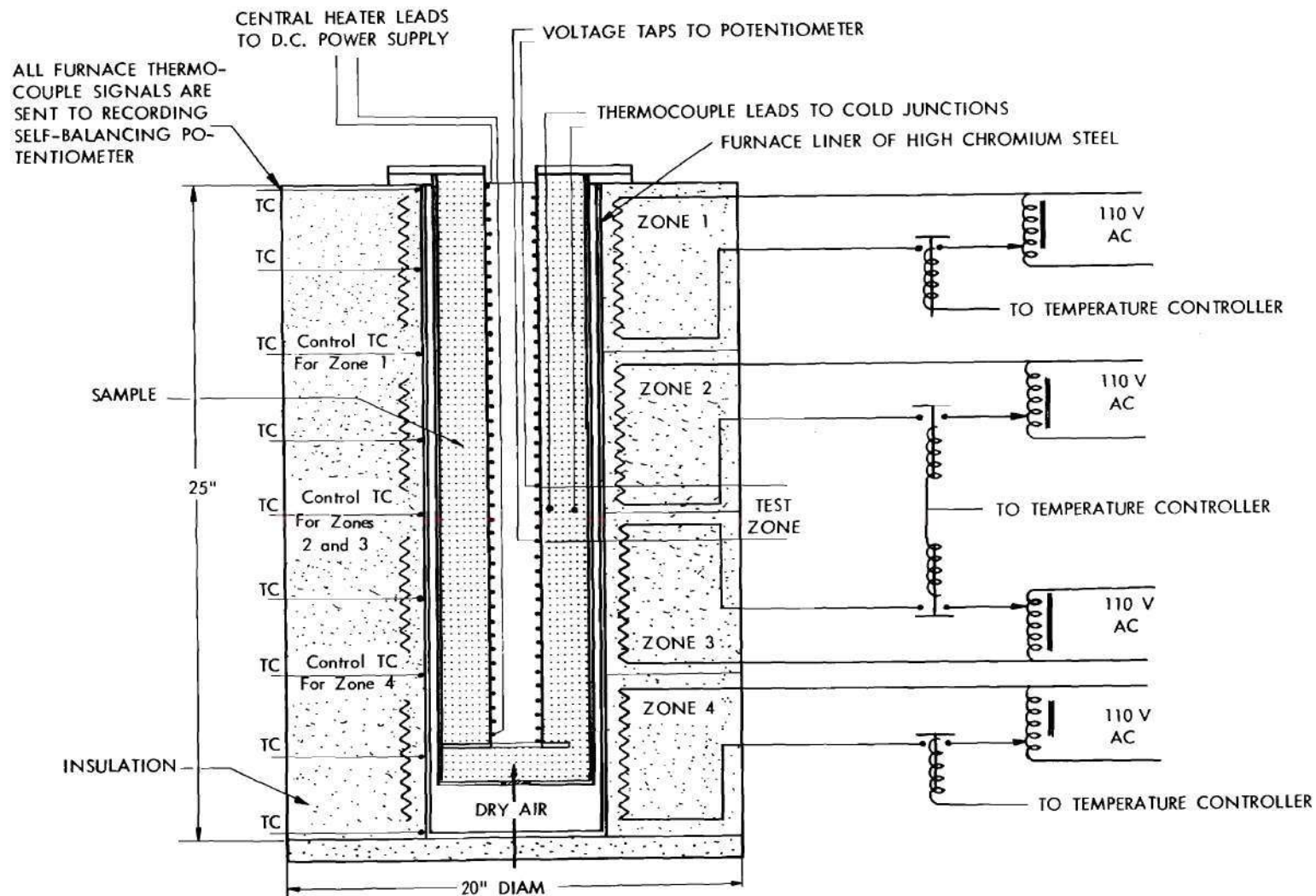
Fig. 3. Schematic Diagram of Sample Container in Controlled-Temperature Furnace.

which were very nearly concentric cylinders. The isotherms were adjusted
to this configuration and maintained by guard heaters which could be
sensitively trimmed by adjustable voltage supplies. Twelve thermocouples
were located in the test zone in a circular pattern in two ranks concen-
tric with the central heater (Figure 4). Each rank had six thermocouples.
The temperatures of the thermocouples in the two ranks were measured, and
an average temperature was determined for each rank by taking an arith-
metic average of the temperatures indicated by the six thermocouples in
that rank.

Sample Container

The sample container was fabricated from Inconel pipe and was
about 4 inches in inside diameter, 4-1/2 inches in outside diameter, and
about 24 inches long. The container accommodated a 1-inch Inconel tube
(14BWG) that was about 22 inches long and was welded to the center of
the top flange. The Inconel tube was centered at the bottom by an
Inconel spacer or "spider" in which the tube was free to turn (Figure 5).
The spacer was prevented from turning by two small lugs projecting from
the side wall of the container. The top flange held six pairs of thermo-
couples which were spring-loaded to prevent them from bowing under expan-
sion. This was found to be necessary to maintain their radial positions
in the container (Figures 5 and 6). To prevent any motion of the portion
of the thermocouples outside the container being transmitted to the por-
tion of the thermocouples inside the test zone, ceramic spacers in the
upper portion of the container were necessary (Figures 5 and 6). The
ceramic spacers were machined from Lava "A"—an aluminum silicate—and
were spring-loaded to maintain their longitudinal position. The top and

OUTER RANK OF
THERMOCOUPLES

INNER RANK OF
THERMOCOUPLES

THERMOCOUPLE DISTANCE
FROM CENTER LINE
(NOMINAL)

1	1 5/8"	2	7/8"
3	"	4	"
5	"	6	"
7	"	8	"
9	"	10	"
11	"	12	"
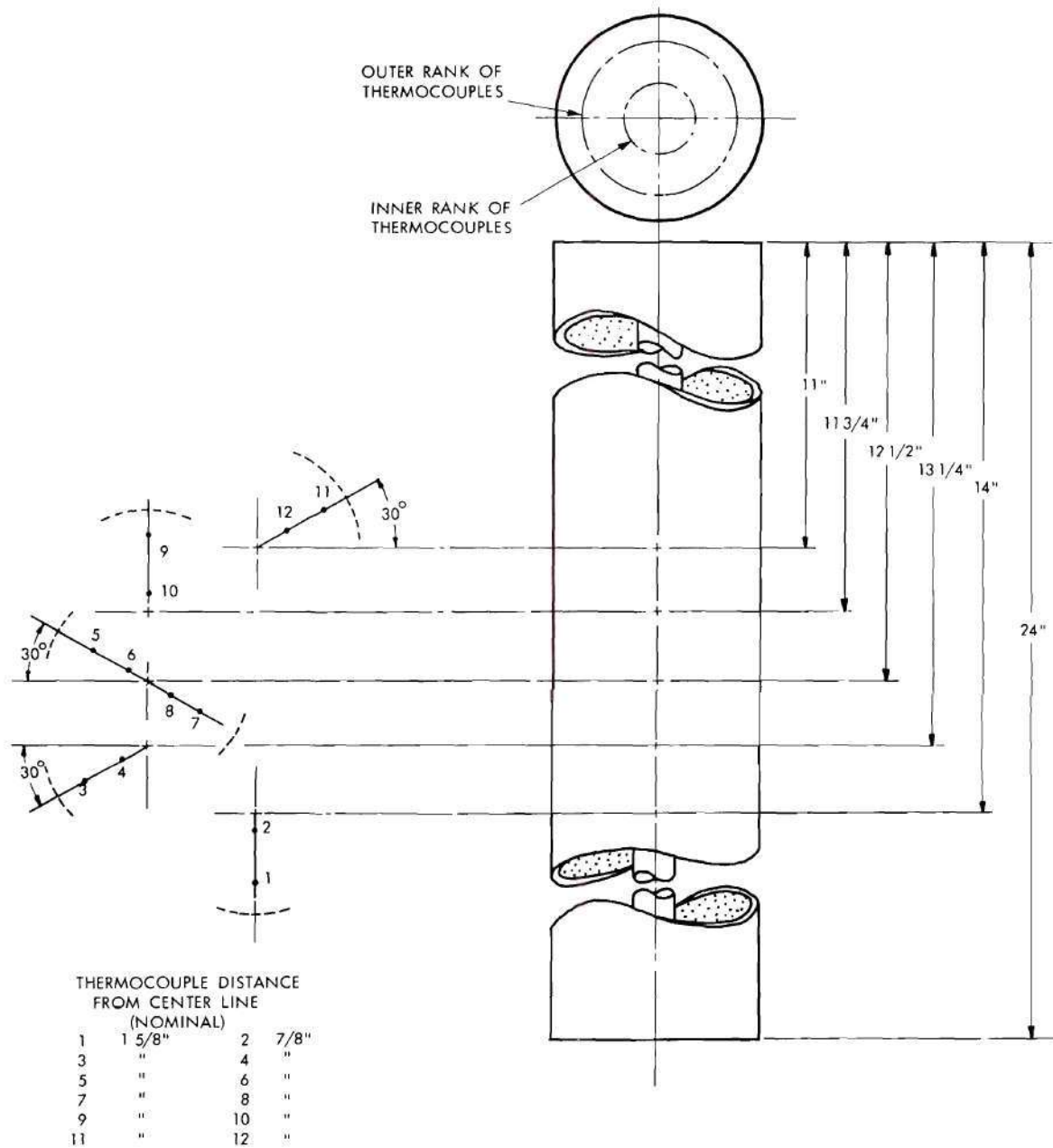
Fig. 4. Longitudinal, Radial, and Azimuthal Locations of Thermo-
couples in Sample Container.

CERAMIC SPACER

CENTRAL HEATER TUBE

MARKERS INDICATE THERMOCOUPLE LOCATION

INCONEL SPACER
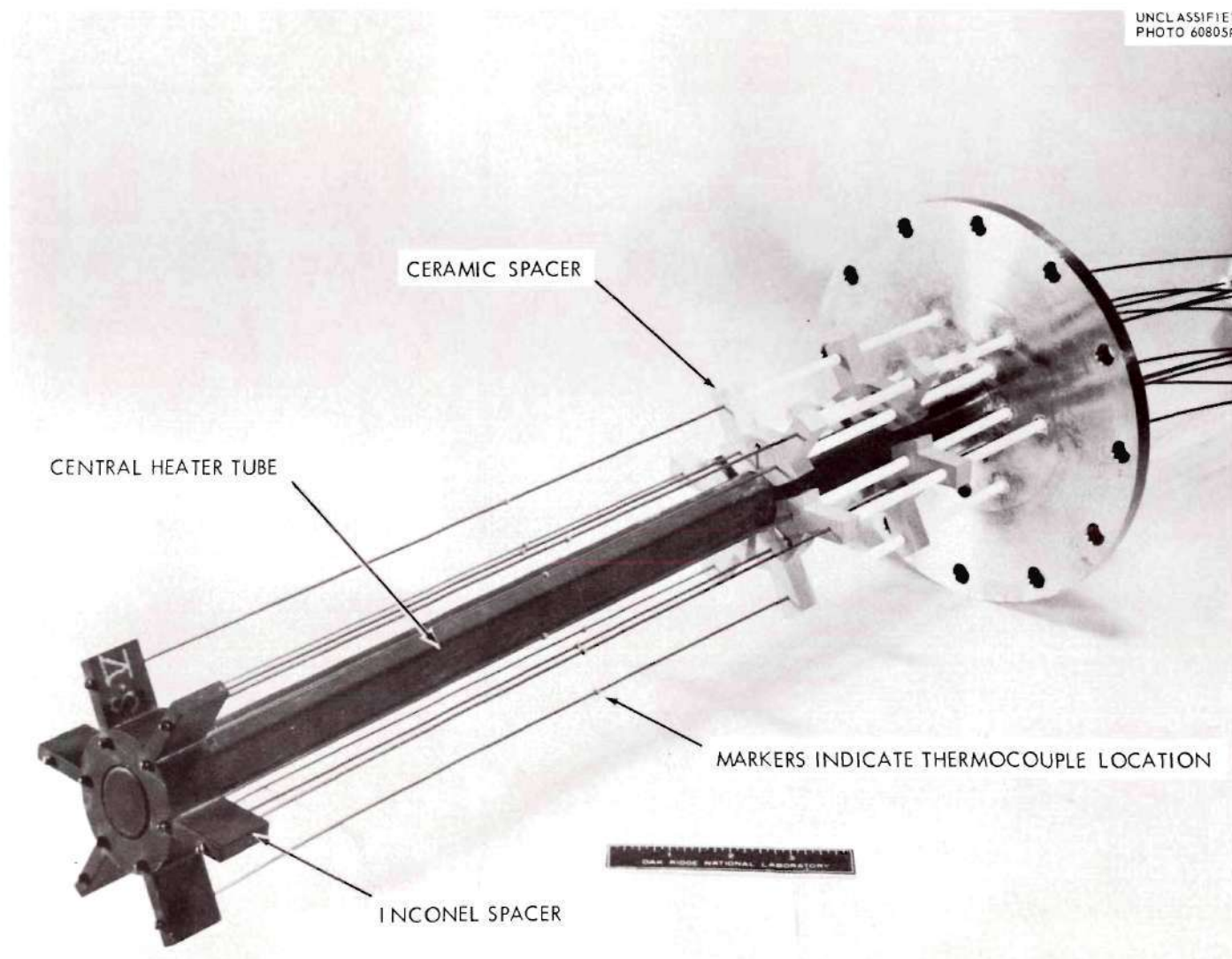
Fig. 5. Sample Container Top Flange and Central Heater Tube.

THERMOCOUPLE TENSION SPRINGS

SPRING GUIDES (removed to show springs)
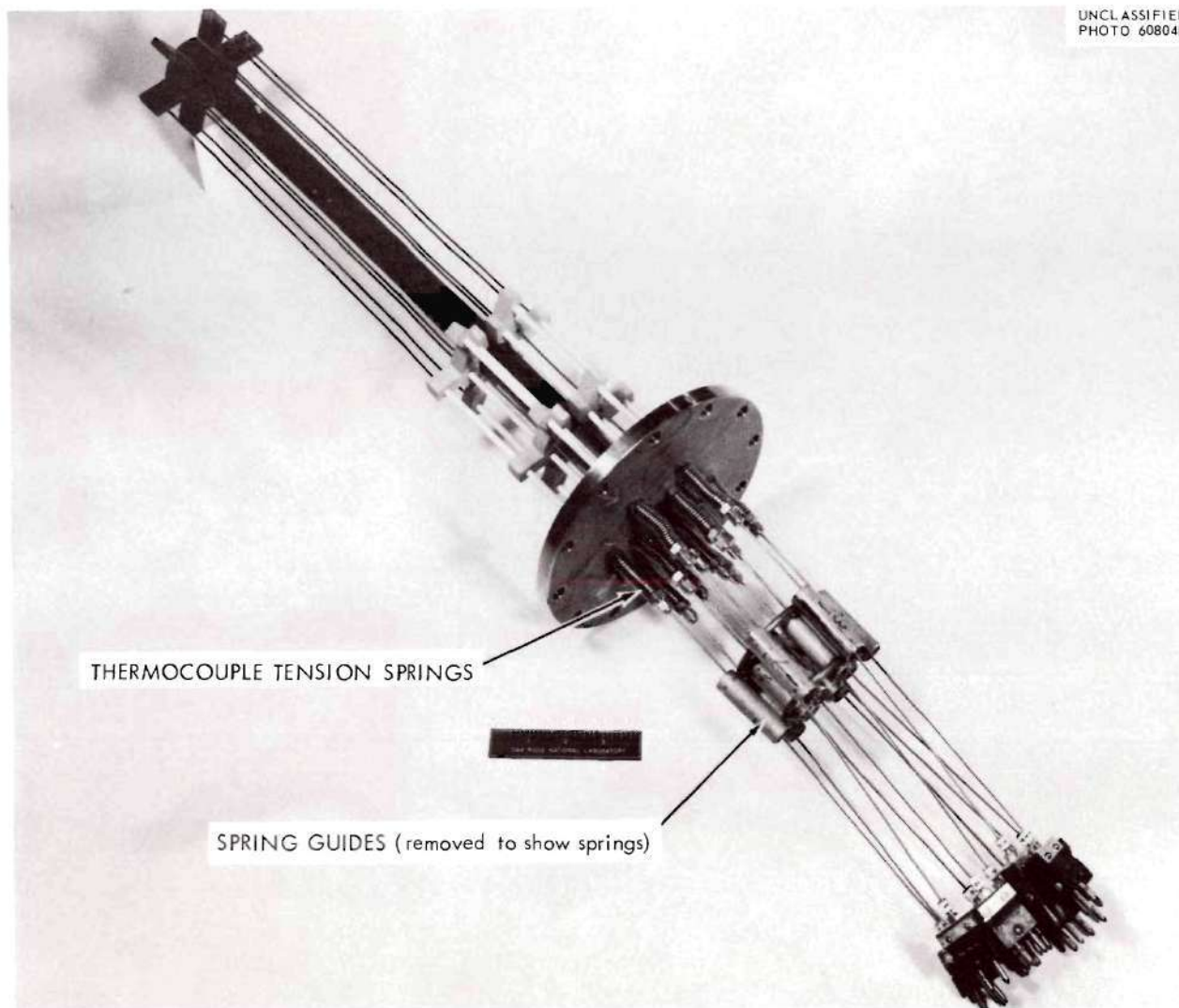
Fig. 6.   Thermocouple Tension Springs and Spring Guides.

bottom flanges were sealed to the sample container using corrugated stainless steel gaskets. Five containers were fabricated and used.

Furnace

The 5 kva controlled-temperature furnace was used to maintain a chosen temperature level as well as to establish vertical cylindrical isotherms in the test zone. The furnace was constructed of four resistance heater bands clamped to a high-chromium steel tube. Each heater band or zone was about 6 inches high and was powered separately (Figure 3). The temperatures of the top and bottom zones were controlled by off-on pyrometer type temperature control instruments with proportional and reset action. The middle two zones, although powered separately, were controlled by the same thermocouple. In two furnaces the temperatures of this middle zone were controlled by off-on null-balance temperature recorder-controller instruments with proportional and reset action. In the third furnace, temperatures of the middle zone were controlled by the pyrometer type instruments mentioned above. An over-all view of the controls for the three furnaces is shown in Appendix II (Figure 48). The three furnaces behaved similarly. Under steady-state conditions the furnaces as operated gave temperatures in the test zone constant to approximately $\pm 0.2^{\circ}F$ at about $200^{\circ}F$ and constant to approximately $\pm 1.5^{\circ}F$ at about $1500^{\circ}F$ for periods up to 72 hours.

Central Heater

For steady-state measurements the platinum-wound resistance heater—Appendix II, Figure 49(a)—was lightly coated with alundum cement and inserted into the 1-inch Inconel tube. The platinum wire was wound on a

ceramic core made of Lava "A". For unsteady-state measurements the top and bottom flanges were modified to accommodate insulating glands to isolate electrically the 1/8-inch, 347 stainless steel tube, resistance heater—Appendix II, Figure 49(b) and (c)—from the sample container. Three platinum-wound and three stainless steel tube resistance heaters were constructed and used.

Central Heater Power Supply

Direct current power to the central heater, either platinum wound or stainless steel tube, was supplied by a solid state power supply of the transistor-magnetic type. The model used (Appendix II, Figure 48) had an output which was continuously adjustable over the range 0-36 volts and 0-20 amperes.

Power Measuring Equipment

Power to the central heater was determined from measured voltage and current. The potential drop across the portion of the heater in the test zone was measured using a potentiometer (Rubicon Type B) in conjuntion with a volt box (Appendix II, Figure 47). The current in the heater was measured using the potentiometer in conjunction with a standard shunt in a current lead as well as with the volt box (Appendix II, Figure 47).

Temperature Measuring Equipment

All temperatures were measured with chromel-alumel thermocouples which had been calibrated to within 0.25 per cent of the values given in NBS Circular 561 at the steam point and aluminum melting point or checked against those which had been calibrated. The thermocouples distributed throughout the test zone were swaged assemblies of either 28 or 30 AWG

wire with magnesia insulation and with 1/16 inch outside diameter sheathing tubes of either 310 stainless steel or Inconel. The Inconel sheathing was more satisfactory than the 310 stainless steel because of Inconel's better resistance to steam corrosion. The thermocouple welded to the wall of the "probe" heater was 24 AWG wire.

The emfs of the thermocouples in the powder sample were determined with the potentiometer, and the emf of the "probe" thermocouple was recorded on a self-balancing variable range potentiometer with a chart speed of four inches per minute. All thermocouple emfs were converted to temperatures using NBS Circular 561. An over-all view of the cold junctions, potentiometer, and accessories is shown in Appendix II (Figure 50).

CHAPTER IV

CHARACTERIZATION OF MATERIALS

Selection of meaningful methods to characterize particle matter
is a problem common to many fields of science and engineering. The
properties of a multicomponent two phase system, such as a powder made
of solid and gas, cannot be adequately described without taking into
account such factors as total void fraction, particle size, particle-
size distribution, surface characteristics of the particles, shape
factors, pore size, and pore-size distribution. The gross properties
of powders are determined by three major sub-classes of properties.
The first class is described by the properties of the pure bulk com-
ponents. These properties are retained by the components in the mixture.
Examples are thermal conductivity and heat capacity of the bulk solid
and the gas; and hardness, coefficient of linear expansion, and x-ray
crystal pattern of the bulk solid. The second class is described by
properties created by subdividing the solid. Examples are particle
size, particle-size distribution, surface characteristics, shape
factors, pore size, and pore-size distribution. The third class is
described by properties belonging to the solid-gas system. Examples
of this class are bulk or apparent density, effective thermal conductivity,
permeability, and other transport properties of the system. In the
measurement of properties in classes two and three above it is assumed
that the powder is isotropic (i.e., no preferred orientation of the
particles) and that the sample examined or measured is large enough so

that selection of another similar sample or a larger sample will not materially change the measured values.

The behavior of a powder (or any particulate matter) should be determined by the properties of the pure components, the particle parameters, and the manner in which they are combined as stated above. However, it is difficult to determine which of the pure component properties and particle parameters are most important, and even more difficult to determine how each affects the behavior of the multicomponent system. Much of the data in the literature on the effective thermal conductivity of systems which appear similar (based on k_c, k_d, V_d and particle size) actually vary widely. For example, Schotte (62) compares data on five glass beads-air systems at temperatures not too far apart and with almost the same void fraction and finds that the results differ by a factor of 2.4. One of the principal tenets of the present work is that such differences found in apparently similar systems may easily be real, and are explicable in terms of more subtle factors such as particle-size distribution, surface conditions (roughness, cleanliness, adsorbed films, etc.), mechanical (not gas) pressure on the system, and other factors. To promote and support this belief, powders used in this study were extensively characterized.

The solid materials used for thermal conductivity measurements were magnesia, alumina, and lime-stabilized zirconia powders that were produced from the respective electrochemically refined (fused in an electric furnace) oxides which had been crushed. The supplier of the materials, Norton Company, Worcester, Massachusetts, designates the alumina as Alundum, Type:38; the magnesia as Magnorite, Type: Electrical;

and the zirconia as Lime Stabilized (Cubic) Zirconia, Type: "H". The as-received magnesia and zirconia powders were individually blended in a Patterson-Kelly twin shell laboratory blender before any measurements were made. The purpose of blending was to ensure homogeneity since there seemed to be a floating of fines during shipment of the powders. With the exception of this blending, the magnesia powders designated MgO (E-98) and MgO (E-227) and the zirconia powders designated ZrO_2 (H30F) and ZrO_2 (H14F) were used as-received. The alumina powder designated Al_2O_3 (E-98) was prepared by mixing appropriately sized fractions of powder to give a powder having a particle-size distribution like that of the MgO (E-98) powder. The alumina powder designated Al_2O_3 (B45F) was obtained by taking a selected cut of an as-received alumina powder. The designations in parentheses following the chemical formula of a powder are codes used for convenience in this study and correspond, in most cases, to the supplier's code.

Analysis by x-ray diffraction indicated that the materials were magnesia, alpha-alumina, and cubic zirconia. Spectrochemical analyses of the oxides indicated that the principal impurities in the magnesia were aluminum (0.01-0.1%), iron (0.01-0.1%), and silicon (0.01-0.1%); that the principal impurities in the alumina were iron (0.01-0.1%), sodium (0.01-0.1%), and silicon (0.01-0.1%); and that the principal impurity in the zirconia (exclusive of the CaO added to stabilize the ZrO_2 in the cubic form) was aluminum (0.01-0.1%). Analyses by flame photometry indicated that the ZrO_2 (H30F) contained 3.58 weight per cent CaO and that the ZrO_2 (H14F) contained 2.57 weight per cent CaO. Thermogravimetric analyses indicated that the weight losses of the

powders on heating to 1832°F varied from 0.024 to 0.134 weight per cent (Table 1). The complete thermograms for each powder are presented in Appendix III (Figure 51). The surface area per unit weight, as determined by BET nitrogen adsorption, and the "absolute," "true," or "pore-free" density, as determined by pycnometric techniques, of the powders are given in Table 1. The surface area and density measurements indicate that the particles have few or no closed internal pores as would be expected for fused and crushed material. The particles are irregular in shape. However, they are neither plate-like nor needle-like, which are shapes that tend to destroy homogeneity of packing structure (Figure 7).

For irregular particles the term "particle size" is arbitrary, but should be unambiguous. The particle size measurements used in this work were selected using the excellent treatments of small particle measurement techniques, their ranges of applicability, and limitations by DallaValle (63), Orr and DallaValle (64), or Herdan (65) as a guide.

The particle size as determined by sieving is taken to be the arithmetic average of the sizes of the openings of the screen which passes the particle and that which retains it. The logarithmic-probability plots of cumulative weight in per cent versus size for the powders used are shown in Figures 8 to 13. The tabular data from which these plots were made are given in Appendix III (Tables 6 to 8). The median particle size, logarithmic (to base e) standard deviation, and mean particle size for each powder obtained from these data are given in Table 2.

Table 1. Properties of Magnesia, Alumina, and Zirconia Powders.

Powder	Pore-free Density[a] (g/cc)	Surface Area[b] (m^2/g)	Weight Loss on Heating to 1832°F (%)	Minimum Volume Fraction Solid[d] $V_{d\ min}$	Maximum Volume Fraction Solid[e] $V_{d\ max}$
MgO (E-98)	3.59	0.076	0.058	0.494	0.651
MgO (E-227)	3.58	0.062	0.125	0.452	0.610
Al$_2$O$_3$ (E-98)	3.98	0.043	0.134	0.457	0.633
Al$_2$O$_3$ (B45F)	3.95	0.034	0.079	0.426	0.528
ZrO$_2$ (H30F)	5.60	0.116	0.030	0.534	0.764
ZrO$_2$ (H14F)	5.63	0.081	0.024	0.573	0.801

Determined as follows:

[a] Gas pycnometer.

[b] BET nitrogen adsorption.

[c] Thermogravimetric analysis.

[d] Procedure on page 56.

[e] Procedure on page 56.

MgO (E-98)

MgO (E-227)

Al$_2$O$_3$ (E-98)

Al$_2$O$_3$ (B45F)

ZrO$_2$ (H30F)

ZrO$_2$ (H14F)
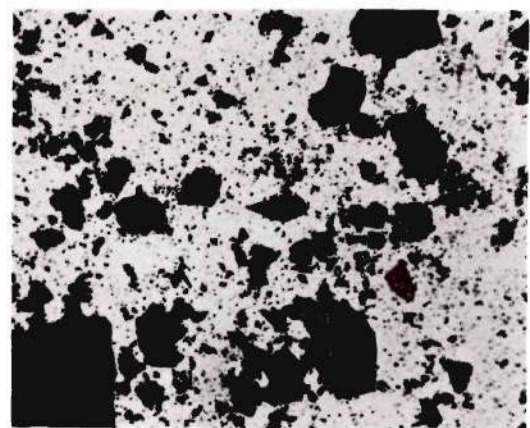
100 MICRONS

Fig. 7. Photomicrographs of Powders.
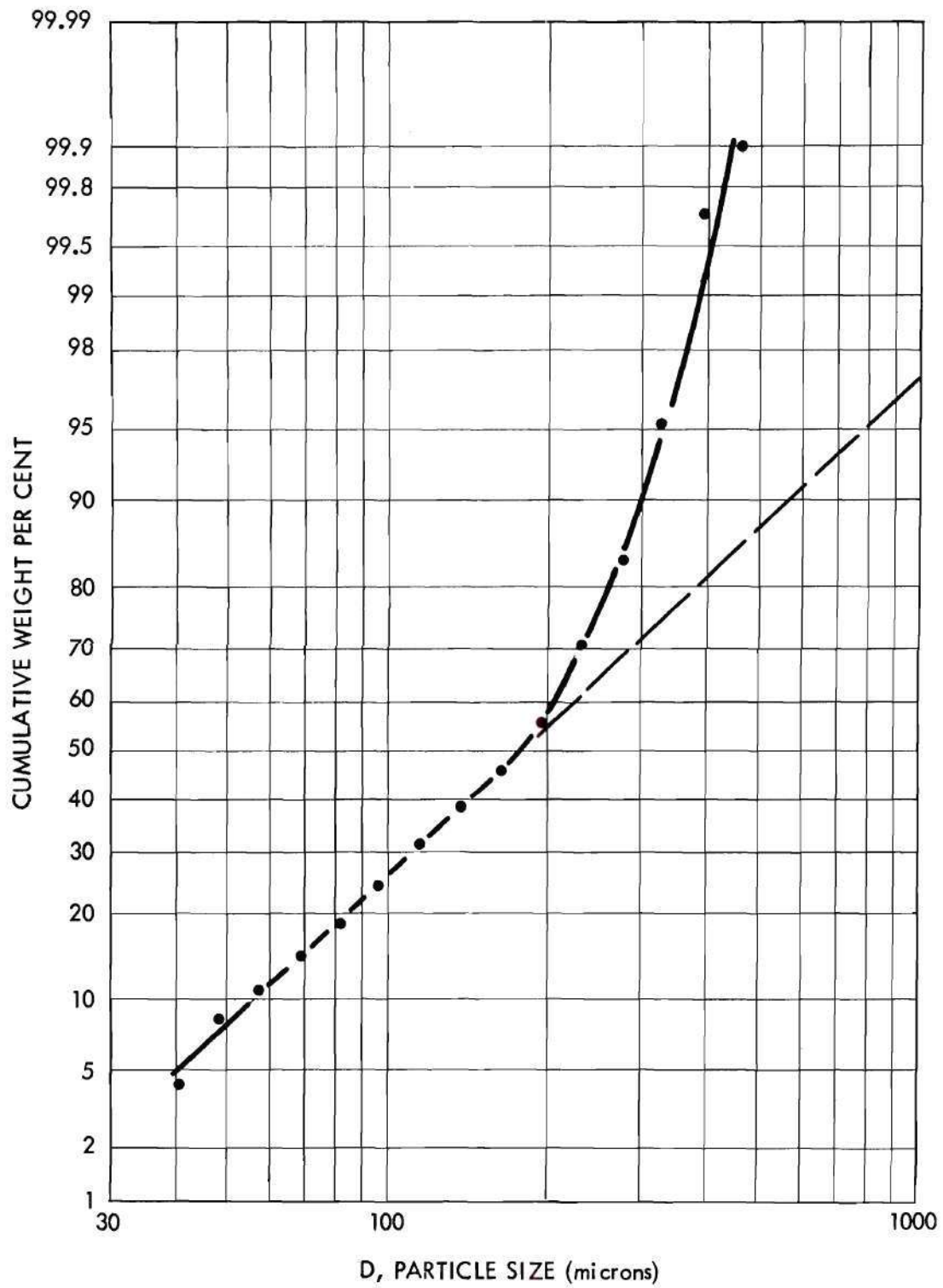
Fig. 8.   Particle-Size Distribution of MgO (E-98) by Sieving.
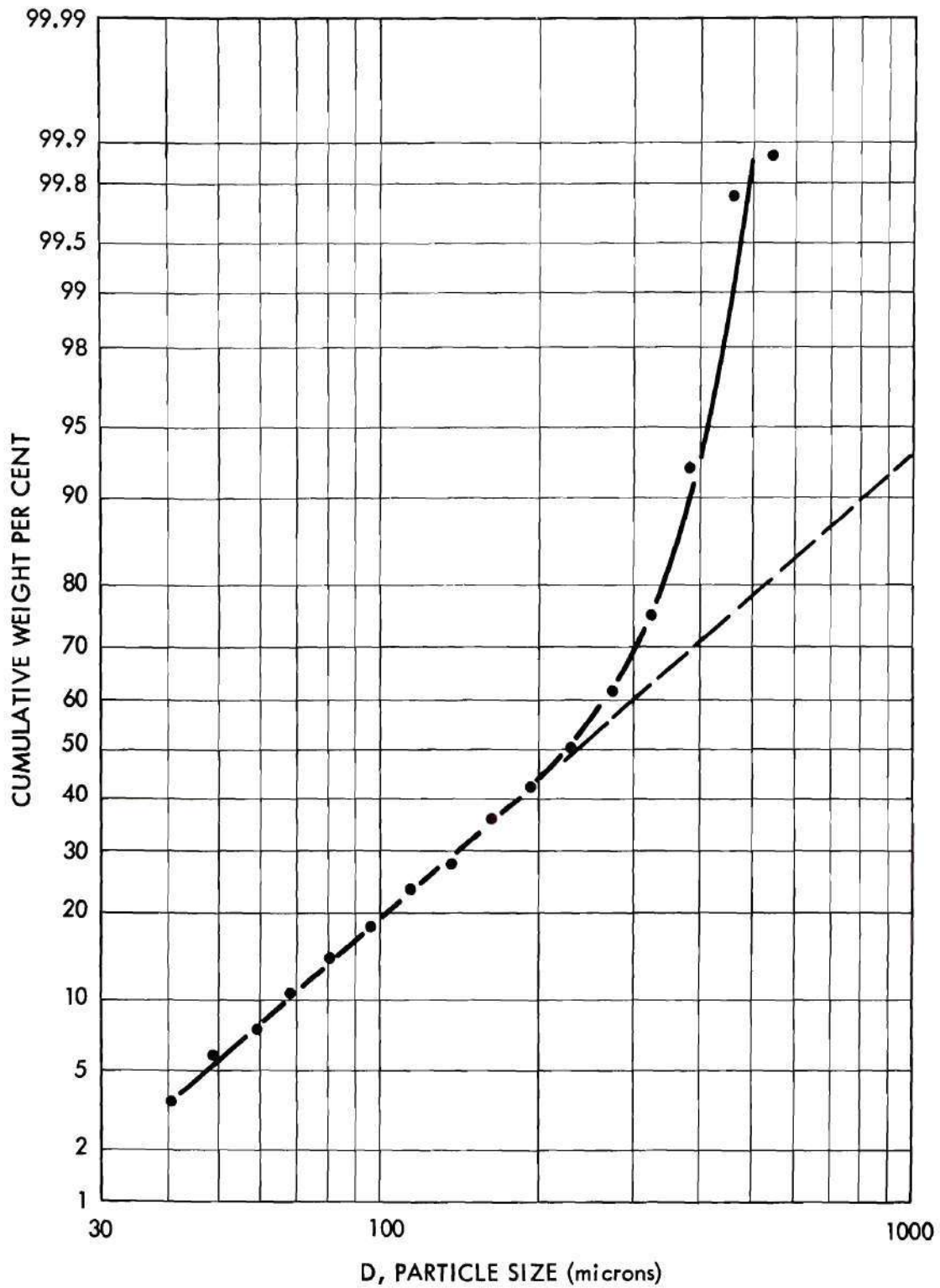
Fig. 9. Particle-Size Distribution of MgO (E-227) by Sieving.
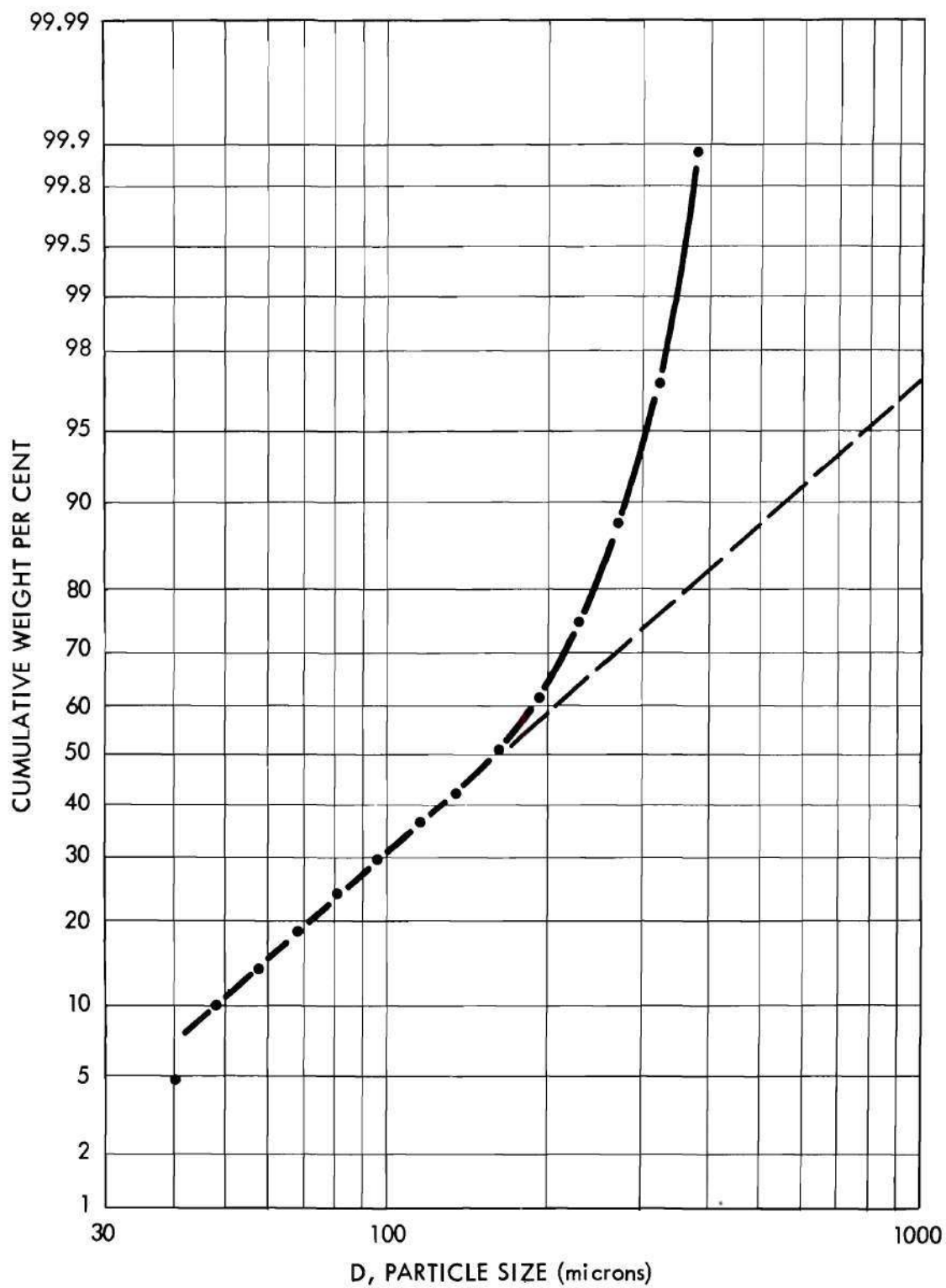
Fig. 10. Particle-Size Distribution of Al_2O_3 (E-98) by Sieving.
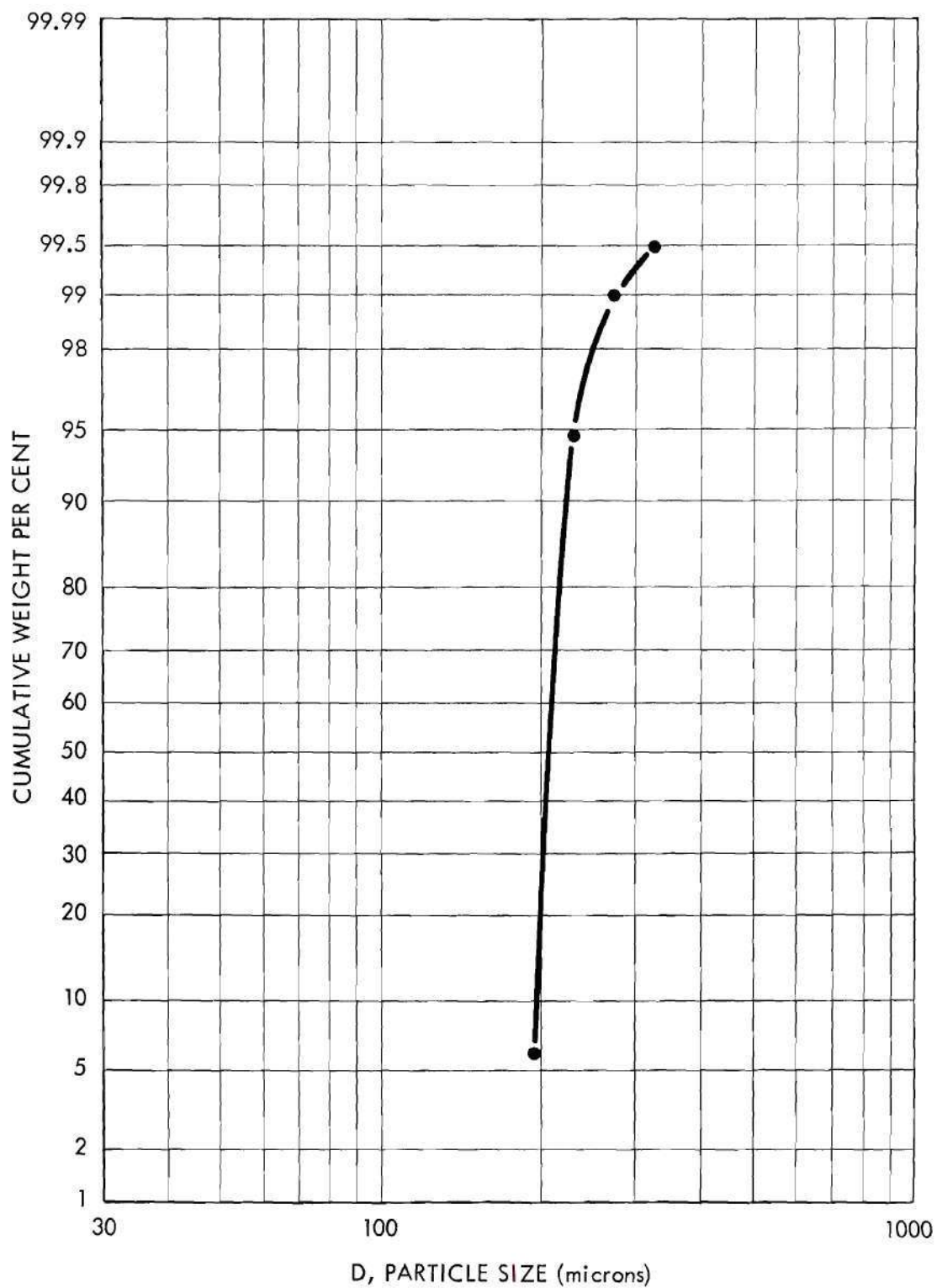
Fig. 11.   Particle-Size Distribution of Al_2O_3 (B45F) by Sieving.
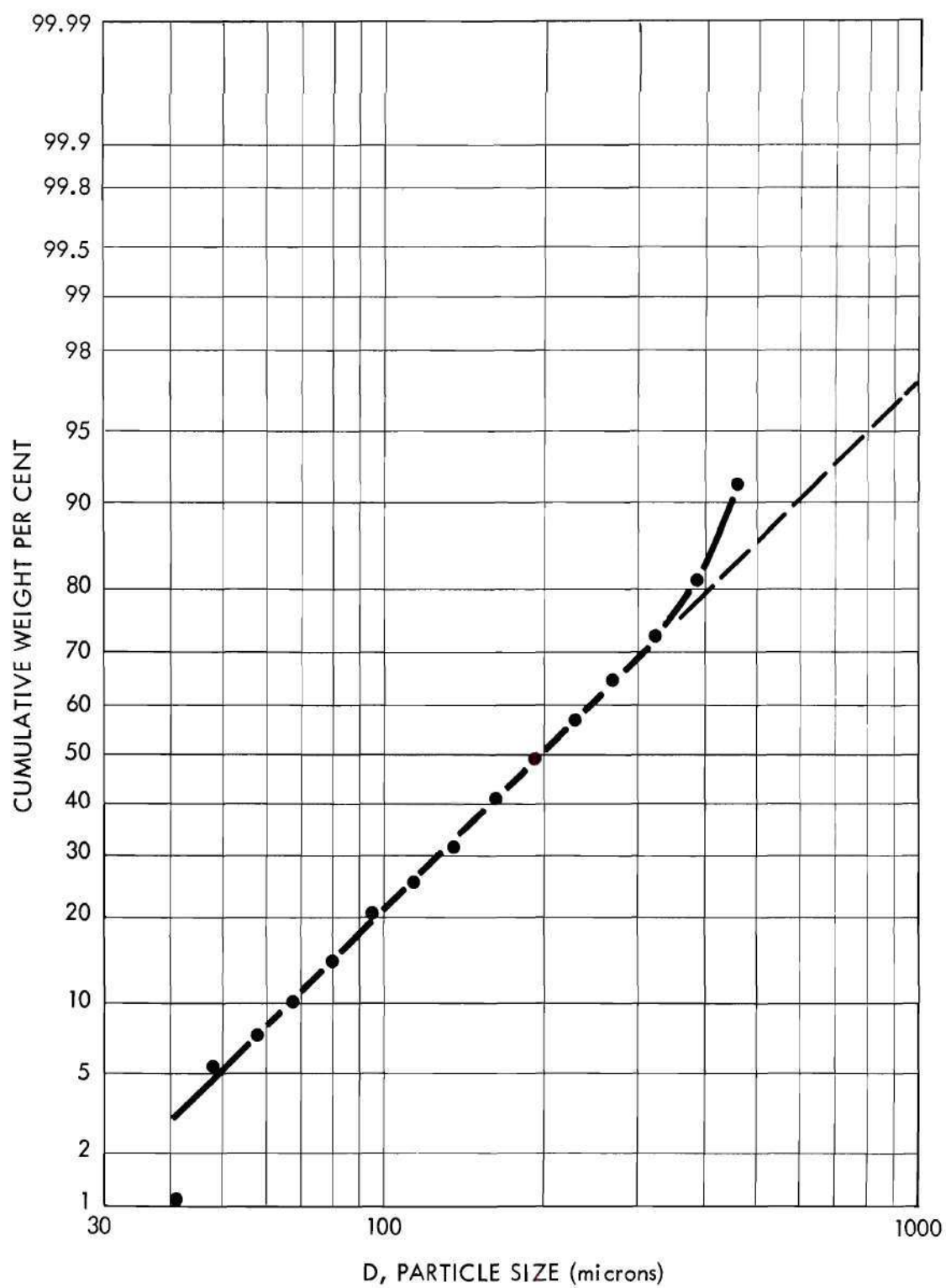
Fig. 12.   Particle-Size Distribution of ZrO_2 (H30F) by Sieving.
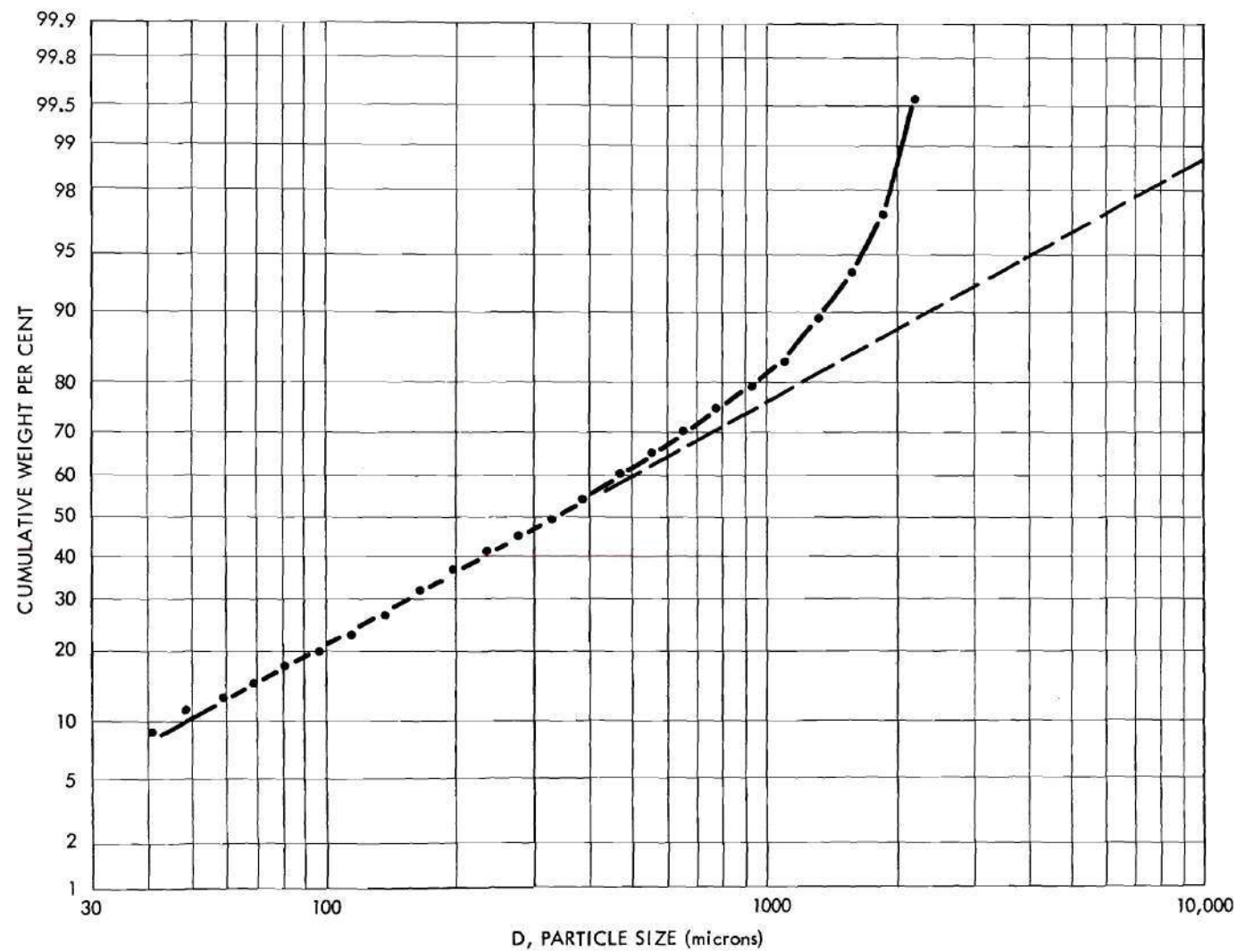
Fig. 13. Particle-Size Distribution of ZrO_2 (H14F) by Sieving.

48

Table 2. Parameters of Magnesia, Alumina, and Zirconia Powders Obtained from Screen Analysis

Powder	Median Particle Size,[a] $D_{50\%}$ (microns)	Logarithmic (to base e) Standard Deviation,[b] S_{ln}	Mean Particle Size,[c] D_m (microns)	Points of Truncation[d] Lower, D_a (microns)	Points of Truncation[d] Upper, D_b (microns)	$\int_{D_a}^{D_b} \frac{e^{-u^2/2}}{\sqrt{2\pi}} du$
MgO (E-98)	180	0.892	268	23	328	0.739
MgO (E-227)	235	0.949	369	19	432	0.735
Al_2O_3 (E-98)	166	0.959	263	13	308	0.737
Al_2O_3 (B45F)	211	0.055	211	e	e	e
ZrO_2 (H30F)	198	0.880	292	36	555	0.853
ZrO_2 (H14F)	333	1.499	1023	20	1950	0.851

Determined as follows:

[a] Fifty per cent value of D from logarithmic probability plot of particle size versus cumulative weight per cent.

[b] $S_{ln} = ln \left[\dfrac{D \text{ at } 84.13\%}{D \text{ at } 50\%} \right]$ using straight line portion of logarithmic plot of particle size versus cumulate weight per cent.

[c] $D_m = D_{50\%} e^{1/2 (S_{ln})^2}$.

[d] Procedure on page 52.

[e] Distribution has too few points for meaningful determination of points of truncation.

The size of particle as determined by sedimentation is expressed as the diameter of a sphere that would fall with a velocity equal to the observed falling velocity of the particle. This method gives the so-called apparent Stokes' diameter. These results are tabulated in Appendix III (Table 9).

The sieving and sedimentation techniques given above yield weight or volume fractions of the various sizes. For purposes of comparison, a linear measure of size as a function of the number of particles, as determined by microscopic measurement of one powder, MgO (E-98), is presented in Appendix III (Table 10). As a general rule, if the number distribution of particle size obeys a specific distribution law, the weight distribution does not, and vice-versa. However, the logarithmic normal distribution is one of the distribution laws for which, if the weight distribution is logarithmic normal, the number distribution is logarithmic normal with the same logarithmic standard deviation (66). The results of MgO (E-98) as determined by sieving and microscopy are compared in Figure 14. It may be seen that the distributions follow a logarithmic normal law with logarithmic (to base e) standard deviations of 0.892 and 0.936, as determined by sieving and microscopy, respectively.

Although a complete population was used as a sample in the operations which gave the information plotted in Figures 8 to 14, the individual values of observations below a smallest particle size, D_a, and above a largest particle size, D_b, are not specified. A distribution of this type is called a censored distribution because the obtainable information has in a sense been "censored" either by nature or by the observer.
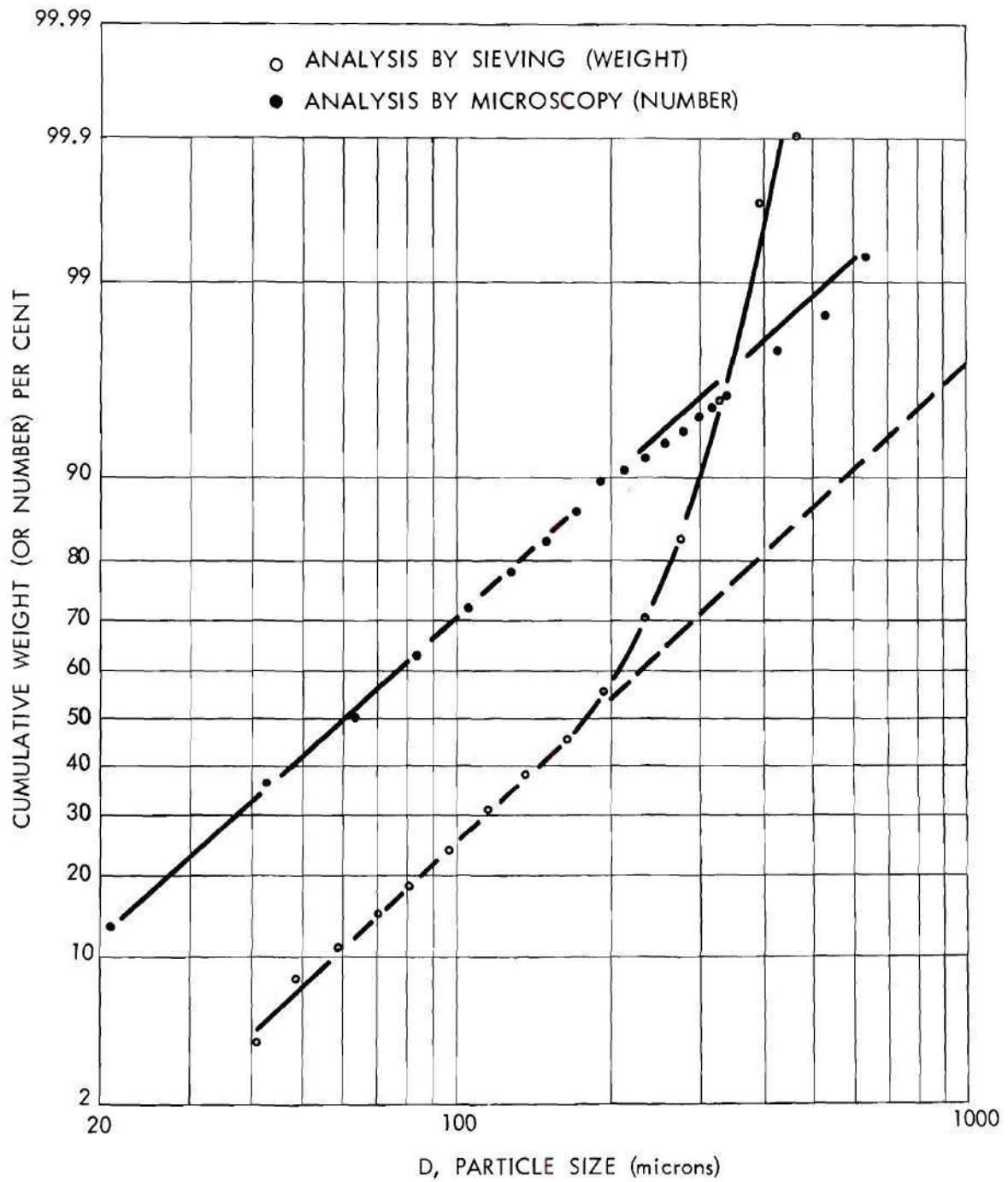
Fig. 14. Particle-Size Distribution of MgO (E-98) by Sieving and by Microscopy.

In other words a logarithmic normal distribution with parameters, $D_{50\%}$ and S_{ln}, describes a system with

$$\int_{-\infty}^{+\infty} \frac{e^{-u^2/2}}{\sqrt{2\pi}} \, du = 1 \tag{29}$$

where

$$u = \frac{1}{S_{ln}} \ln \frac{D}{D_{50\%}} \, , \tag{30}$$

D = particle size,

$D_{50\%}$ = median particle size, and

S_{ln} = logarithmic (to base e) standard deviation.

Any real powder represents only a portion of the above integral. Determination of the points of truncation of a population (the smallest and largest particles in this case) is mathematically very difficult. For instance, see the treatment of censored distributions and truncated populations given by Hald (67) or Kendall and Stuart (68).

The scheme used to obtain points of truncation for the powders of this study was as follows: (a) The original size analysis (Appendix III, Tables 6, 7, and 8) of each powder was plotted on arithmetic (Figure 15) or semi-logarithmic paper (Figure 16) as particle size versus cumulative weight (or volume) per cent. (b) The best straight line through the points was extrapolated to 0% and 100% to obtain values for D_a and D_b, respectively. It was assumed that any particle sizes excluded from the distribution by this scheme occurred so infrequently that their exclusion did not significantly alter the heat flow pattern of the powder and that they could be considered not present at all.
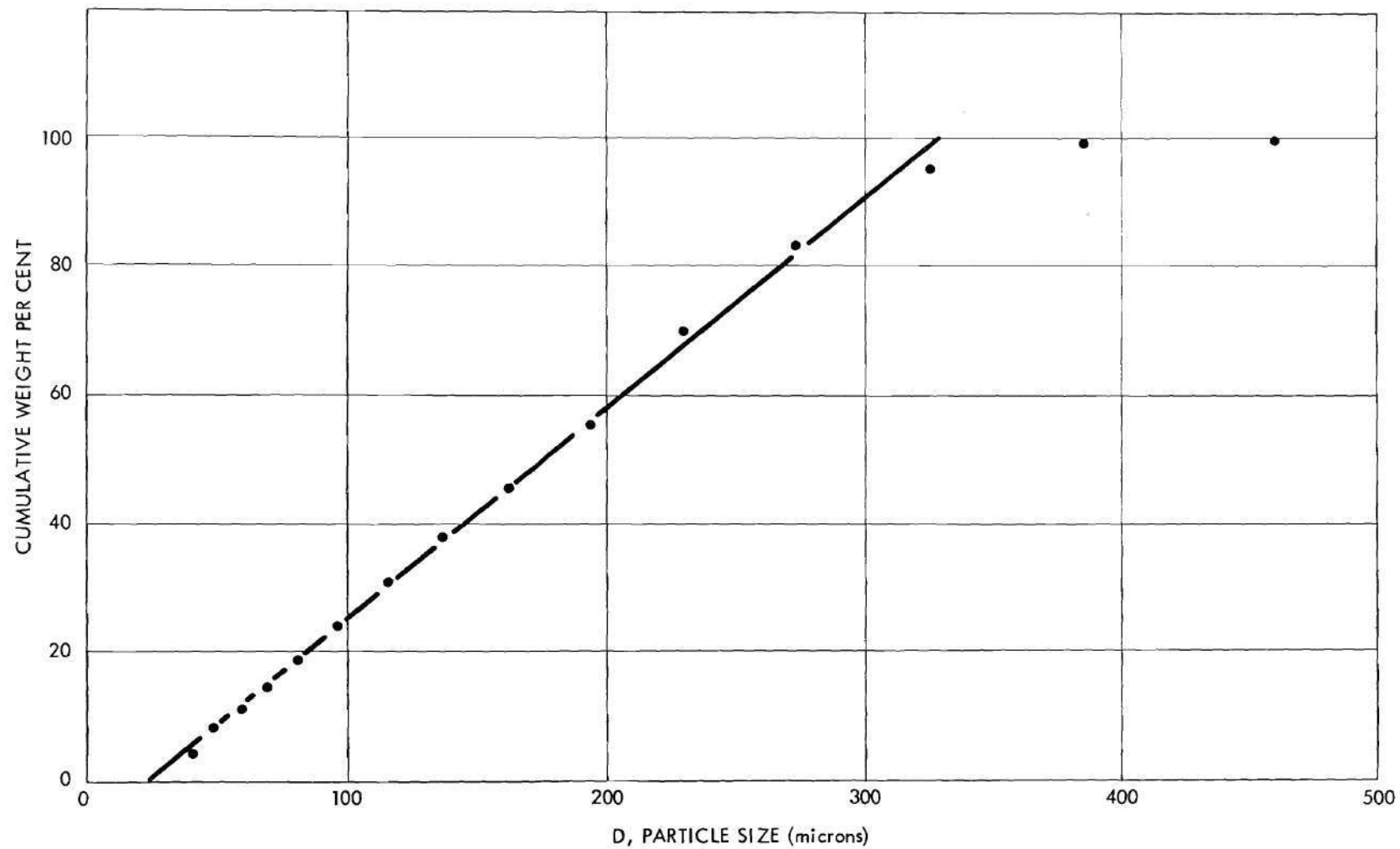
Fig. 15. Graph Used to Determine Points of Truncation of MgO (E-98) Particle-Size Distribution.
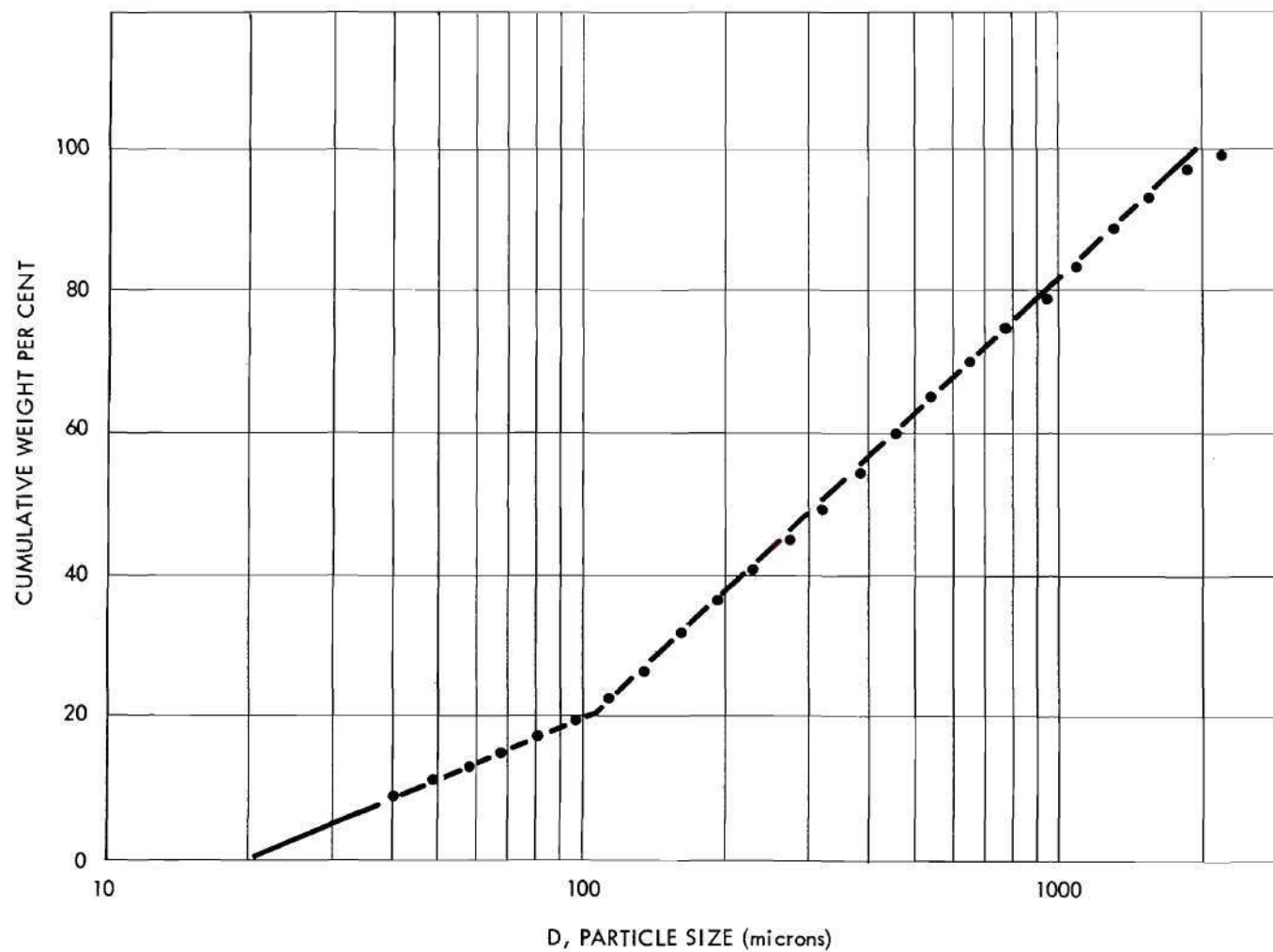
Fig. 16. Graph Used to Determine Points of Truncation of ZrO$_2$ (H14F) Particle-Size Distribution.

For each powder studied the points of truncation as determined by the scheme given above are tabulated in Table 2. The value of the integral

$$\int_{D_a}^{D_b} \frac{e^{-u^2/2}}{\sqrt{2\pi}} \, du$$

where D_a = lower point of truncation and D_b = upper point of truncation for each powder is tabulated in Table 2.

The interrelation between volume fraction solid and particle shape is complicated. For single-sized spheres the volume fraction solid in a powder is a function of arrangement only and can be calculated from geometry for the six orderly arrangements possible (69 and 70). These are theoretical packings, and in practice the volume fraction solid for single-sized spheres may be less than the most open packing (cubic) because groups of spheres may arch and leave gaps. However, in any statistically describable packing of spheres there will be a packing pattern, made up of combinations of the six theoretical arrangements and arches, which is repeated in identical form throughout the body of spheres. For packings of unequal spheres a wider range of volume fraction solids is possible, since the smaller spheres are able to fit into the openings between the larger spheres. For packings of ir-regularly shaped and non-uniformly sized particles almost any volume fraction solid is possible. For a given powder, the amount which can be put into a given container can be increased by compacting, for instance, by tapping the container. This increase in volume fraction solid in the container is caused by factors such as the breaking of arches, the better fitting-together of particles, (for example, a

concave surface of one particle slips into the convex surface of another), and the filling up of voids between larger particles by smaller ones (71).

In order to determine for each powder what range of volume fractions to expect, a "minimum volume fraction," $V_{d\ min}$, and a "maximum volume fraction," $V_{d\ max}$, were determined for each powder (Table 1).

$V_{d\ min}$ was determined by filling a funnel, having a spout which extended to the bottom of a graduated cylinder, with a charge of powder. The funnel was raised slowly so that the powder would fall through essentially no distance in filling the cylinder—obviously the emergent powder is under some head because of the unsupported weight of the column of powder in the spout. In practice a 500 gram charge of powder was placed in a 60^0, 15 centimeters diameter funnel with a 35 centimeters extension spout having a one centimeter inside diameter. The spout extended to the bottom of a standard 500 milliliter graduated cylinder. The funnel was raised at about 0.06 centimeter per minute and the powder allowed to flow out. The flow was sporadic because of the intermittent slipping nature of the powder. At no time, however, did the spout pull free of the released mound of powder before additional powder was released from the spout. Results obtained by this method were very reproducible. A drawing of the apparatus is given in Appendix III (Figure 52).

$V_{d\ max}$ was determined by placing a 500 gram charge of powder in a steel cylinder 17 centimeters long and 5.2 centimeters inside diameter. The cylinder was raised 0.6 centimeter and dropped to a metal plate 120 times per minute. Dropping was continued until the volume of powder ceased to diminish — usually about three hours. A drawing of the apparatus is given in Appendix III (Figure 53).

CHAPTER V

EXPERIMENTAL PROCEDURE

Procedures for sample holder calibration, sample preparation, and equipment operation were standardized in the interest of producing consistent results.

Sample Holder Calibration

The radial distances of thermocouples from the wall of the 1-inch Inconel tube were determined by taping a glass microscope slide to the Inconel tube and a pair of thermocouples on the same radius (Figure 17). The slide was then sprayed with acrylic base lacquer. After the lacquer dried, the slide was removed, and the distances from the edge of the slide to the unlacquered strips which had been shielded by the thermocouple were measured with a micrometer. The distance from the center of an unlacquered strip to the 1-inch Inconel tube plus one-half the diameter of the tube gave the radial location of the thermocouple (Figure 17). Of the numerous measuring techniques tried, including methods using x-rays of the assembled and filled container, this spraying technique proved most satisfactory. The volume of the assembled sample container was determined by filling it with water. The nominal volume of an assembled sample container was 4.35 liters.

1"- INCONEL TUBE

1/16" SHEATHED
THERMOCOUPLE

GLASS MICROSCOPE
SLIDE

UNLACQUERED STRIP
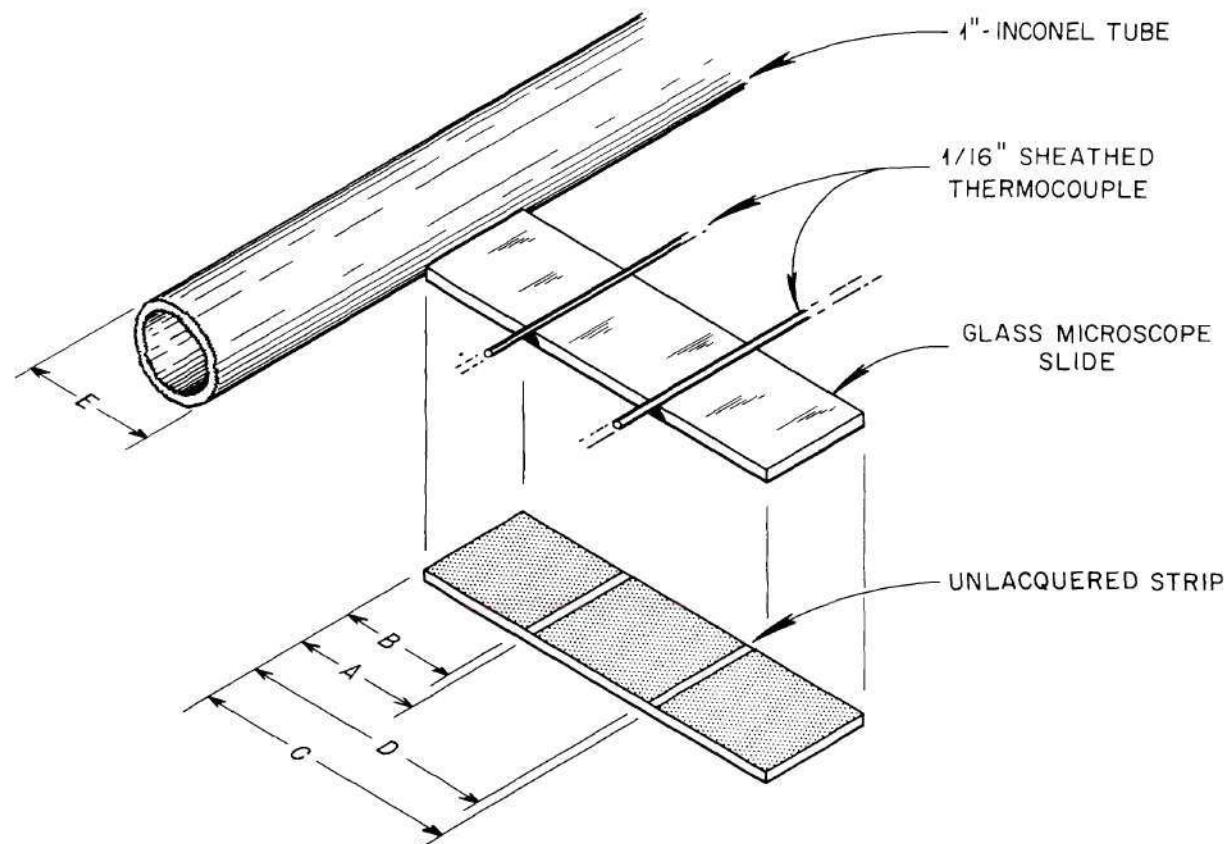
INNER RADIUS = 1/2 (A+B+E)
OUTER RADIUS = 1/2 (C+D+E)

THERMOCOUPLE JUNCTION IS ASSUMED TO BE AT CENTER OF SHEATHED ASSEMBLY

Fig. 17. Scheme for Determining Radial Distances of Thermocouples.

Sample Preparation

The powder to be tested was poured into the sample container through the open bottom (steady-state) of the inverted container, or through a hole in the top flange (unsteady-state). The mass of powder added to achieve a desired volume fraction solid was chosen to satisfy the relation

$$V_d = \frac{M_S}{\rho_{PF} V_T} \tag{31}$$

where M_S = mass of solid,

ρ_{PF} = density of pore-free solid (Table 1), and

V_T = volume of test cylinder.

In practice, the mass of solid (determined using a platform balance) was taken as the mass of powder measured in air, since the maximum error that can be introduced into V_d by neglecting the mass of air is on the order of 0.02 per cent for the systems studied. The sample container was tapped while the powder was being added. In order to differentiate between the several volume fractions obtainable with the same powder, the following convenient expression was used

$$P_d = \frac{V_d - V_{d\ min}}{V_{d\ max} - V_{d\ min}}, \tag{32}$$

where P_d is defined as degree of packing,

V_d = observed volume fraction solid,

$V_{d\ min}$ = minimum stable volume fraction obtainable (as determined by procedure in Chapter IV), and

$V_{d\ max}$ = maximum volume fraction obtainable (as determined by procedure in Chapter IV).

In systems with low degrees of packing—about 0.2, tapping the container with the side of the fist was sufficient to put all the powder into the sample container. In systems with an intermediate degree of packing—about 0.5, tapping with a rubber mallet was sufficient to put the powder into the sample container. In systems with a high degree of packing—approaching unity, tapping with a hard plastic or steel hammer was required to put the powder into the sample container. After filling the container, the end flange was fastened to the sample container which was slowly rotated end-over-end in a specially designed tumbling assembly (Figure 18) at about 10 rpm. Powders at low degrees of packing settled under their weight during rotation so that the container was not completely filled. ZrO_2 (H3OF) at $V_d = 0.58$ is the only powder used in this study with such a low degree of packing; it was not rotated. Powders at intermediate degrees of packing were rotated from 6 to 8 hours. Powders at high degrees of packing were rotated for about 24 hours. The longer rotating times were necessary to eliminate density variations in the system. A measure of whether or not density variations existed in a system was the closeness of readings of thermocouples at the same radial distance from the heater but at different axial positions.

Steady-State Measurements

The filled container, after rotation, was placed in the furnace. The platinum-wound heater was inserted down the inner tube, and power supply leads were attached to it. The various heater voltage taps and thermocouple lead wires were attached. The dry air supply line was
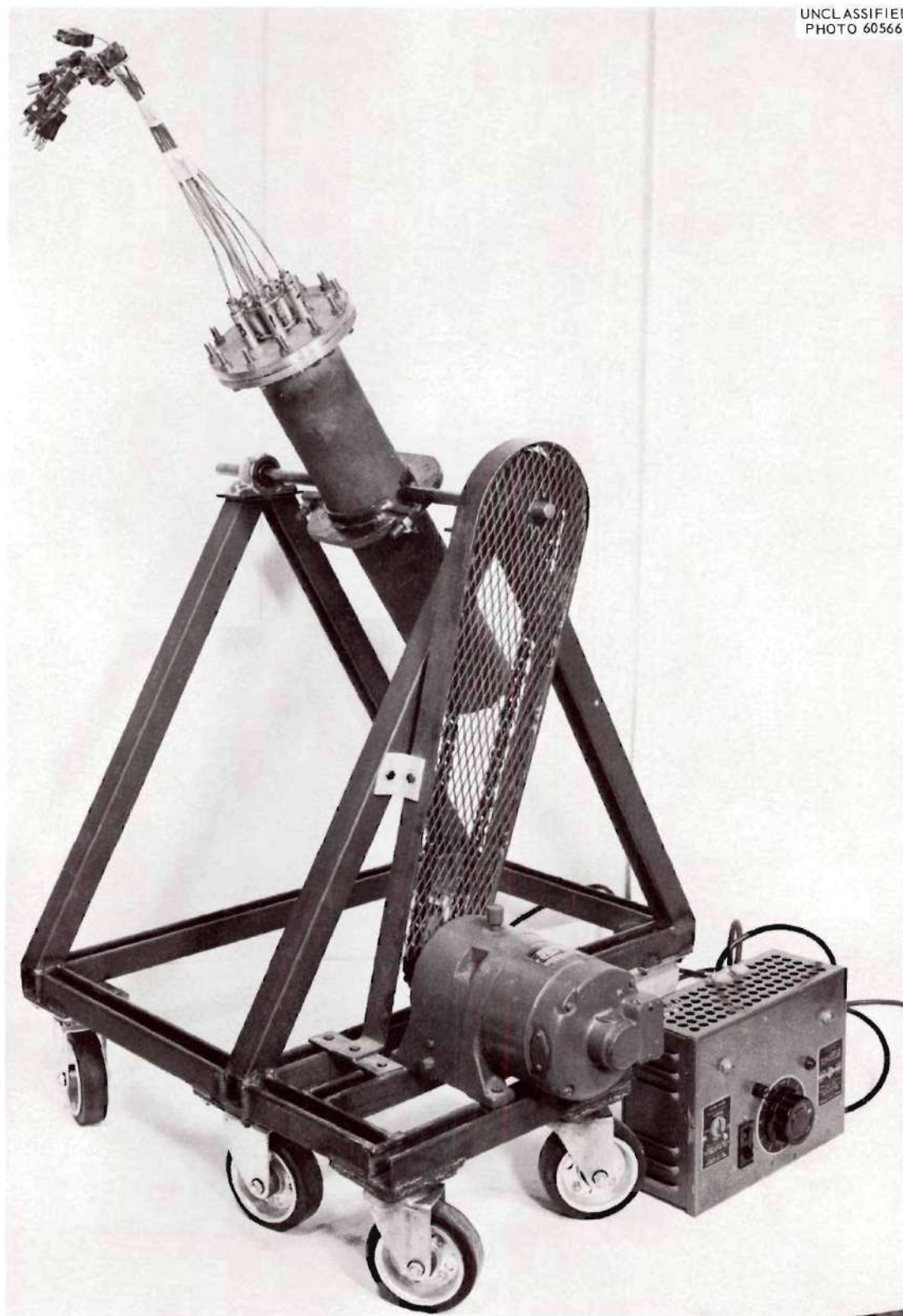
Fig. 18. Sample Container Tumbling Assembly.

connected to the bottom of the sample container and air forced through the can at 30-40 milliliters per minute. The temperature of the system was raised to about $850^{\circ}F$ for magnesia and alumina and to about $1050^{\circ}F$ for zirconia. The system was held at the appropriate temperature, with air flowing through the powder, for about 24 hours to insure complete removal of sorbed water. With typical power inputs to the furnace and heater, the system reached essentially a steady-state Δt between thermocouples in about 45 to 60 minutes. The steady-state temperature was essentially reached in 4 to 6 hours. However, at least 24 hours were allowed to elapse between any two successive sets of readings. Sets of measurements or readings were made at approximately each $200^{\circ}F$ interval. After reaching steady-state, the air supply was continued until about 30 minutes before taking readings. The following measurements were made:

(1) The voltage drop across that section of the platinum heater located in the test zone.

(2) The voltage drop across the standard shunt used to determine the current in the platinum-wound heater.

(3) The voltages of the thermocouples in the test zone.

Unsteady-State Measurements

The filled containers were rotated and placed in the furnace. The power leads to the stainless steel heater and the thermocouple lead wires were attached. As with the steady-state sample containers, the air supply line was attached and air admitted to the can at 30-40 milliliters per minute. The system was heated to about $850^{\circ}F$ or $1050^{\circ}F$ and held for about 24 hours at this temperature. At steady-state temperature, the air flow was stopped and power was supplied to the heater.

The millivolt reading of the thermocouple welded to the heater at the center of the test section was recorded on the self-balancing potenti- ometer. The voltage drop across the portion of the heater in the test section and the current through the heater were measured at about 30 second intervals. The power to the heater was usually supplied for about five minutes.

CHAPTER VI

CALCULATION OF THERMAL CONDUCTIVITY FROM EXPERIMENTAL DATA

Steady-State

For steady-state radial heat flow in a hollow cylinder Fourier's
equation for heat flow gives

$$Q = -k \ (2\pi RL) \ \frac{dt}{dR} \ . \tag{33}$$

Integrating for a cylinder of length L between the limits of radius R_1
at temperature t_1 and radius R_2 at temperature t_2 gives

$$k_m = \frac{Q}{2\pi L \ (t_1 - t_2)} \ \ln \frac{R_2}{R_1} \tag{34}$$

where k_m is the mean value of k over the temperature range t_1 to t_2.
The value of k_m is defined by

$$k_m = \frac{\int_{t_1}^{t_2} k \ dt}{t_2 - t_1} \ . \tag{35}$$

The true conductivity cannot be evaluated without knowledge of the
relation between k and t. If k varies linearly with temperature, the
mean conductivity is also the true conductivity at the mean temperature.
For materials whose temperature-conductivity curve has small curvature
the mean conductivity calculated assuming linear variation of k with t
will closely approximate the true conductivity if the temperature interval
is small. All the k's reported in this study are averaged k_m's and will
be designated by k_e. The value of k_m calculated assuming linear variation

of k over the temperature increment between thermocouples—about 20 to 40°F—are arithmetically averaged at each temperature level to give k_e. A sample calculation to illustrate how steady-state data are used in the evaluation of k_e's is presented in Appendix IV.

Unsteady-State

For a solid of infinite extent, initially at zero temperature, with a constant heat flux through any internally contained cylindrical surface, the temperature rise of the surface for large values of $\tau\theta/R^2$ is given by Carslaw and Jaeger (72) as

$$t = \frac{Q}{4\pi Lk} \ln \left| \frac{4\tau\theta}{\zeta R^2} \right| + \xi \left| \frac{R^2}{\tau\theta} \right| , \tag{36}$$

where ζ = constant = 1.7811 ...,

and the ξ term indicates a temperature whose order of magnitude is $R^2/\tau\theta$. A sample calculation to illustrate the magnitude of the ξ term is presented in Appendix IV. In the range of times where Equation 36 applies, a plot of $\ln\theta$ versus Δt should yield a straight line according to the equation:

$$\Delta t = \frac{Q}{4\pi Lk} \ln \frac{\theta_2}{\theta_1} . \tag{37}$$

If Q and L are known, the thermal conductivity may be obtained from the slope (linear asymptote) of the plot of $\ln\theta$ versus Δt using the expression

$$k_e = \frac{Q}{4\pi L (t_2 - t_1)} \ln \frac{\theta_2}{\theta_1} . \tag{38}$$

If a thermal resistance exists between the heated tube and the solid media, Equation 36 is modified to the following equation (61):

$$t = \frac{Q}{4\pi Lk} \left[\left(\frac{2}{R} \frac{k}{h} \right) + \ln \left(\frac{4\tau\theta}{\zeta R^2} \right) \right] + \xi \left(\frac{R^2}{\tau\theta} \right) \tag{39}$$

where h is a heat transfer coefficient and Equation 37 may be obtained from Equation 39 as well as from Equation 36. A sample calculation to illustrate how unsteady-state data are used in the evaluation of k_e's is presented in Appendix IV.

Fitting of Data

The values of k_m calculated using Equation 34 for each pair of thermocouples were arithmetically averaged at each temperature level to give k_e. These k_e's and temperatures (Appendix IV, Table 11) were fitted by least squares to polynomials of degree one through four. Examination of the results so obtained lead to the conclusion that there was little to be gained by going to a polynominal of higher than second degree; and in fact that higher degree fits followed the data points more scrupulously than experimental scatter and the inherent rates of changes of such systems warranted.

Accuracy and Precision

Accuracy is taken to be the square root of the sum of the squares of the uncertainties in observed quantities. The sign of the uncertainty is assumed just as likely to be positive as negative. Precision is taken to be the reproducibility of a given result when performed repeatedly in the same manner in the same equipment, or in similar equipment.

Steady-State Measurements

Thermal conductivity was calculated from measured or observed quantities using Equation 34. If R_2, R_1, and L are dimensions measured at room temperature, or any convenient temperature t, then Equation 34 can be expressed as follows to account for linear expansion of the components

$$k_e = \frac{Q \, \ln \dfrac{R_2 \, (1 + E_2 t_2)}{R_1 \, (1 + E_1 t_1)}}{2\pi L \, (1 + E_3 t_3) \, \Delta t} \tag{40}$$

where E_1 = coefficient of linear expansion (length/unit length·degree of temperature) between t and t_1.

Q is calculated from measured current and voltage of the resistance heater. The error in measurement of current is estimated at ±0.25 per cent. The error in measurement of voltage is estimated at ±0.15 per cent. These errors arise from degree of regulation (±0.1%) and ripple (±0.005%) in the power supply plus the inherent accuracy limits of the standard shunt (±0.1%), the volt box (±0.04%), and the potentiometer (±0.01%). This leads to an overall error in Q of ±0.4 per cent.

The maximum uncertainty in the location of a thermocouple junction is one sheathing diameter (1/16 inch), so that the total uncertainty in $(R_2 - R_1)$ is about one-eighth inch; therefore, the error in $\ln(R_2/R_1)$ is about 9 per cent. If t_1 and t_2 are not far apart, then $\ln(R_2/R_1)$ is essentially equal $\ln \left[R_2 \, (1 + E_2 t_2)/R_1 \, (1 + E_1 t_1) \right]$.

Estimating the point of electrical contact between two wires which are welded together in order to set an error limit on L is difficult. However, 2 per cent is probably a reasonable estimate for the heaters

used in this study. The magnitude of this uncertainty overshadows the error introduced by neglecting the $(1 + E_3 t_3)$ correction of L. At the highest temperature (1500°F) this correction would be about 0.3 per cent for the ceramic heater.

The thermocouple emf readings were checked against each other at room temperature, the steam point, and the aluminum freezing point. The variation of any thermocouple from the average of all the emfs at the highest temperature was equivalent to a temperature variation on the order of 0.5°F. From a consideration of this variation, it is concluded that the Δt's are accurate to about 3 per cent at the lowest Δt and highest temperature. The square root of the sum of the squares of the above error estimates is approximately ± 10 per cent. Typical variations in k_m calculated from different thermocouple pairs are exemplified by a specific example in Appendix IV (Table 12). Values of k_e plotted in the figures in Chapter VII were obtained by averaging the individual k_m's from the six pairs of thermocouples arranged as shown in Figure 4.

Unsteady-State Measurements

Thermal conductivity was calculated from measured or observed quantities using Equation 38. If L is the distance between voltage taps at some temperature t then Equation 38 may be expressed as follows to account for linear expansion

$$k_e = \frac{Q}{4\pi L \ (1 + E_3 t_3) \ \Delta t} \ln \frac{\theta_2}{\theta_1} . \tag{41}$$

The error in measurement of Q, L, and Δt is estimated to be approximately the same as those for steady-state measurements. The errors

in time measurement were undoubtedly negligible. However, the power
supplies used in this study were constant voltage instruments and not
constant-power instruments, as is required in the solution leading to
Equation 38. This introduces an additional uncertainty of perhaps
$\pm$10 per cent into Q, since an average power was used over the interval
during which $\ln\theta$ versus Δt was approximately linear. Again, the
magnitude of this uncertainty more than overshadows the correction for
linear expansion which for the steel heater amounts to about 0.5 per
cent at 1500°F. The square root of the sum of the squares of the above
error estimates is approximately $\pm$11 per cent.

Experimental Determination of Reproducibility of Measurements

To check the reproducibility of observations, MgO (E-98) at
$V_d = 0.58$ was studied using the steady-state measurement method in dif-
ferent containers, in different furnaces, and with different sets of
thermocouples. The experimental results from the two experiments are
compared in Figure 19. Agreement between the two sets of data is within
about $\pm$3 per cent.
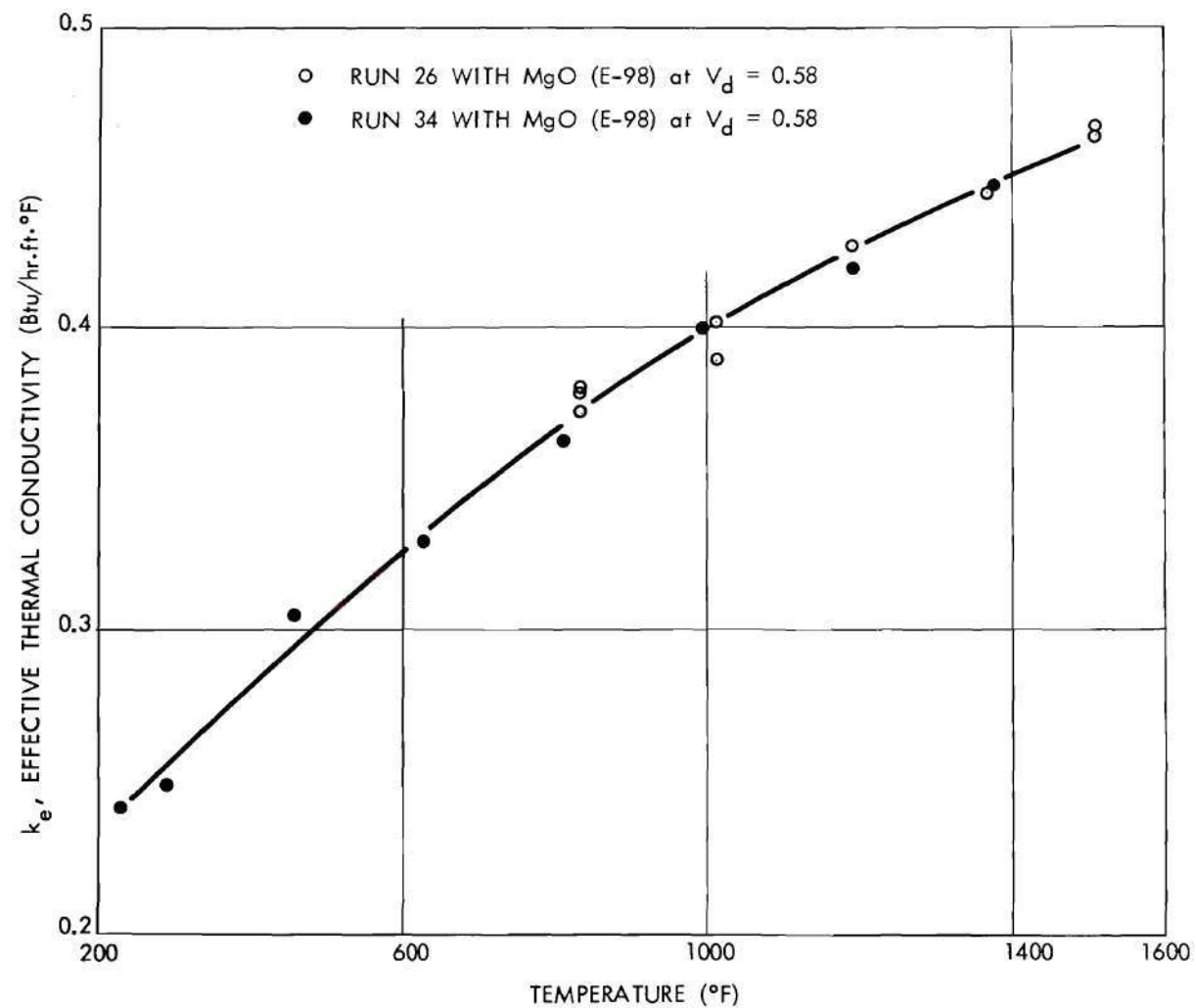
Fig. 19. Experimental Thermal Conductivities of Magnesia Powder Showing Experimental Reproducibility.

CHAPTER VII

RESULTS AND DISCUSSION OF RESULTS

A total of ten individual loadings of magnesia, two of alumina, and four of zirconia were studied. Each loading was studied at about nine temperatures although considerable variation existed among loadings. Of these sixteen loadings only four were studied using the unsteady-state method.

The experimental thermal conductivities of magnesia, alumina, and zirconia powders in dry air at atmospheric pressure between approximately $200^{\circ}F$ and $1500^{\circ}F$ as determined by the steady-state method are plotted in Figures 20, 21, and 22, respectively. The equation for effective thermal conductivity as a function of temperature for each material as determined from steady-state data is presented in Table 3. The method of curve fitting is discussed in Chapter VI. The effective thermal conductivities determined by the unsteady-state method are presented in Table 4. These data are the basis for the following discussion and analysis.

Effect of Temperature

The conductivity of the powder increases with temperature for each material. Since the thermal conductivity of both theoretically dense zirconia and of air increase with temperature, the effective thermal conductivity of a zirconia powder would be expected to increase with increasing temperature. However, the thermal conductivities of
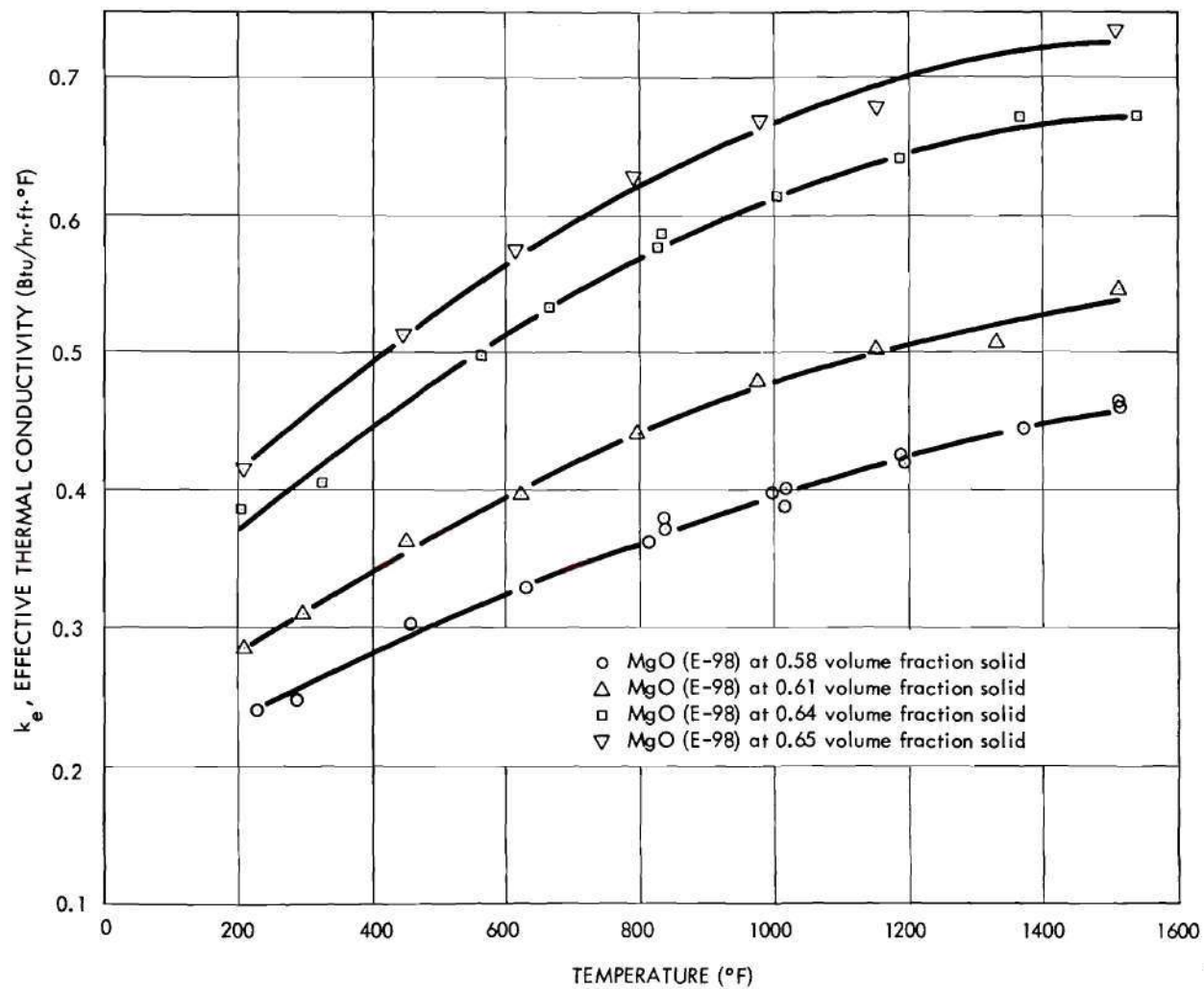
Fig. 20. Effective Thermal Conductivity of MgO (E-98) Powder in Dry Air.
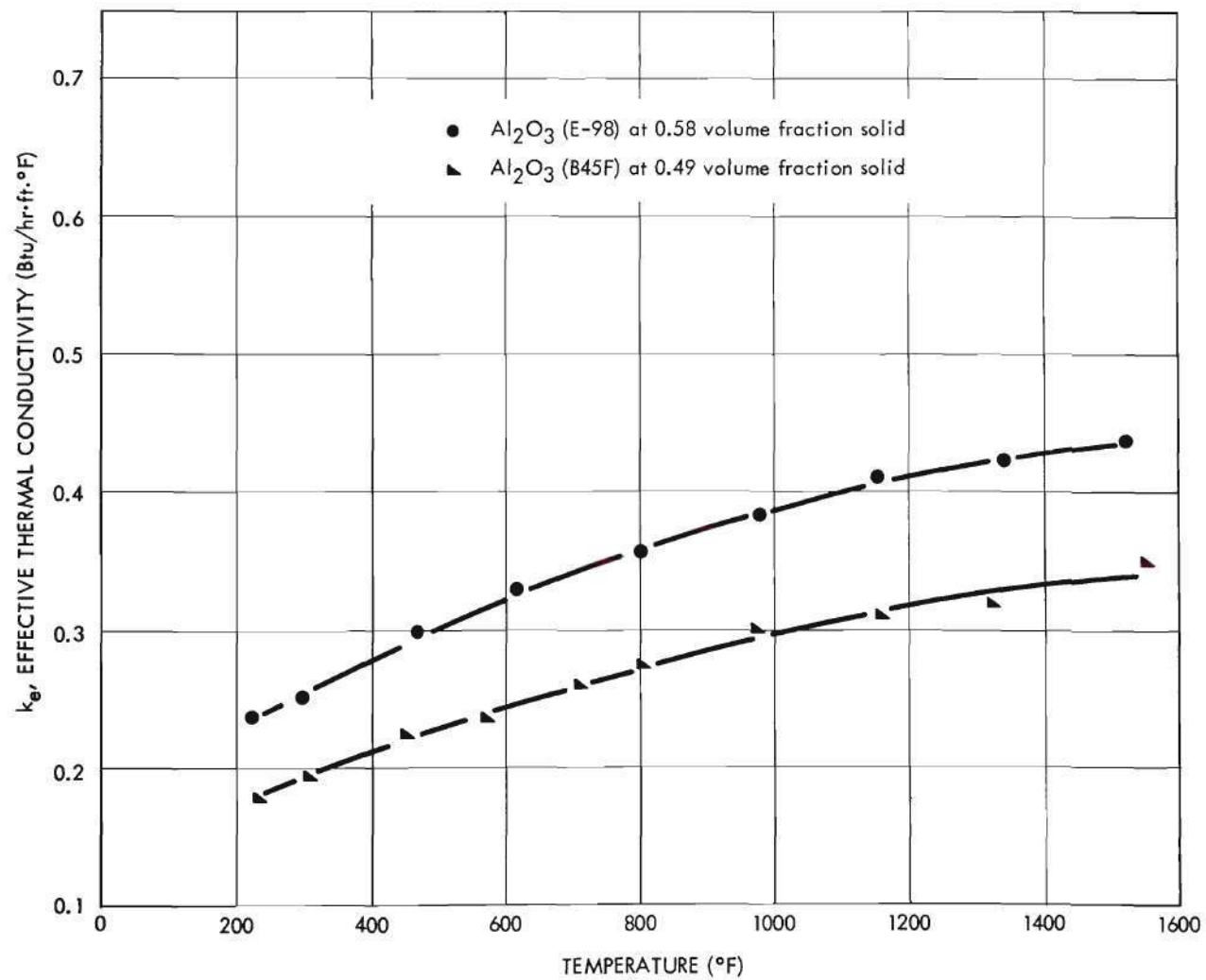
Fig. 21. Effective Thermal Conductivities of Alumina Powders in Dry Air.
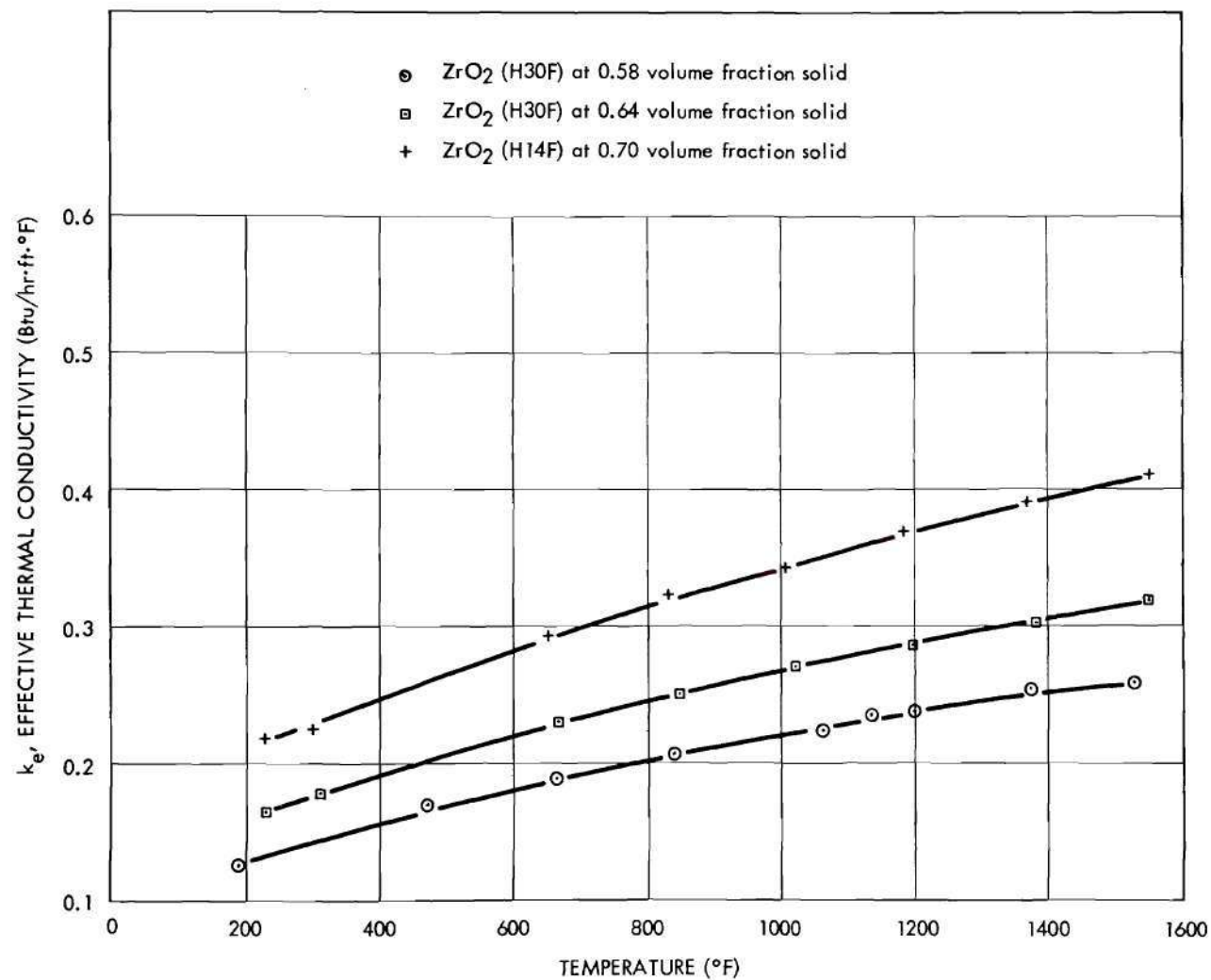
Fig. 22. Effective Thermal Conductivities of Zirconia Powders in Dry Air.

Table 3. Equations for k_e Resulting from Least-Squares Fitting of Steady-State Data[a]

MgO (E-98)

$V_d = 0.58$ $k_e = 0.1788 + 0.2844 \times 10^{-3} \, t - 0.6444 \times 10^{-7} \, t^2$.

$V_d = 0.61$ $k_e = 0.2139 + 0.3634 \times 10^{-3} \, t - 0.9763 \times 10^{-7} \, t^2$.

$V_d = 0.64$ $k_e = 0.2840 + 0.4709 \times 10^{-3} \, t - 1.396 \times 10^{-7} \, t^2$.

$V_d = 0.65$ $k_e = 0.3205 + 0.5032 \times 10^{-3} \, t - 1.534 \times 10^{-7} \, t^2$.

MgO (E-227)

$V_d = 0.61$ $k_e = 0.2089 + 0.3507 \times 10^{-3} \, t - 0.9097 \times 10^{-7} \, t^2$.

Al_2O_3 (E-98)

$V_d = 0.58$ $k_e = 0.1740 + 0.2942 \times 10^{-3} \, t - 0.8070 \times 10^{-7} \, t^2$.

Al_2O_3 (B45F)

$V_d = 0.49$ $k_e = 0.1355 + 0.2129 \times 10^{-3} \, t - 0.5083 \times 10^{-7} \, t^2$.

ZrO_2 (H30F)

$V_d = 0.58$ $k_e = 0.0960 + 0.1622 \times 10^{-3} \, t - 0.3630 \times 10^{-7} \, t^2$.

$V_d = 0.64$ $k_e = 0.1283 + 0.1728 \times 10^{-3} \, t - 0.3274 \times 10^{-7} \, t^2$.

ZrO_2 (H14F)

$V_d = 0.70$ $k_e = 0.1692 + 0.2102 \times 10^{-3} \, t - 0.3530 \times 10^{-7} \, t^2$.

---

[a] All powders in dry air, k_e in Btu/hr·ft·°F, and t in degrees Fahrenheit.

Table 4. Values of k_e Obtained by Unsteady-State Method

Powder	V_d	t (°F)	k_e (Btu/hr.ft.°F)
MgO (E-98)	0.58	215.5	0.250
		445.0	0.290
		570.5	0.319
		698.7	0.349
		843.5	0.382
		983.3	0.398
		997.3	0.385
MgO (E-98)	0.64	212.0	0.367
		339.0	0.414
		446.0	0.454
		767.5	0.567
		901.0	0.581
		1056.7	0.588
ZrO_2 (H30F)	0.64	158.0	0.168
		315.0	0.196
		1045.0	0.285
		1130.5	0.302

theoretically dense magnesia and alumina both decrease with increasing temperature (over the range of temperatures studied); a priori argument would not necessarily predict that the effective conductivity of these powders would increase with increasing temperature. The fact that their conductivities do increase with increasing temperature means that the gas conductivity has more influence on the conductivity of the composite body than does the solid conductivity. This is an important qualitative observation, and has been recognized by such investigators as Smoluchowski (73), Aberdeen and Laby (74), as well as others.

Effect of Volume Fraction Solid, V_d

The data for magnesia (Figure 20) are replotted in Figure 23 as volume fraction solid versus effective thermal conductivity. It should be noted that this powder has a $V_{d\ min}$ of about 0.49 and a $V_{d\ max}$ of about 0.65 (Table 1). Thus, extrapolation beyond these limits should not be attempted. It should also be noted that with increasing V_d the sensitivity of k_e to V_d increases until, at values near $V_{d\ max}$, k_e is critically dependent on V_d.

The thermal conductivities of powders of a given solid often are plotted versus porosity. This type of plot is useful because a range of porosities may be obtained with a given solid. However, in many instances the different porosities on a single plot were obtained using solids having different particle sizes and different particle-size distributions. Thus, the plot obtained is not truly representative of the conductivity of a specific powder at various porosities. Further, since there is a limited porosity range that is physically attainable, it is
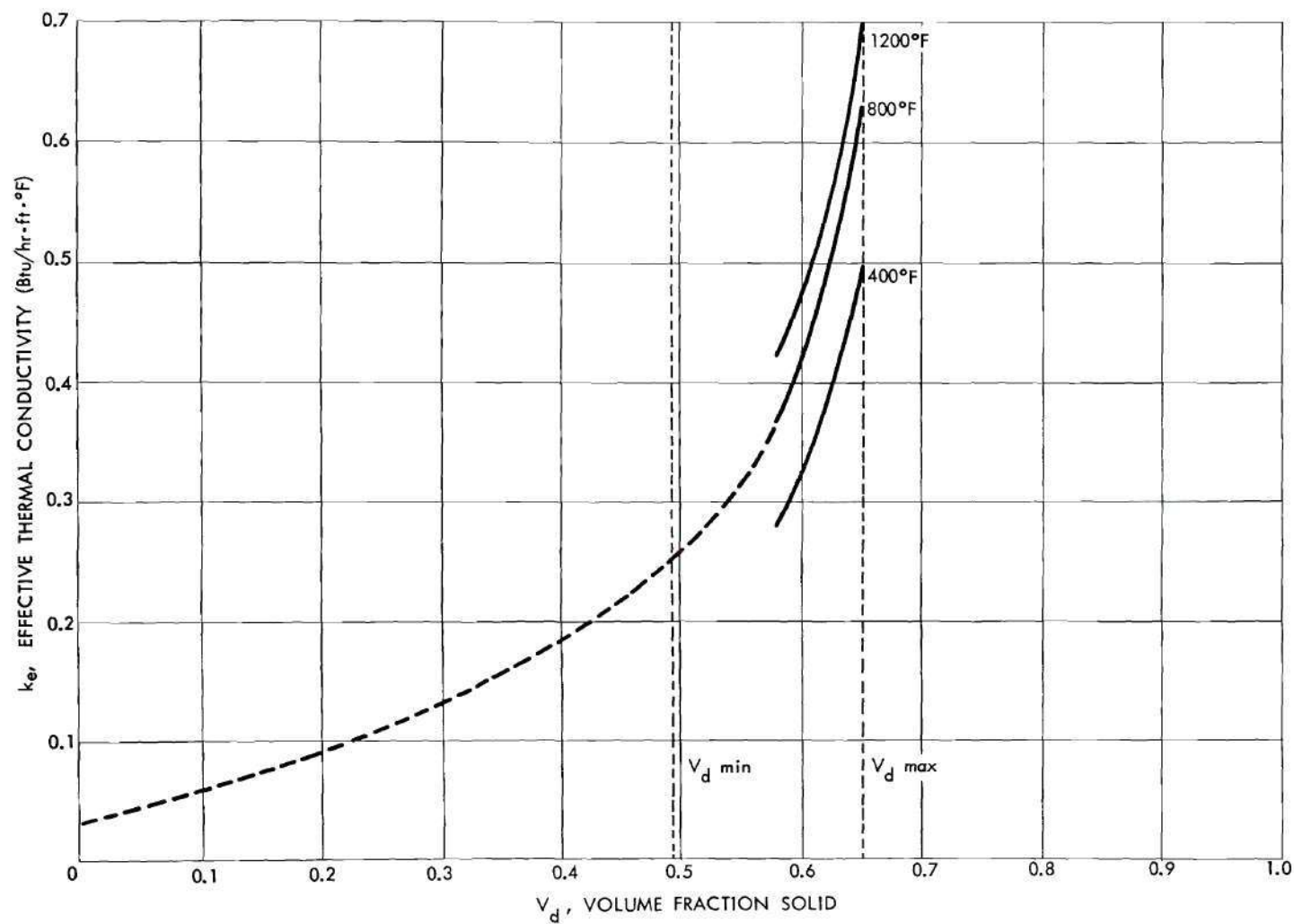
Fig. 23. Effective Thermal Conductivity of MgO (E-98) Powder as a Function of Volume Fraction Solid.

possible to extrapolate such plots into an unreal porosity region for any given powder. This point is illustrated in Figure 23 for a magnesia powder at 800°F and atmospheric pressure. Extrapolation by means of a smooth line to zero per cent solid (k = k of air at 800°F) will permit estimation by interpolation of the conductivity of this magnesia powder at, say 0.40 volume fraction solid. The error in this extrapolation is the failure to take into account that the minimum volume fraction solid that this powder can have without fluidization is about 0.49. At the other extreme, the maximum volume fraction solid obtainable with this powder is about 0.65. Extrapolation to higher volume fractions goes into regions not physically realizable. Obviously, systems having higher and lower volume fractions are possible with other magnesia powders. The point is that these systems cannot be expected to have conductivities which are continuations of the solid line shown in Figure 23. Neither should the conductivity curves be expected to overlap exactly the curve in Figure 23. Each powder will have its own characteristic particle size, particle-size distribution, and points of truncation, and will yield its own characteristic k_e versus V_d curve.

The data in Figure 23 are replotted in Figure 24 as effective thermal conductivity versus P_d. Several more points on the curve presented in Figure 24 would permit reasonably good extrapolation into regions known to exist. Since $V_{d\,min}$ and $V_{d\,max}$ are not exact properties, but depend on the mode of determination, they may be somewhat poorly defined; however, they are fairly reproducible, and they do present the data in a form convenient for extrapolation for comparison with other
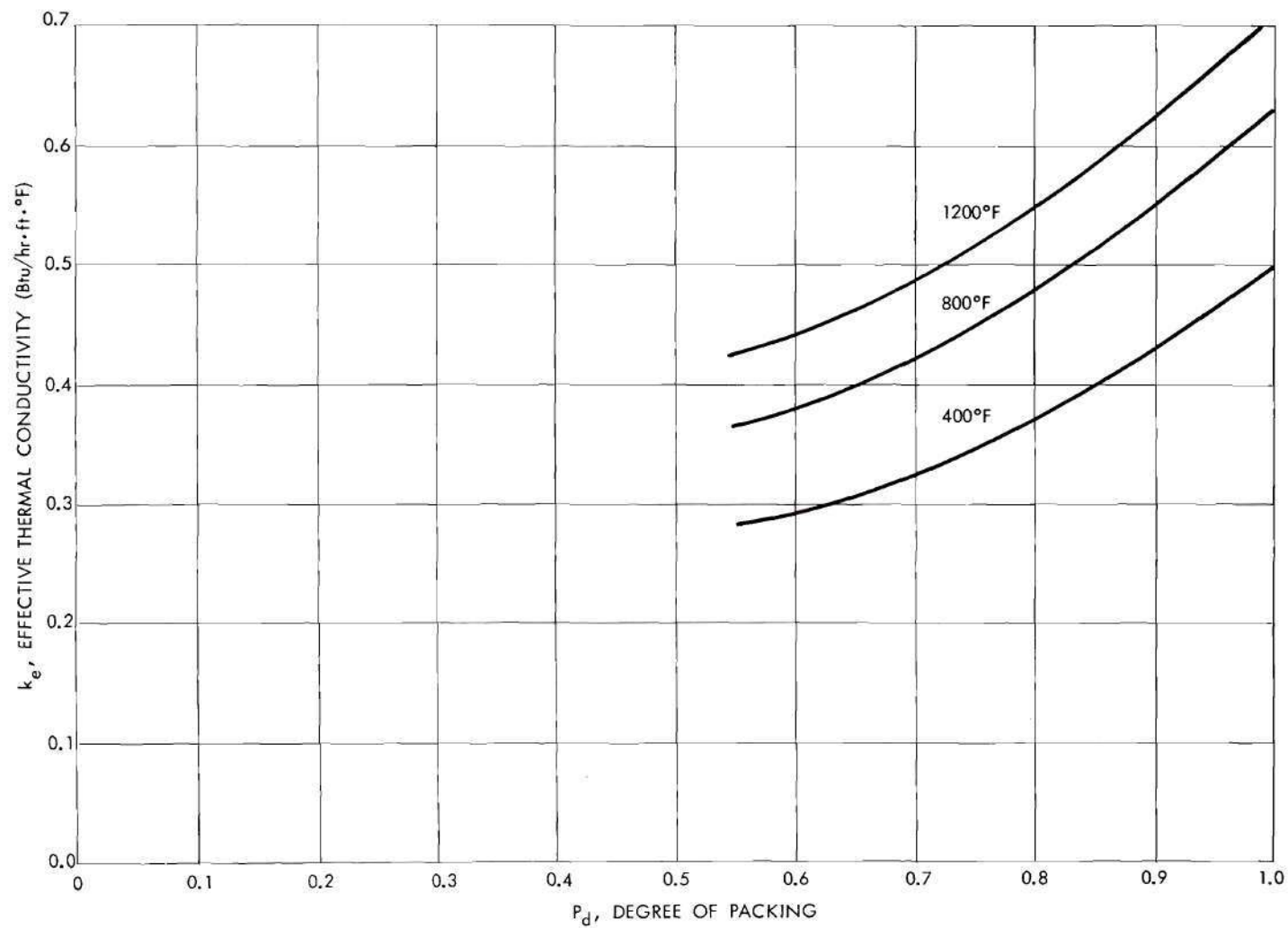
Fig. 24. Effective Thermal Conductivity of MgO (E-98) Powder as a Function of Degree of Packing.

powders. Such comparisons are more meaningful than those obtained from the extrapolation of customary plots, since these partially compensate for the variability in conductivity brought about by powder characteristics. If $V_{d\ min}$ and $V_{d\ max}$, no matter how determined, are known, the apparent density of the system may be back-calculated from P_d.

Any significant change in $V_{d\ min}$ and $V_{d\ max}$ for a powder indicates that the powder has changed characteristics. Thus they serve as quick, rough checks on variation in the particle size and particle-size distribution of a powder.

Effect of Dry Air Purge

Initial experiments with magnesia and zirconia were conducted without a purge of air that had been dried by passage through a $CaSO_4$ tower. The differences between the purged and the unpurged powders is shown in Figure 25 for two different packings of magnesia. It is clear that careful work, especially at the lower temperatures, requires inclusion of a gas clean-up procedure, and exclusion of untreated gas in subsequent handling. From the thermograms of the powders and the assumption that water is the principal sorbed species it may be calculated that in every case there is more than enough sorbed water to result in monolayer coverage. The assumption of water as the principal sorbed species is supported by the fact that rapid weight losses on heating occur at about the temperatures for $Mg(OH)_2$ decomposition to MgO plus H_2O, $Al(OH)_3$ decomposition to Al_2O_3 plus H_2O, and $Zr(OH)_4$ decomposition to ZrO_2 plus H_2O. It should be noted that once the powders had been purged with treated gas there was no effect of continued purging, even if allowed to continue while measurements were being made.
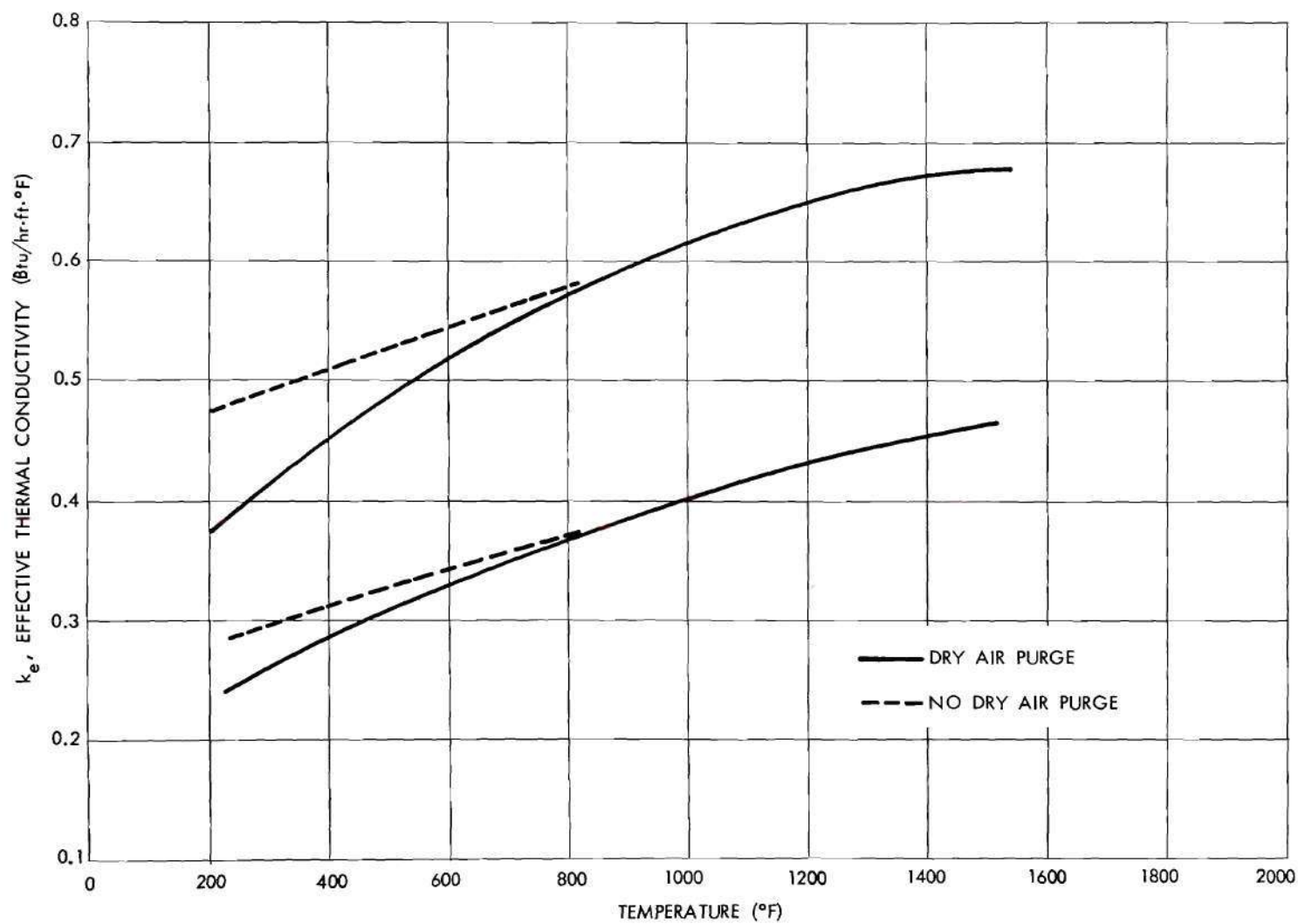
Fig. 25.   Effect of Dry Air Purge on Effective Thermal Conductivity of MgO (E-98) Powder.

Effect of Temperature "Retracing"

Initial experiments were made with increasing temperature to about 1500°F and indicated an increase in conductivity with increasing temperature as expected (Figure 26, Curve A). From 1500°F the experiments were continued in order of decreasing temperature and indicated that conductivity increased with decreasing temperature (Figure 26, Curve B). Although the example in Figure 26 is from results on a sample which had not been air-dried, the same behavior was observed on dried and undried samples. Since the sample container had in no way been shaken or handled, this anomalous behavior on cooling was totally unexpected. It is explicable on the basis of a change in packing of the powder, as is apparent from Figure 20. However, inspection of the powder through the top hole used for container volume calibration showed no perceptible settling of the powder. Rescreening of the powder indicated no change in particle-size distribution. The powder was repacked and essentially the same results were obtained (Figure 26) in experiments made with increasing and decreasing temperature. A possible explanation of this effect is based on the difference in expansion of the solid refractories and the Inconel. At high temperature the powder may settle slightly (not visibly perceptible), and as the system cools the powder is compressed. This mechanical pressure on the particles causes a better particle-to-particle contact so that the effective conductivity of the powder is enhanced. Since the linear expansion of Inconel is greater than that of magnesia, alumina, or zirconia, such a compression of the powder is possible. Also, sintering as an explanation of the effect does not seem reasonable by virtue of the low temperature, and of the fact that the
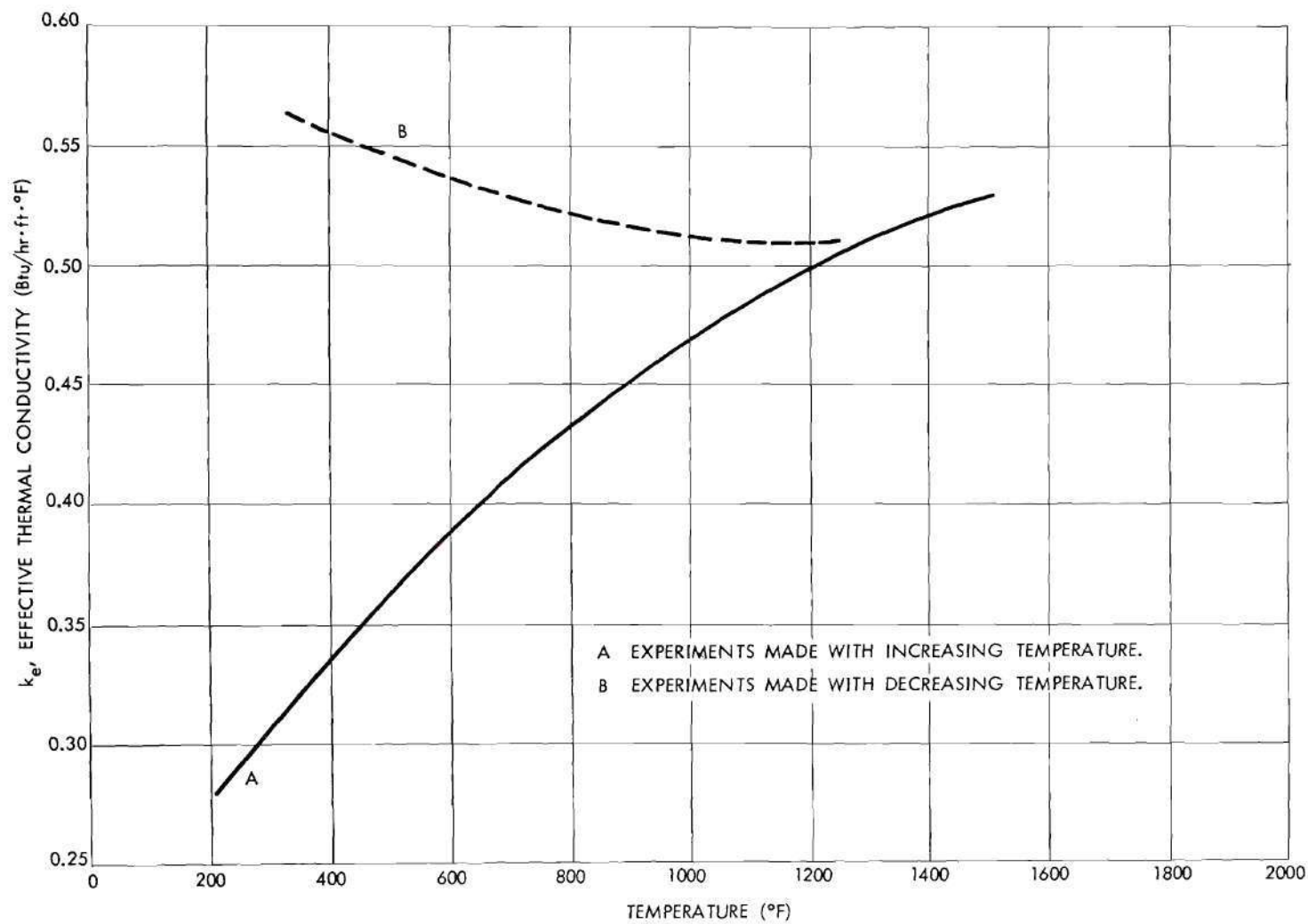
Fig. 26. Effect of Temperature "Retracing" on Effective Thermal Conductivity of MgO (E-227) Powder.

particle-size distribution of the powder did not change. The effect was observed in every case in which the experiments were performed with decreasing temperature after reaching the highest temperature. The effect was more pronounced the higher the degree of packing of the powder.

Comparison of MgO (E-98) and MgO (E-227)

Two magnesia powders with the particle-size distributions shown in Figures 8 and 9 were packed to 0.61 volume fraction solid. The experimental thermal conductivities of the powders as a function of temperature are shown in Figure 27. Within the limits of reproducibility, the two powders have the same thermal conductivity. It is interesting to note that although these powders have different $V_{d\ min}$'s and $V_{d\ max}$'s, they have the same $V_{d\ max}-V_{d\ min}$ range (Table 1). In addition, although they have different particle-size distributions, they have essentially the same value (Table 2) for the quantity

$$\int_{D_a}^{D_b} \frac{e^{-u^2/2}}{\sqrt{2\pi}}\ du\ .$$

Comparison of MgO (E-98) and Al_2O_3 (E-98)

A magnesia powder and an alumina powder with the particle-size distributions shown in Figures 8 and 10 were packed to 0.58 volume fraction solid. The experimental thermal conductivities of the powders as a function of temperature are shown in Figure 28. The fact that the alumina powder has a slightly lower conductivity than the magnesia powder (Figure 28) can be explained by the slightly lower conductivity
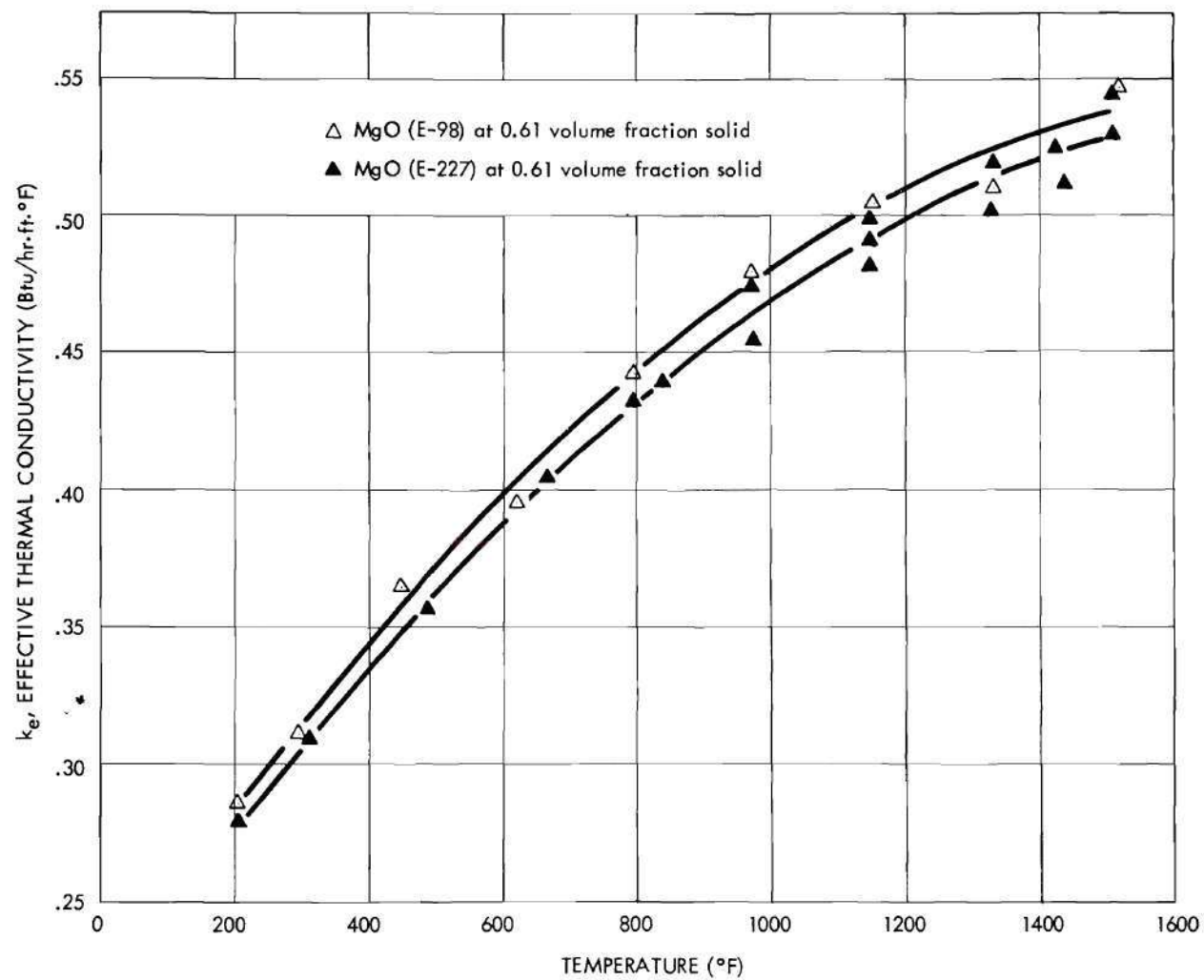
Fig. 27. Comparison of Effective Thermal Conductivities of Similar Magnesia Powders.
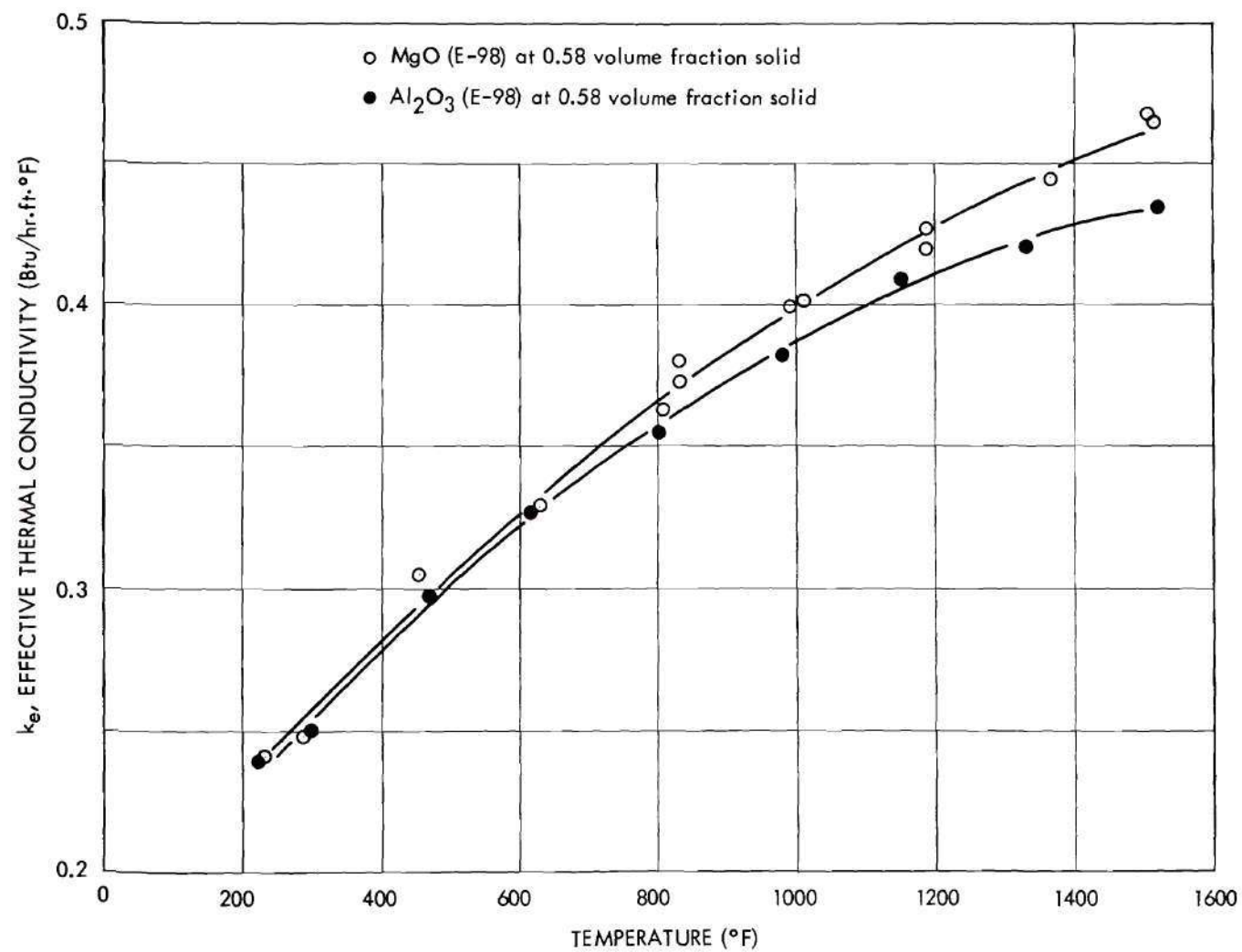
Fig. 28. Comparison of Effective Thermal Conductivities of Magnesia and Alumina Powders.

of the dense, polycrystalline alumina. The conductivity at $800^{\circ}F$ of alumina is about 7 and of magnesia is about 9 Btu/hr·ft·$^{\circ}F$ (Figure 1). However, the above results are not conclusive, since the spread in data is not outside the precision of the measurements. Also, the surface properties of the two powders are not necessarily the same and this may account for the differences observed.

Comparison of Steady-State and Unsteady-State Methods

The steady-state and unsteady-state methods used to measure thermal conductivity give results which agree to within about 7 per cent (Figures 20, 21, 22, and Table 4). Contrary to the observation of most investigators (working at ambient temperatures), the unsteady-state method did not offer any time saving over the steady-state method. The time-limiting factor was the same for both methods—namely, heating of the system composed of sample, sample container, and furnace to temperature level.

CHAPTER VIII

COMPARISON WITH PREVIOUS EXPERIMENTAL RESULTS

In general, previously reported measurements have been made on powders inadequately characterized to permit a meaningful comparison with the present results. However, in the case of one specific packing and particle-size distribution of magnesia such a comparison is possible. The experimental results of the investigation with MgO (E-98) at V_d = 0.58 in air at atmospheric pressure can be compared (Figure 29) with the data of Deissler and Eian (36). Their magnesia powder had a similar particle-size distribution and was also packed to 0.58 volume fraction solid and run in air at pressures varying from about 14 psia at 200°F to about 24 psia at 800°F. The screen analyses for the two powders are given in Figure 30. They indicate that the two powders have, within the limitations of a sieving technique, the same particle-size distribution.

Over the temperature range 200°F to 800°F in which the comparison can be made, the results of the present study and those of Deissler and Eian are essentially the same. The tendency of the present data to fall below that of Deissler and Eian may be explained on the basis of pressure effects. Deissler and Eian observed that the "breakaway" pressure for their powder was about 15 psia at 340°F and increased with increasing temperature. The term breakaway pressure as used by Deissler and Eian refers to that pressure below which the thermal conductivity of a powder at a fixed temperature is reduced by reducing the gas pressure. The fact that the present data falls below their data at 400-500°F is in accord with their observed breakaway pressures.
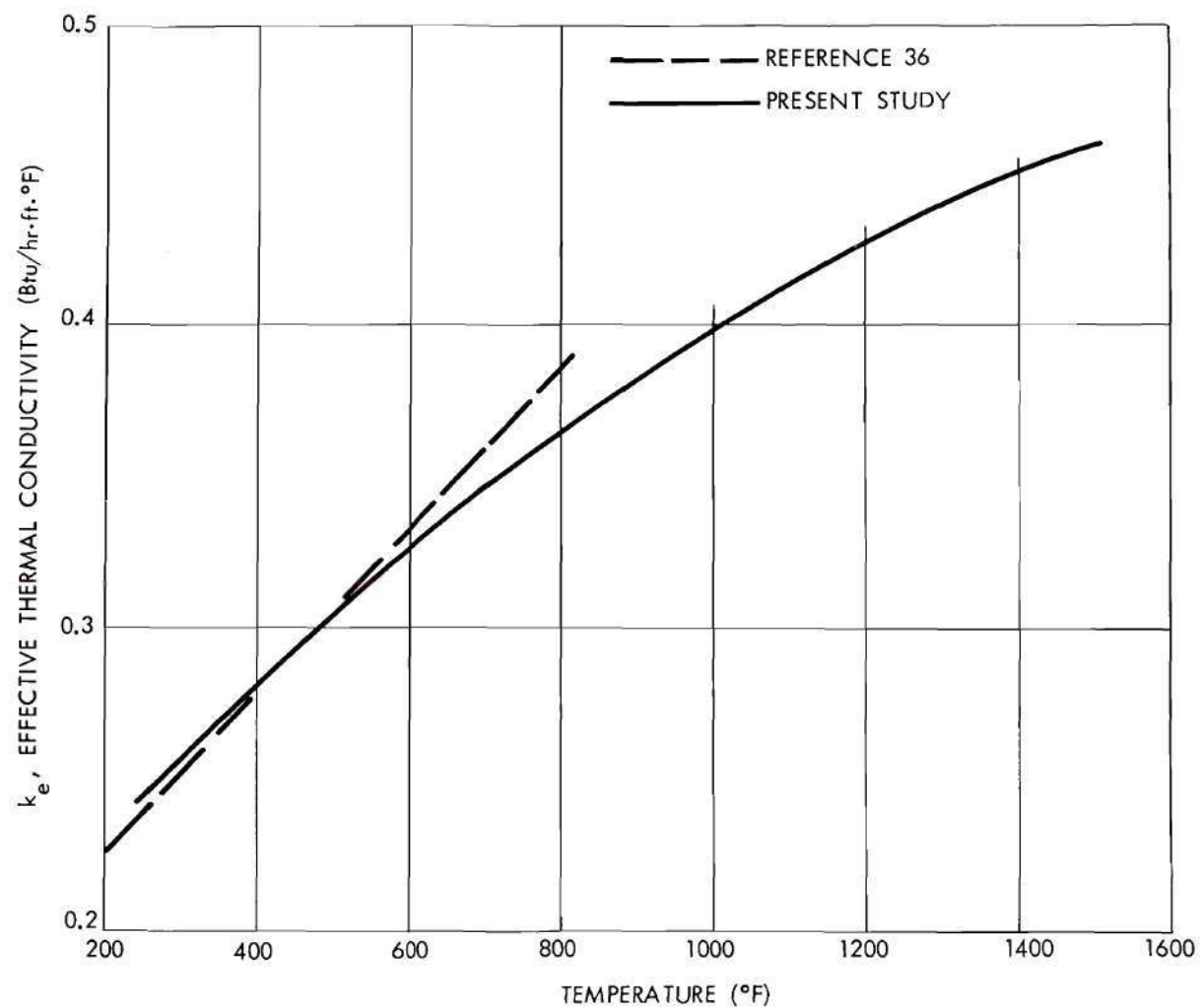
Fig. 29. Comparison of Present Results with MgO (E-98) Powder with Those of Previous Investigators.
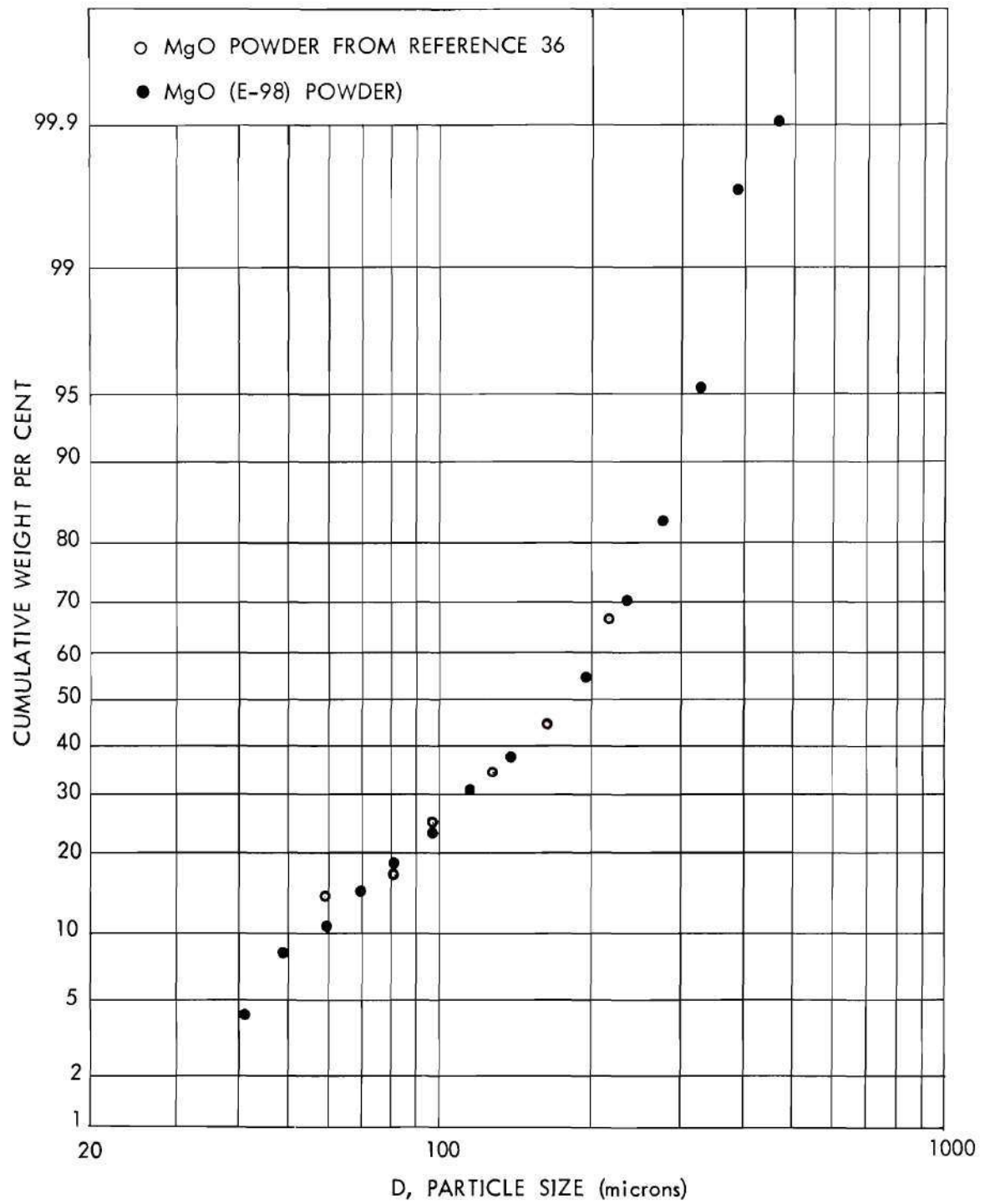
Fig. 30. Comparison of Particle-Size Distributions of Two Magnesia Powders.

CHAPTER IX

THEORETICAL DEVELOPMENT AND ILLUSTRATIVE EXAMPLE

An expression based on established theory that will not only ac-
count for measured effective conductivities but that will also predict
effective conductivity from the properties of the pure components and
the physical properties of the system is desirable in order to under-
stand heat transfer in powders.   Many correlations have been reported
in the literature to predict the effective conductivity of such systems
(see Chapter II).   As mentioned previously, most prediction methods ex-
press the thermal conductivity of a powder as a function of the thermal
conductivities of the two phases, the volume concentrations of the two
phases, and the distribution of the two phases in the system.   These
expressions are either exact mathematical solutions for an assumed
geometrical configuration or simple integrations of Fourier's equation
for an assumed configuration with an assumed heat flow or temperature
pattern.   Although the particles in a powder may be of uniform shape
and size they will not be arranged in an exact pattern.   Construction
of a model that represents reasonably well the heterogeneous material
under consideration and calculation of the effective conductivity of
this model has proved difficult.

Heat Transfer in Powders

Heat transfer is assumed to occur in a powder by the following
mechanisms:

(1) Convection by the fluid phase.

   (a) Natural.
   (b) Forced.

(2) Conduction through solid and fluid phases.

   (a) Conduction by solid only.
   (b) Conduction by solid and fluid in series and in parallel.

(3) Radiation between the solid surfaces.

Generally the contribution of each mechanism has been correlated in terms of the properties that affect it, and the effective thermal conductivity of the body is made up of the added contributions from each mechanism. Assuming that the effective thermal conductivity, k_e, of a powder is made up of additive contributions from the mechanisms outlined above

$$k_e = k_{nc} + k_{fc} + k_{sc} + k_{gsc} + k_r \tag{42}$$

where k_{nc} = conductivity by natural convection,

   k_{fc} = conductivity by forced convection,

   k_{sc} = conductivity by solid only,

   k_{gsc} = conductivity by gas and solid, and

   k_r = conductivity by radiation.

Convection

For granular materials, if the sizes of the pores are small, the contribution of natural convection to the over-all transfer of heat is probably negligibly small. Waddams (44) concluded from his experiments that natural convection is appreciable as a factor in the flow of heat through granular materials only when the average diameter of the grains is about one-fourth inch or greater. From a theoretical considera-

tion of the majority of published (from year 1933 to 1948) thermal conductivities on porous media, Wilhelm et al. (34) concluded that natural convection is negligible for particle diameters of 3 to 4 millimeters, pressures up to 10 atmospheres, and temperatures up to about $600^{\circ}F$.

Kunii and Smith (75) studied beds with fluid flow in a direction parallel and countercurrent to heat flow. The values of effective thermal conductivity increased significantly with mass velocity of the fluid. For instance, the thermal conductivity of a glass bead bed (diameter of bead about 1 millimeter) increased by a factor of about 3 when the Reynolds number increased from 0 to about 0.6. Willhite, Kunii, and Smith (37) showed from experimental data for beds of glass beads (diameter of bead about 0.9 millimeter) that for heat transfer perpendicular to the direction of fluid flow and Reynolds numbers from 0 to 6.6 there was no effect of flow on the conductivity.

Conduction

Heat transfer through the particles of a powder independent of the gas phase or so-called "straight-through" or "residual" solid conductivity has been approximated experimentally by evacuating the gas phase (16, 33, 41, 73, and 76). Masamune and Smith (45) present a semi-empirical method for predicting solid-to-solid conductivity from data on effective thermal conductivities in vacuum. These investigations indicate that the "straight-through" conductivity for an in vacuo powder is on the order of several thousandths to several hundredths of the conductivity of the solid. Moreover, in explaining observed conductivities, the success of correlations (19, 20, 33, 36, and 37) based only on point

contact would indicate that "straight-through" conductivity or k_{sc} is significant only when other modes of transfer are effectively suppressed. From their theoretical study of 53 systems with fluid phase continuous—solid phase discontinuous, Wilhelm et al.(34) concluded that heat transfer is almost purely conductive provided the particle size, gas pressure, and temperature are not too high. They also concluded that the effective conductivity of the mixture is more dependent upon the thermal conductivity of the continuous phase than upon the conductivity of the discontinuous phase. For example, Deissler and Boegli (51) point out that the effective conductivity of a magnesium oxide powder measured in helium was about five times that of the same powder in argon.

Radiation

Radiation may contribute significantly at high temperatures in coarse powders and at sufficiently high temperatures may predominate. For a bed of 3.8 millimeters diameter alumina spheres the ratio of heat transferred by radiation to that transferred by conduction was estimated by Hill and Wilhelm (77) to increase with average bed temperature from the order of 0.1 at about $200^{o}F$, to 1.2 at about $1800^{o}F$. Theoretical expressions (20, 62, 78, and 79) derived to account for radiant heat transfer usually express an effective radiant conductivity in terms of the geometry of the pore space, the emissivity of the walls of the pore, and the third power of the absolute temperature. These are reviewed and compared by Chen and Churchill (79).

Simplified Model

In order to obtain a simplified system which will permit calculation of an effective thermal conductivity by summing series and parallel

conduction through the fluid and solid phases, following Tsao's (32) lead, a homogeneously heterogeneous powder (Figure 31) in which the isotherms are planes perpendicular to the x-axis will be considered.

The heterogeneous material shown in Figure 31(a) is sliced into many thin layers which are parallel to the x-y plane. Each layer is of such thickness that it is essentially "full" of solid; i.e., there is little or no pure series fluid associated with a particle in the z-direction. In other words, the slices are as shown in Figure 31(c) and not as shown in Figure 31(b).

The particles in each such slice are moved without rotation along the x-axis until they again touch each other. Assuming heat flow perpendicular to y-z plane, based on adding resistances in series, this does not change the effective conductivity of the slice. This movement does not destroy the particle distribution in the x-direction. However, it does destroy the particle distribution in the y and z-directions. The body as modified above is sliced into many thin layers which are parallel to the y-z plane. Each layer is again of such thickness that it is essentially "full" of solid. Based on adding conductances in parallel, the particles in each slice can be pushed into a pore-free rectangle without destroying the effective thermal conductivity of the slice. After these rearrangements, the model shown in Figure 32(a) is obtained.

For the modified body shown in Figure 32(a), let

X = length of representative cell,

S = solid area perpendicular to heat flow, and

D_s = solid length parallel to heat flow.

CONTINUOUS PHASE

DISCONTINUOUS PHASE

(a)

HETEROGENEOUS BODY OF TWO PHASES

x-AXIS PERPENDICULAR
TO PAGE

SLICES IN z-DIRECTION
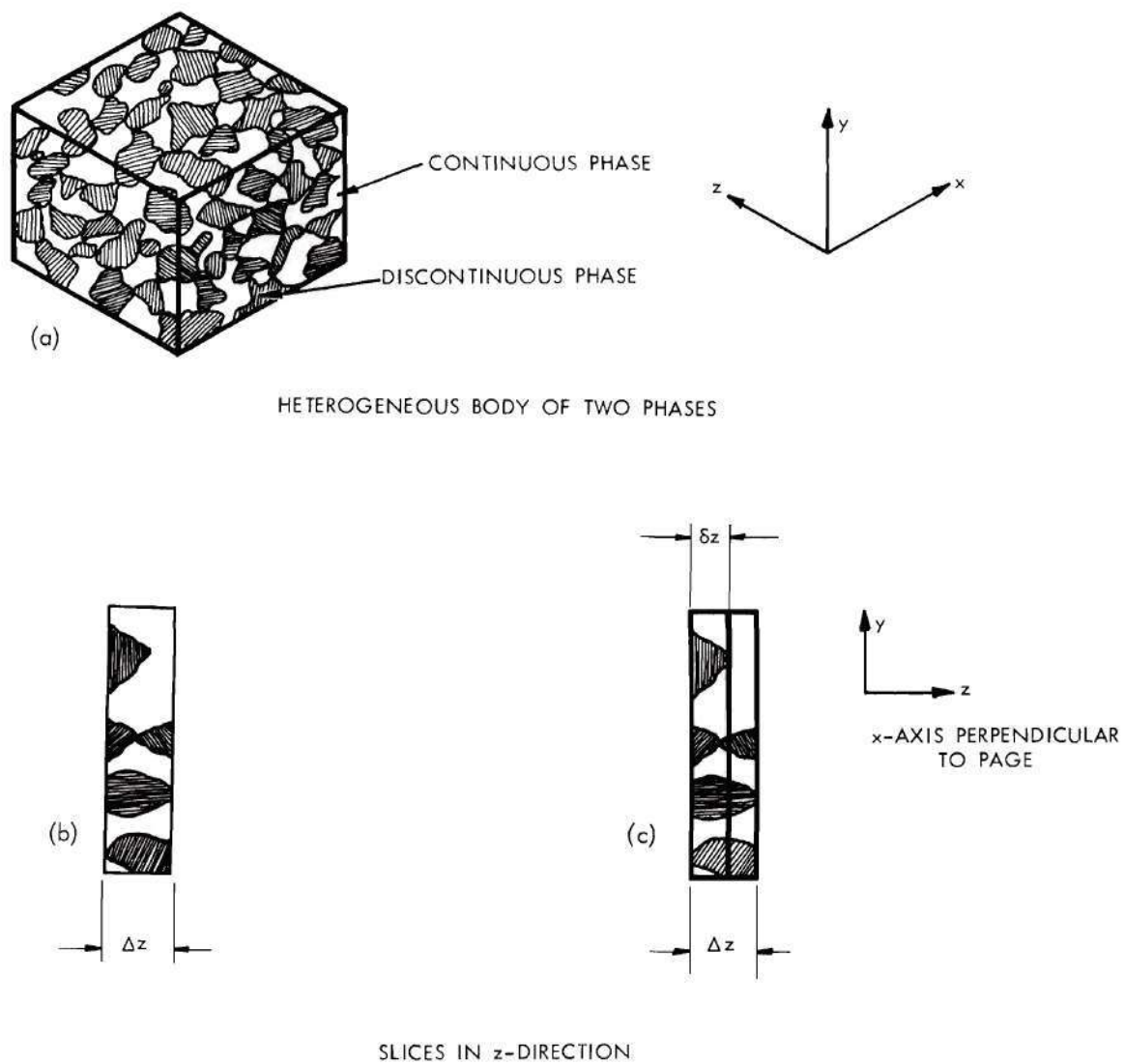
Fig. 31. Representation of the Gas-Powder System.
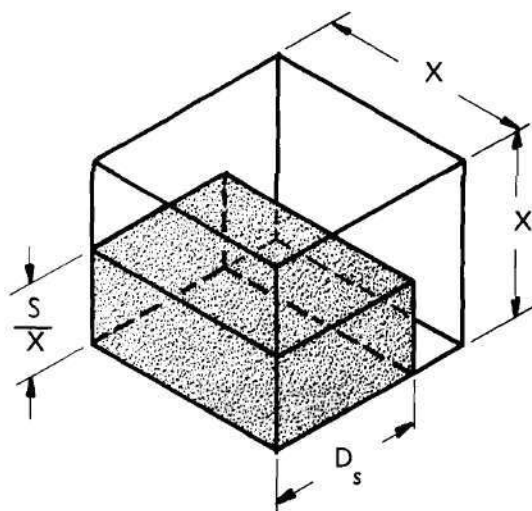
(a) SIMPLIFIED HETEROGENEOUS BODY OF TWO PHASES
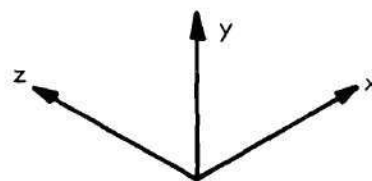
HEAT FLOW Q, PERPENDICULAR TO y-z PLANE
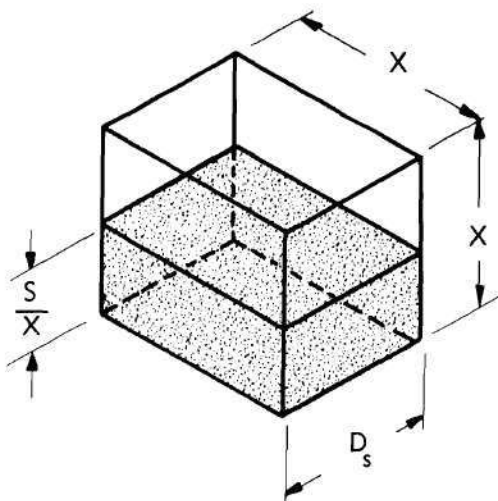
(b) PORTION OF SIMPLIFIED BODY BETWEEN $x = 0$ AND $x = D_s$
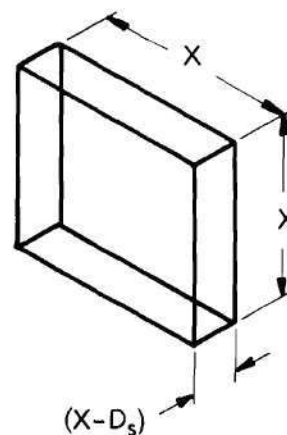
(c) PORTION OF SIMPLIFIED BODY BETWEEN $x = D_s$ AND $x = X$

Fig. 32. Representation of Simplified Gas-Powder System.

Consider that portion of the simplified body shown in Figure 32(b).

Let

$$Q_{gsc} = q_1 + q_2 \tag{43}$$

where q_1 = heat flow in fluid, and

q_2 = heat flow in solid.

If k_d = conductivity of solid particles,

k_c = conductivity of fluid in pores, and

Δt_1 = temperature drop across D_s,

then

$$q_1 = -k_c (x^2 - S) \frac{\Delta t_1}{D_s} , \tag{44}$$

and

$$q_2 = -k_d (S) \frac{\Delta t_1}{D_s} , \tag{45}$$

so

$$Q_{gsc} = -\left[k_c (x^2 - S) + k_d (S) \right] \frac{\Delta t_1}{D_s} . \tag{46}$$

Now consider that portion of the simplified body shown in Figure 32(c). For this portion of the simplified body

$$Q_{gsc} = -k_c x^2 \frac{\Delta t_2}{X - D_s} \tag{47}$$

where Δt_2 = temperature drop across $X-D_s$.

But

$$Q_{gsc} = -k_{gsc} (x^2) \frac{\Delta t_{total}}{X} \tag{48}$$

and

$$\Delta t_{total} = \Delta t_1 + \Delta t_2 .$$ (49)

Thus, combining Equations 46, 47, 48, and 49 gives

$$k_{gsc} = \frac{k_c}{\left[\dfrac{\dfrac{D_s}{X}}{\left(1 - \dfrac{S}{X^2}\right) + \dfrac{k_d}{k_c}\left(\dfrac{S}{X^2}\right)}\right] + \left(1 - \dfrac{D_s}{X}\right)} .$$ (50)

It may be shown that if $D_s = X$, then $S/X^2 = V_d$ and Equation 50 reduces to Equation 3 which is the expression for laminae parallel to the flow of heat. Also, if $D_s = V_d X$, Equation 50 reduces to Equation 4 which is the expression for laminae perpendicular to the heat flow.

If the assumption is made that $D_s = V_d^{1/3}X$ then Equation 50 reduces to Equation 22 which is Russell's equation (46). It is interesting to note that if the original powder were cubical particles in a cubic lattice so that the true relation between D_s and X is $D_s = V_d^{1/3}X$, the movement of particles used in arriving at the model given in Figure 32(a) does not destroy this relation.

In order to use Equation 50 a relation between D_s and X in the direction of heat flow is needed. To obtain such a relation define a shape factor

$$\alpha \equiv \frac{S}{D_s^2}$$ (51)

Inspection of Figure 32(a) will show that α is a shape factor which determines how much of the solid may be considered to be in parallel with the surrounding fluid and how much may be considered to be in series.

Multiplying both sides of Equation 51 by D_s gives

$$\alpha = \frac{SD_s}{D_s^3} \, .$$ (52)

But, it may be seen from Figure 32(a) that

$$SD_s = V_d X^3 \, .$$ (53)

Therefore, combining Equations 52 and 53 gives

$$\frac{D_s}{X} = \left(\frac{V_d}{\alpha}\right)^{1/3} \, .$$ (54)

Considering again a cubical array of cubes (Russell's model), one sees that α calculated from Equation 54 equals unity as it should for this array. This qualitatively explains why Russell's equation gives low results when applied to powders. In any real packing of cubes, α will be less than unity since the cubes will be twisted and turned in space. Substituting Equation 54 into Equation 50 still gives an equation with α as an unknown quantity. The quantity α is, however, a property of the particles and can be related to the heterogeneous body through a volume balance of the two phases. A variety of methods are available to obtain α. The one used in this study is presented below.

Consider particles having a particle-size distribution obtained by a technique that gives weight per cent as a function of some characteristic length. For example, with a screen analysis this is equivalent to obtaining volume per cent as a function of screen openings, if the density of the particles is known. Most crushed materials, as represented by most of the materials in this study, follow a logarithmic normal distribution (Table 2). For such materials, considering a representative unit length of solid,

$$\int_{D_a}^{D_b} \frac{e^{-u^2/2}}{\sqrt{2\pi}} \, du = \frac{\text{volume of solid}}{\text{a normalizing volume of solid}} \, . \qquad (55)$$

That is, it is the fraction of the total volume (contained between the limits $D = 0$ and $D = +\infty$) which is contained between the limits D_a and D_b; i.e., it is the volume between D_a and D_b when

$$\int_{-\infty}^{+\infty} e^{-u^2/2} \, du = \sqrt{2\pi} \, . \qquad (56)$$

Let G_s represent the number of series gas lengths associated with the representative unit length of solid.

Thus,

$$(1 + G_s)^3 = \frac{\text{volume of representative cell}}{\text{a normalizing volume of solid}} \, . \qquad (57)$$

Combining Equations 52 and 57 gives

$$\frac{\int_{D_a}^{D_b} \frac{e^{-u^2/2}}{\sqrt{2\pi}} \, du}{(1 + G_s)^3} = \frac{\text{volume of solid}}{\text{volume of representative cell}} \, . \qquad (58)$$

which is V_d.

Now, examining Figure 32(a) again, it may be seen that also

$$G_s = \frac{X - D_s}{D_s} \, . \qquad (59)$$

Cubing Equation 59 gives

$$(1 + G_s)^3 = \frac{X^3}{D_s^3} \, . \qquad (60)$$

Comparing Equations 54, 58, and 60 shows that

$$\int_{D_a}^{D_b} \frac{e^{-u^2/2}}{\sqrt{2\pi}} \, du = \alpha \tag{61}$$

for these materials. In some materials, for instance uniformly sized materials such as the Al_2O_3 (B45F) powder (Table 2) used in this study, the relation between D_s and X may be difficult to determine.

So far in the derivation of Equation 50, the conductivity of the gas in the pores has been assumed to be that of the pure bulk gas at the temperature and pressure of the system. However the work of numerous investigators (16, 33, 41, 45, 73, and 76) has shown that the thermal conductivity of a powder-gas system is decreased by decreasing pressure at a much faster rate than can be explained by the decrease in conductivity of the pure gas by reduced pressure. One theoretical approach to the problem is through the use of the temperature jump distance (80). Schotte (62) applied the relationship based on the heat transfer between close parallel plates given by Kennard (81) to relate the normal thermal conductivity of a gas to the apparent thermal conductivity. The derivation which follows is essentially the one presented by Schotte. Kennard gives the heat conducted per unit area per unit time through a gas of conductivity k_g between two parallel plates separated by a relatively small distance d, per degree difference in temperature between them, as

$$q^o = \frac{k_g}{d + j_1 + j_2} \tag{62}$$

where j_1 and j_2 are the temperature jump distances of the two surfaces. Assuming that j_1 and j_2 are equal, the apparent conductivity of the gas can be expressed as

$$k_g^o = q^o d = \frac{k_g}{1 + \frac{2j}{d}} . \qquad (63)$$

Kennard also shows that (82)

$$j = \left(\frac{2 - a}{a}\right)\left(\frac{2}{\gamma + 1}\right)\left(\frac{k_g}{\eta C_{vg}}\right)\lambda . \qquad (64)$$

where a = thermal accommodation coefficient for gas-solid surface,

γ = ratio of gas heat capacity at constant pressure to heat capacity at constant volume,

η = viscosity of gas,

C_{vg} = gas heat capacity at constant volume,

λ = mean free path for gas molecule = $\dfrac{BT}{\pi \rho^2 P \sqrt{2}}$, $\qquad (65)$

T = absolute temperature,

P = absolute pressure,

ρ = molecular diameter of gas as determined from viscosity, and

B = Boltzmann constant.

Combining Equations 63, 64, and 65

$$k_g^o = \frac{k_g}{1 + Z\left(\dfrac{2 - a}{a}\right)\left(\dfrac{\gamma}{1 + \gamma}\right)\left(\dfrac{T}{Pd\,\rho^2\,N_{Pr}}\right)} \qquad (66)$$

where $N_{Pr} = \dfrac{\eta C_{pg}}{k_g}$ = Prandtl number,

C_{pg} = gas heat capacity at constant pressure, and

Z = a constant = 5.08×10^{-24} for foot, pound, degree Rankine units.

Solution of Equation 66 requires a knowledge of the accommodation coefficient as well as the average heat transfer distance, d, between particles. Experimental values of the accommodation coefficient (83,

84, and 85) reported in the literature vary widely for any given gas depending on temperature, pressure and strongly on the condition of the surface. However, all measured values are greater than zero and less than one, so that a reasonable estimate of accommodation coefficients may be possible from a consideration of all the experimental values available. For the simplified model presented in Figure 32(a) the value of d is $X - D_s$.

If Equation 50 is modified by substituting k_g^o for k_g in the space between the solid surfaces, that is, in the volume which is $(X-D_s)$ by X by S/X of Figure 32(c), then

$$k_{gsc} = \frac{k_g^*}{\left[\frac{\frac{D_s}{X}}{\frac{k_g}{k_g^*}\left(1 - \frac{S}{X^2}\right) + \frac{k_d}{k_g^*}\left(\frac{S}{X^2}\right)} + \left(1 - \frac{D_s}{X}\right)\right]} \qquad (67)$$

where

$$k_g^* = k_g\left(1 - \frac{S}{X^2}\right) + k_g^o\left(\frac{S}{X^2}\right). \qquad (68)$$

The radiation contribution depends upon the temperature level and gradient. The net radiation heat transfer between two bodies can be expressed as

$$q_r = n_r^2 \, \sigma \, F_\epsilon F_a \, A_r \, (T_1^4 - T_2^4) \qquad (69)$$

where n_r = refractive index of media between surfaces,

σ = Stefan-Boltzmann constant,

F_ϵ = emissivity factor,

F_a = angle (or "view") factor, and

A_r = radiating surface area.

Factoring the term $(T_1^4 - T_2^4)$ to $(T_1 - T_2)(T_1 + T_2)(T_1^2 + T_2^2)$, and assuming that approximately, $(T_1 + T_2) = 2T$ and $(T_1^2 + T_2^2) = 2T^2$, gives

$$q_r = 4n_r^2 \ \sigma \ F_\epsilon F_a \ A_r \ T^3 \ \Delta T \qquad (70)$$

Assuming that a particle surface area is small compared to the "visible" surface of the enclosing particles, Equation 70 reduces to

$$q_r = 4n_r^2 \ \sigma \ \epsilon \ A_r T^3 \ \Delta T \qquad (71)$$

where ϵ = emissivity.

Defining an effective radiation thermal conductivity by analogy with Fourier's equation yields

$$q_r = -k_r A_r \frac{(-\Delta T)}{D_r} . \qquad (72)$$

Combining Equations 71 and 72 gives

$$k_r = 4n_r^2 \ \sigma \ \epsilon \ D_r T^3 \qquad (73)$$

where D_r is an effective inter-particle distance for radiation. The average radiating surface for heat flow in the x-direction is S. However, the average effective inter-particle distance in the x-direction is not expected to be $X-D_s$ because the model giving the distance $X-D_s$ does not truly represent the physical system of particles for heat transfer by radiation. It is desired to relate k_r to the average radiating surface in the x-direction in a manner more nearly representing

the original random distribution of particles. This may be accomplished by the following approach:

$$S\ D_r = (1 - V_d)\ X^3\ ,\qquad(74)$$

and

$$S\ D_s = V_d X^3\ .\qquad(53)$$

Combining Equations 74 and 53

$$D_r = (\frac{1}{V_d} - 1)\ D_s\ .\qquad(75)$$

Combining Equations 73 and 75

$$k_r = 4n_r^2\ \sigma\ \epsilon\ (\frac{1}{V_d} - 1)\ D_s\ T^3\ .\qquad(76)$$

Different techniques for measuring particle sizes can give different numbers for the same parameter. For example, the median particle size as determined by sieving, sedimentation, or microscopy is not the same (varying sometimes by factors of 2 or 3). For instance the median particle size of MgO (E-98) was 180 microns as determined by sieving and 60 as determined by microscopy. Obviously the method of obtaining particle size will influence the result from Equations 67 and 76. In contrast in the equation for k_{gsc} (Equation 50) all lengths occur as ratios. Thus, if the method used to measure the relation between X and D_s is valid, it should give essentially the same value for $\frac{D_s}{X}$ as any other method.

Since k_{nc}, k_{fc}, and k_{sc} may be assumed to be negligible for the powders in this investigation, substitution of Equations 67 and 76 into

Equation 42 gives

$$
k_e = \cfrac{k_g^{*}}{\left[\cfrac{\dfrac{D_s}{X}}{\dfrac{k_g}{k_g^{*}}\left(1-\dfrac{S}{X^2}\right)+\dfrac{k_d}{k_g^{*}}\left(\dfrac{S}{X^2}\right)}+\left(1-\dfrac{D_s}{X}\right)\right]}
$$

$$
+ 4n_r^2 \, \sigma \, \epsilon \, \left(\frac{1}{V_d}-1\right) D_s \, T^3 \ . \tag{77}
$$

This is the equation used to compare with experimental results.

Illustrative Example

As a specific example of the calculations involved in the above theory, consider a magnesia powder — MgO (E-98) — in air at atmospheric pressure and having a volume fraction solid of 0.58.

The basic equation for calculating k_e for such a system is Equation 77 above. Auxiliary equations (repeated for convenience) are

$$
\alpha = \int_{D_a}^{D_b} \frac{e^{-u^2/2}}{\sqrt{2\pi}} \, du \tag{61}
$$

which is needed to evaluate α;

$$\frac{D_s}{X} = \left(\frac{V_d}{\alpha}\right)^{1/3} \tag{54}$$

which is needed to evaluate D_s/X;

$$k_g^* = k_g \left(1 - \frac{S}{X^2}\right) + k_g^o \left(\frac{S}{X^2}\right) \tag{68}$$

which is needed to evaluate k_g^*; and

$$k_g^o = \frac{k_g}{1 + Z \left(\frac{2 - a}{a}\right) \left(\frac{\gamma}{1 + \gamma}\right) \left(\frac{T}{Pd \, \phi^2 \, N_{Pr}}\right)} \tag{66}$$

which is needed to evaluate k_g^o.

All the properties of the bulk components in Equations 66, 68, and 77 are in the literature for magnesia and air as well as for most other common solids and gases. It should be noted that the accommodation coefficient, a, is a possible exception to this statement. However, as mentioned previously, a reasonable estimate of accommodation coefficients may be possible from a consideration of experimental values which are available in the literature. Sources of values of properties used in calculation of this example are given in Chapter X.

It will be recalled that according to Equation 42 the value of k_e is made up of k_{gsc} and k_r, which appear as the two principal terms in Equation 77. Further, k_{nc}, k_{fc}, and k_{sc} are not included in the sum of terms comprising k_e because of their negligible contributions under the experimental conditions.

At $1500^{\circ}F$, for magnesia $k_d = 4.84$ Btu/hr·ft·$^{\circ}F$ and $\epsilon = 0.42$; for air $k_g = 0.0408$ Btu/hr·ft·$^{\circ}F$, $\gamma = 1.33$, $\not{b} = 10.8 \times 10^{-10}$ foot, $N_{Pr} = 0.718$, n_r is taken as unity, and the accommodation coefficient, a, is taken as 0.9.

From Table 2 the value of α (Equation 61) is 0.739 for this magnesia powder.

From Equation 54

$$\frac{D_s}{X} = \left(\frac{V_d}{\alpha}\right)^{1/3} = \left(\frac{0.58}{0.739}\right)^{1/3} = 0.9224 \; .$$

Combining Equations 53 and 54

$$\frac{S}{X^2} = V_d \left(\frac{\alpha}{V_d}\right)^{1/3} \; . \tag{78}$$

From Equation 78 above

$$\frac{S}{X^2} = 0.58 \left(\frac{0.739}{0.58}\right)^{1/3} = 0.629 \; .$$

From Figure 32(a) it may be seen that

$$d = \left(\frac{X}{D_s} - 1\right) D_s \tag{79}$$

or

$$d = \left[\left(\frac{\alpha}{V_d}\right)^{1/3} - 1\right] D_s \; . \tag{80}$$

To determine d from Equation 80, a value must be assigned to D_s. From a particle-size distribution, many characteristic particle "sizes" may be obtained—the median, the mean, the mode, and numerous "averages". Of these sizes, the mean (first moment of the distribution) is the only one that weights volume with distance. Therefore, D_s is taken to be the mean particle size. It should be noted that for the systems in this study there is little difference in calculated values of k_e if D_s is taken to be the median particle size. From Table 2 for this magnesia powder

$$D_s = D_m = 268 \text{ microns}$$

and thus, from Equation 80,

$$d = 22.5 \text{ microns} .$$

Now, substituting into Equation 66

$$k_g^o = \frac{0.0408}{1+5.08 \times 10^{-24} \left[\frac{1.1}{0.9}\right]\left[\frac{1.33}{2.33}\right] \left[\frac{1960}{2116(22.5)(3.28 \times 10^{-6})(10.8 \times 10^{-10})^2(0.718)}\right]} ,$$

$$k_g^o = 0.0387 \text{ Btu/hr} \cdot \text{ft} \cdot {}^o\text{F}.$$

From Equation 68

$$k_g^* = 0.0408\ (0.371) + 0.0387\ (0.629),$$

$$k_g^* = 0.0395 \text{ Btu/hr} \cdot \text{ft} \cdot {}^o\text{F}.$$

Substituting the appropriate values above into Equation 77,

$$k_e = \cfrac{0.0395}{\left[\cfrac{0.9224}{\left(\cfrac{0.0408}{0.0395}\right)(0.371) + \cfrac{4.84}{0.0395}(0.629)}\right] + 0.0776}$$

$$+ 4\,(1.73\text{x}10^{9})(0.42)\left(\frac{1}{0.58} - 1\right)(268)(3.28\text{x}10^{6})(1960)^3 \,,$$

$$k_e = 0.441 + 0.014,$$

$$k_e = 0.455 \text{ Btu/hr} \cdot \text{ft} \cdot {}^{\text{o}}\text{F.}$$

This predicted value of k_e at $1500 {}^{\text{o}}$F compares well with the experimental value shown in Figure 20. If the calculation above is repeated taking D_s as the median particle size then

$$k_e = 0.436 + 0.009,$$

$$k_e = 0.445 \text{ Btu/hr} \cdot \text{ft} \cdot {}^{\text{o}}\text{F.}$$

For a comparison of k_{gsc}, k_r, and k_e calculated—for a different powder—taking D_s to be the mean particle size and the median particle size see Table 5.

CHAPTER X

COMPARISON OF RESULTS WITH THEORETICAL EXPRESSIONS

Comparison of Experiments with Selected Earlier Correlations

The correlations (Chapter II) chosen for comparison with the experimental data are those of Fricke (24) with values for the semiprincipal axes suggested by de Vries (28) and of Willhite, Kunii, and Smith (37). These are repeated below for convenience.

Fricke's equation is

$$k_e = k_c \left[\frac{1 + V_d \left(F \frac{k_d}{k_c} - 1\right)}{1 + V_d (F - 1)} \right] ; \tag{7}$$

for spheroids $(f_1 = f_2 \neq f_3)$

$$F = \frac{1}{3} \sum_{i=1}^{3} \left[1 + \left(\frac{k_d}{k_c} - 1\right) f_i \right]^{-1}, \tag{8}$$

and

$$\sum_{i=1}^{3} f_i = 1 . \tag{9}$$

Fricke's equation is chosen as an example of an exact, i.e., mathematically rigorous, solution to the equation for disturbance of steady linear flow of heat in a uniform medium by an object of different conductivity buried in it. Woodside and Messmer found that de Vries' form of Fricke's equation, namely, $f_1 = f_2 = 1/8$ and $f_3 = 3/4$, showed fair agreement with their experimental values for quartz sand,

glass bead, and lead shot packs (16). Thus, this equation represents an exact solution which has been compared with experimental data for several granular materials.

Willhite, Kunii, and Smith's equation is

$$k_e = k_c \left[1 + V_d \left(1 - \frac{k_c}{k_d} \right) + V_d \left(\frac{\Omega}{\omega} \right) \left(1 - \frac{k_c}{k_d} \right)^2 \right] \tag{19}$$

where

$$\omega = \frac{1}{2} \frac{\left(1 - \frac{k_c}{k_d} \right)^2 \sin^2 \beta}{\ln \left\langle \frac{k_d}{k_c} - \left(\frac{k_d}{k_c} - 1 \right) \cos \beta \right\rangle - \left(1 - \frac{k_c}{k_d} \right) \left(1 - \cos \beta \right)}, \tag{20}$$

and

$$\sin^2 \beta = \frac{V_d}{13.23 \, V_d - 5.36} . \tag{21}$$

They took the quantity Ω equal to 1/2 or 2/3. In the present comparison Ω is taken as 2/3 since this value gave better agreement between the calculated and the experimental conductivities of this investigation than a value of 1/2.

The correlation of Willhite, Kunii, and Smith represents an approximate solution to the problem of calculating heat transfer through granular material. It is based on an extension of the work of Kunii and Smith (38) who had extended the earlier work of Yagi and Kunii (39) on a model which assumed cubic and tetrahedral packings of uniform spheres and linear heat flow. This correlation is chosen for comparison with the experimental results of the present investigation since it has been compared with good results to a large body of existing data on packed

beds, and since it relates the number of points of contact in the packed beds to the void fraction. This last fact is important because the controlling factor in the flow of heat is probably the fluid in the immediate vicinity of these points of contact.

The experimental results obtained in this study with magnesia, alumina, and zirconia powders in air are compared with the above correlations in Figures 33 to 42. The thermal conductivities of dense solid magnesia, alumina, and zirconia used in these calculations were taken from Kingery et al. (86) and the thermal conductivities of air were taken from Glassman and Bonilla (87).

It may be seen that Fricke's equation with values for the semi-principal axes suggested by de Vries gives values for k_e that are lower than experimental values for the magnesia and alumina powders (k_d/k_c varying from about 1200 to 100). Although the calculated k_e's do not correspond to the experimental ones in absolute value, they do correspond fairly well in their temperature variation (Figures 33 to 39). This suggest that the k_e's calculated by Fricke's equation for the magnesia and alumina powders can be brought into better agreement with the experimental k_e's in absolute value if the particles are assumed to be spheroids with a ratio of major to minor axis somewhat greater than six (de Vries' value). For the zirconia powders (k_d/k_c varying from about 60 to 30), the predicted k_e's and experimental k_e's are in excellent agreement (Figures 40 to 42). These results are in agreement with the observation of Hamilton and Crosser (88), namely, that the factor F (Equation 8) will not depend strongly on particle shape unless the ratio of k_d to k_c is about 100 or more.
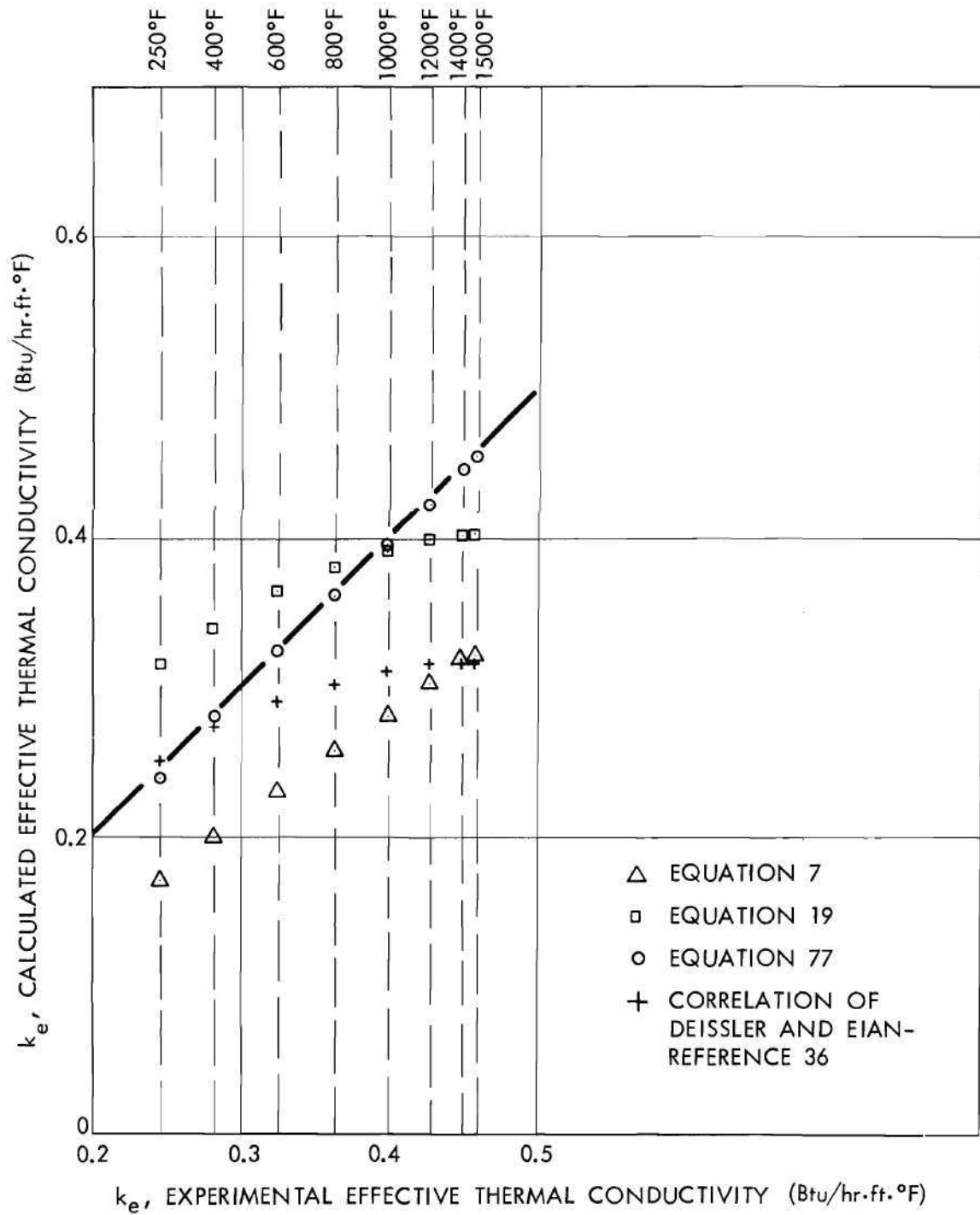
Fig. 33. Comparison of Experimental and Calculated Effective Thermal Conductivities of MgO (E-98) Powder in Dry Air at V_d = 0.58.
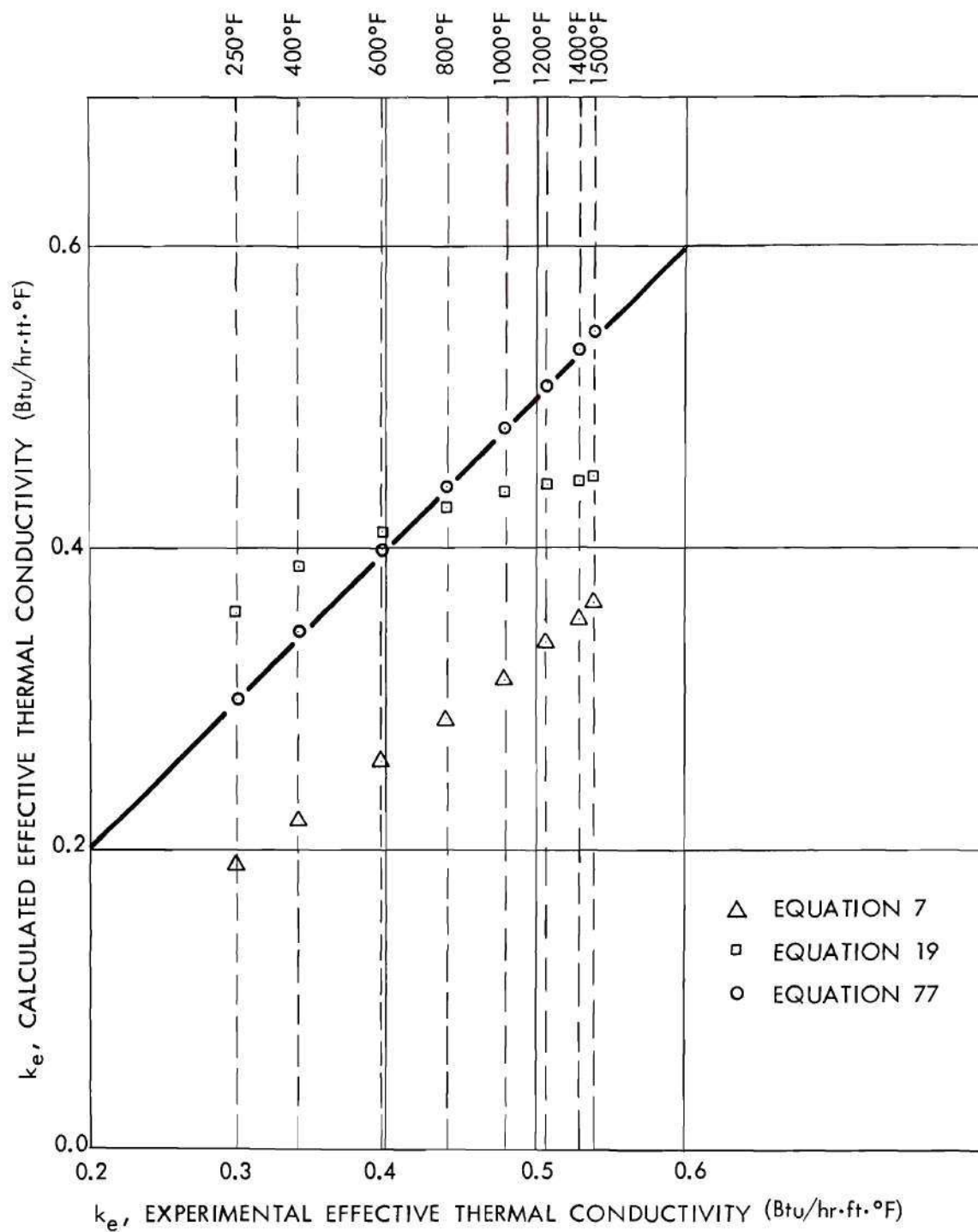
Fig. 34. Comparison of Experimental and Calculated Effective Thermal Conductivities of MgO (E-98) Powder in Dry Air at V_d = 0.61.
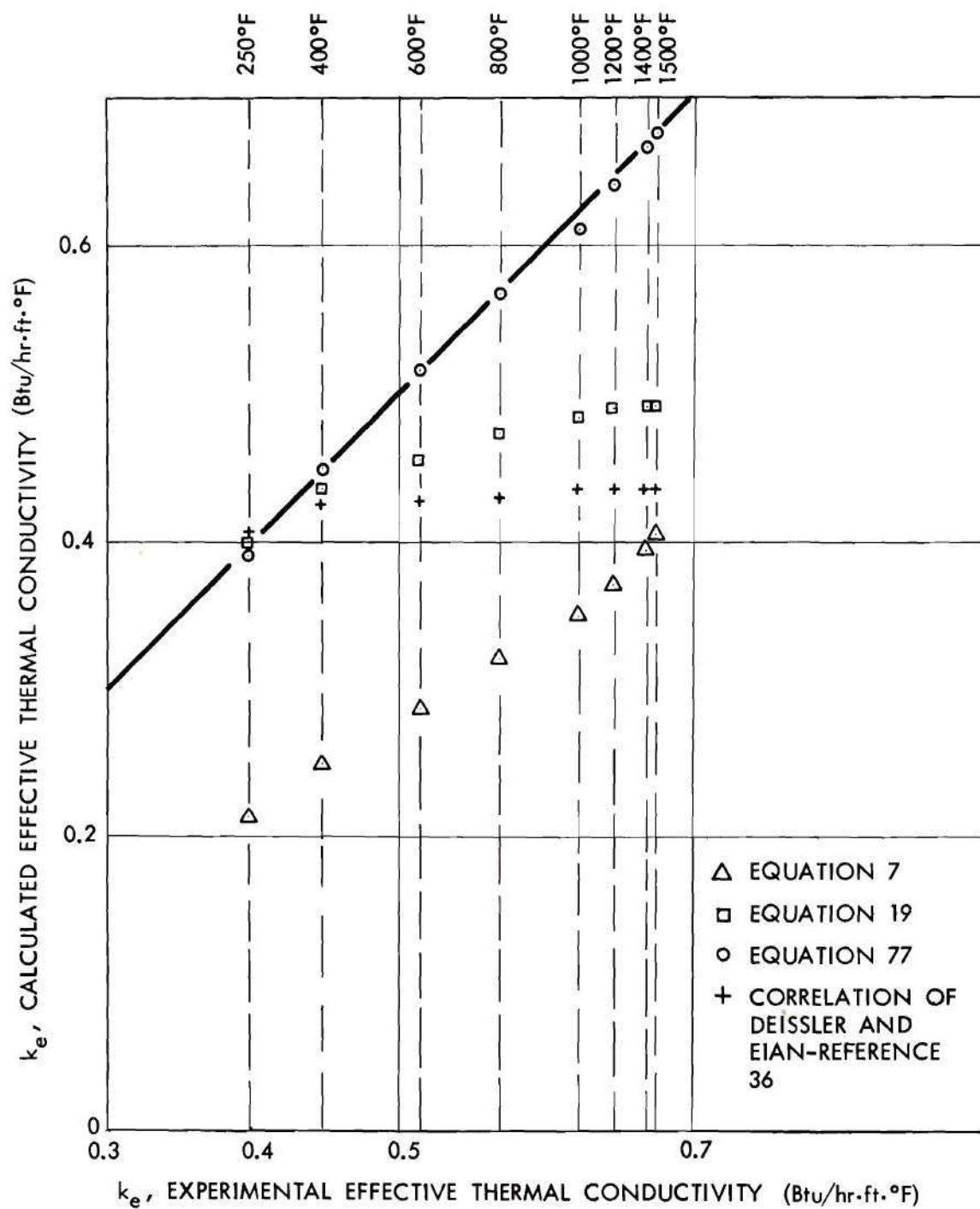
Fig. 35. Comparison of Experimental and Calculated Effective Thermal Conductivities of MgO (E-98) Powder in Dry Air at V_d = 0.64.
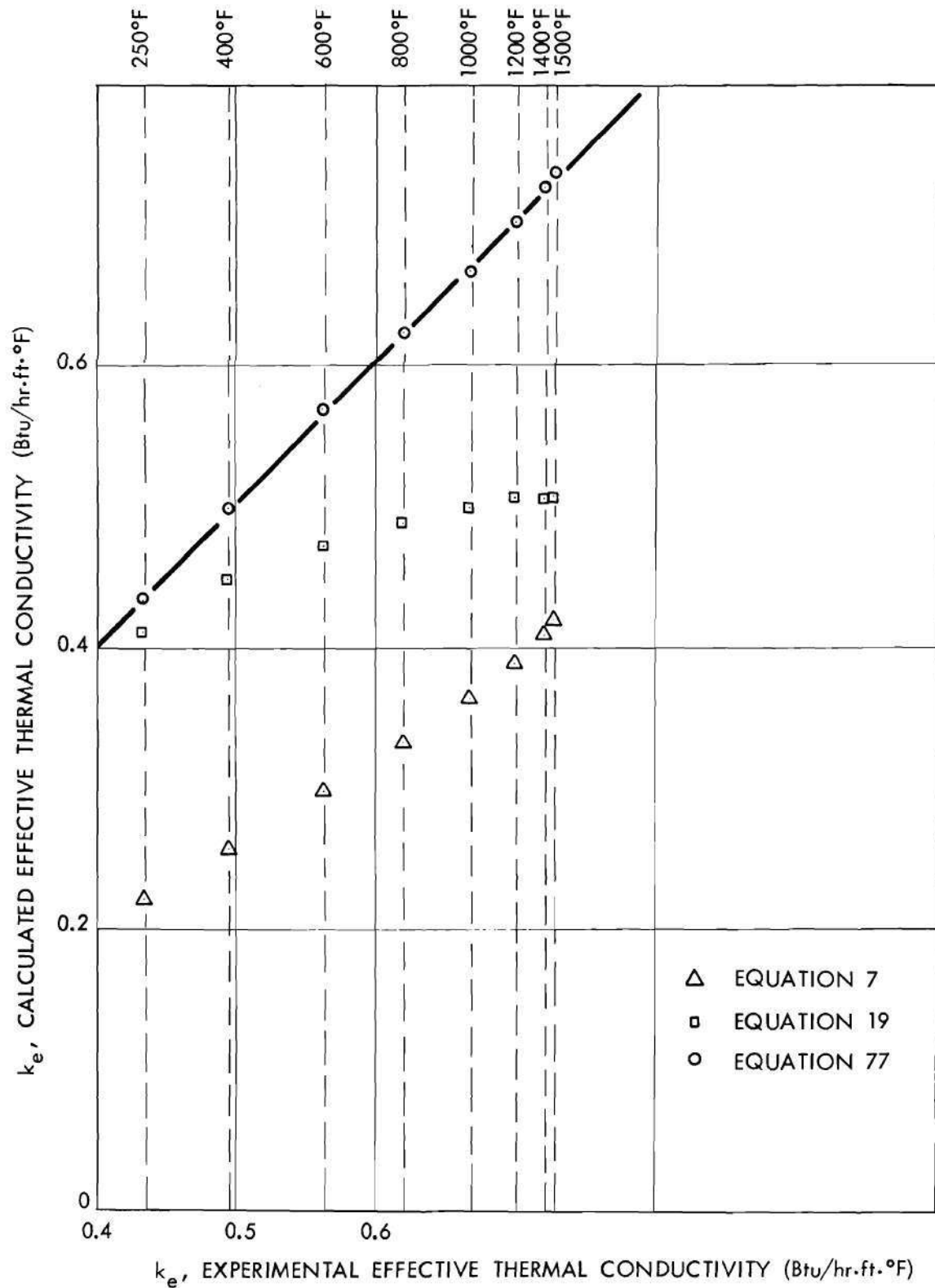
Fig. 36. Comparison of Experimental and Calculated Effective Thermal
Conductivities of MgO (E-98) Powder in Dry Air at $V_d = 0.65$.
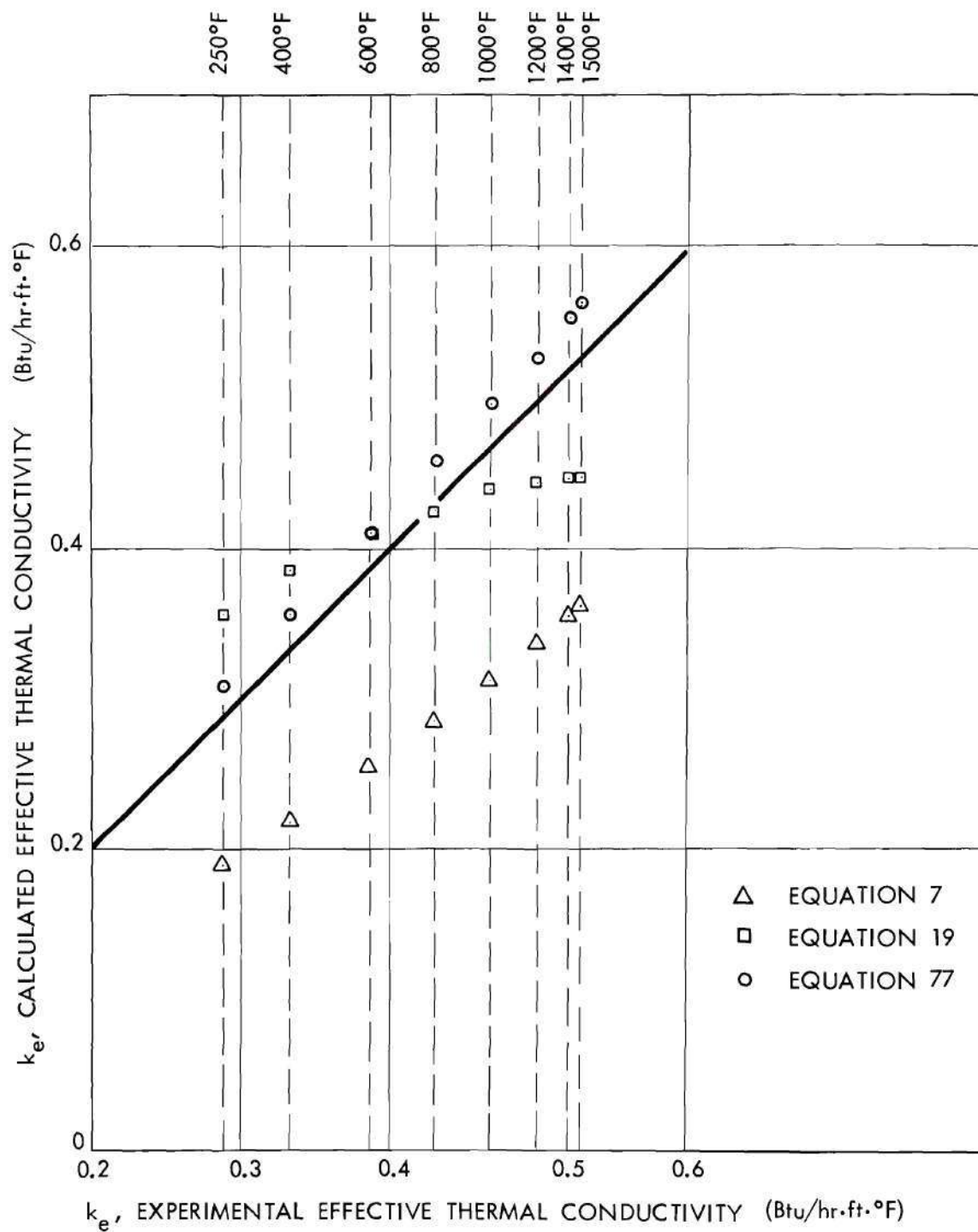
Fig. 37. Comparison of Experimental and Calculated Effective Thermal Conductivities of MgO (E-227) Powder in Dry Air at $V_d = 0.61$.
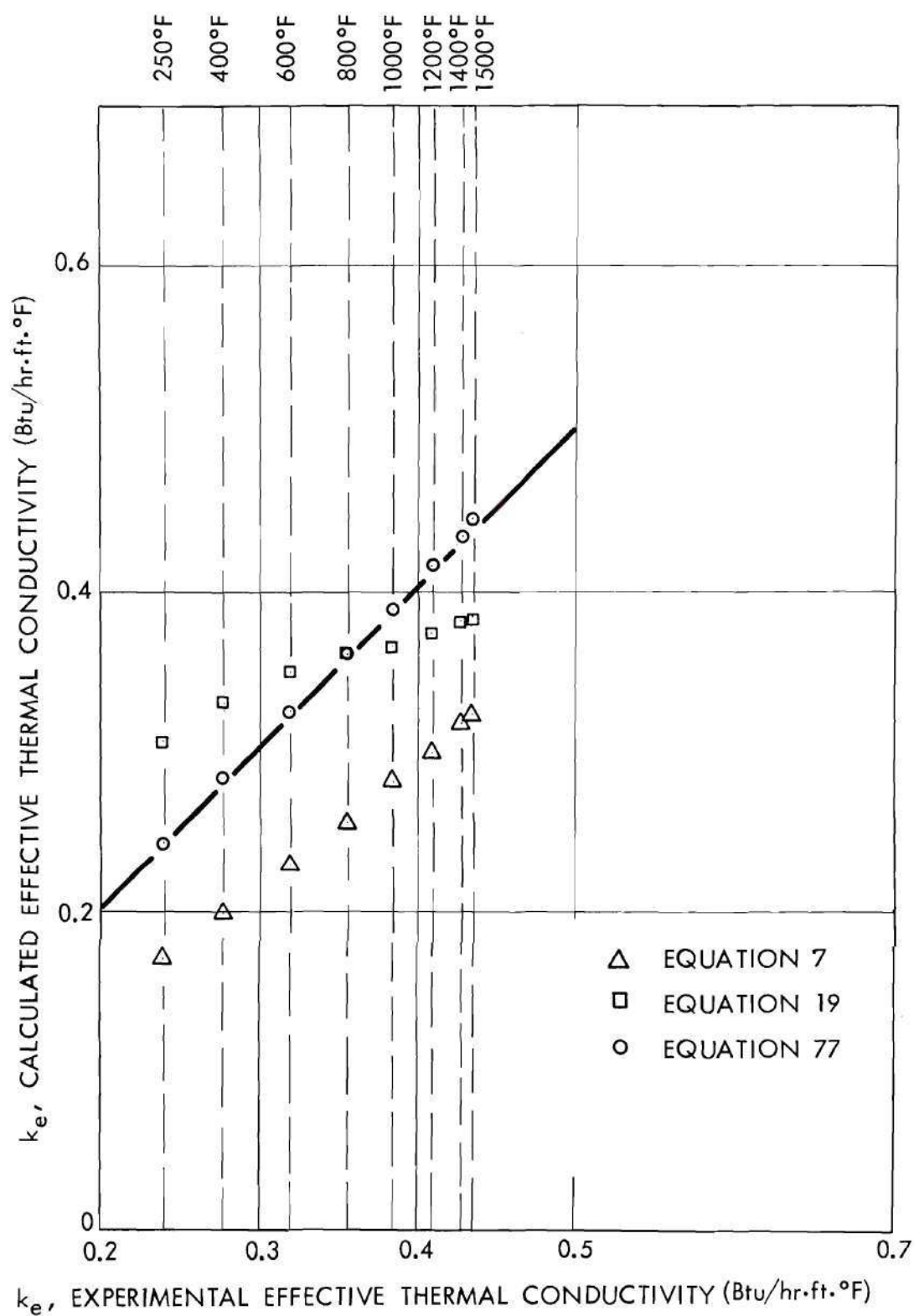
Fig. 38. Comparison of Experimental and Calculated Effective Thermal Conductivities of Al_2O_3 (E-98) Powder in Dry Air at V_d = 0.58.
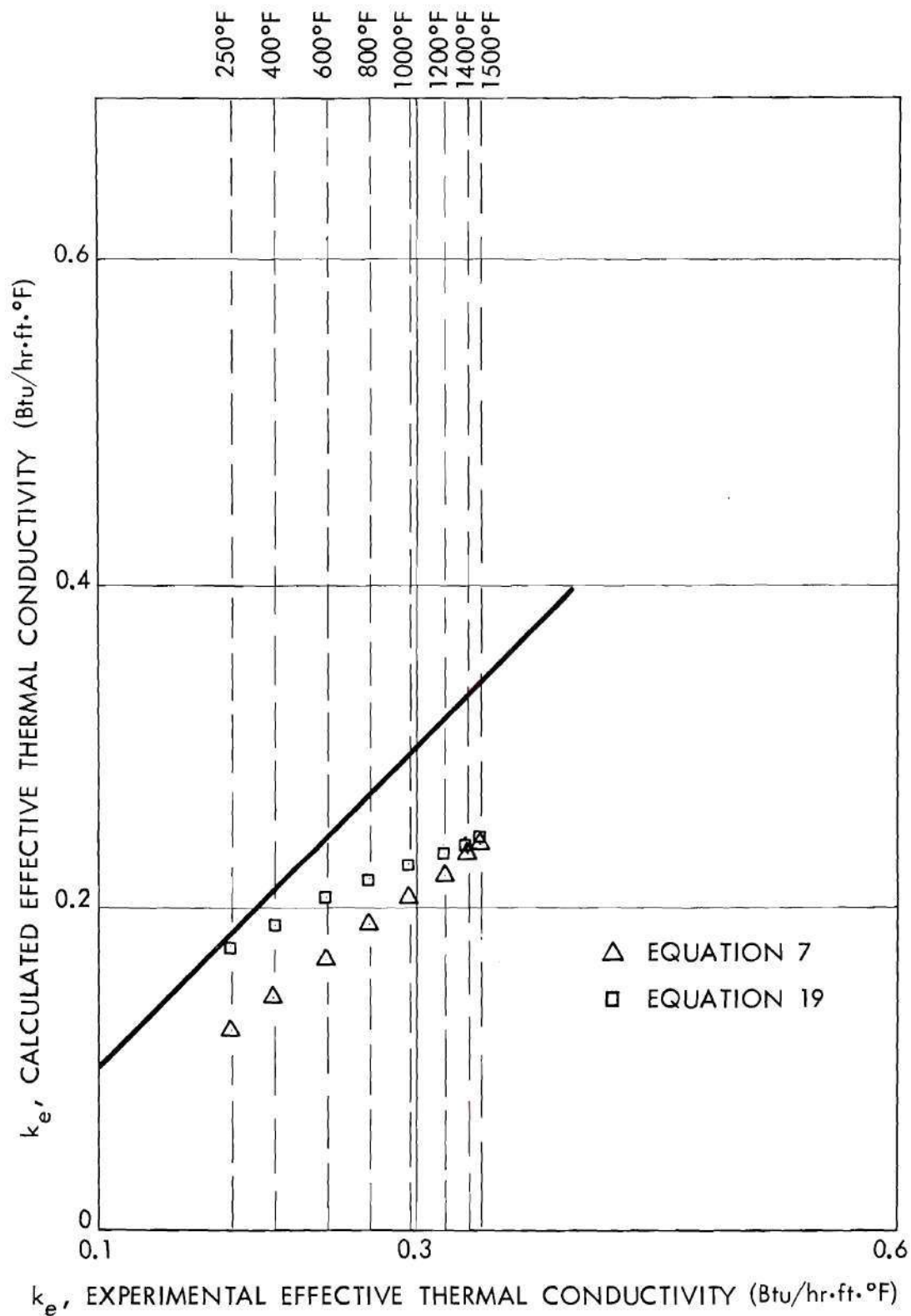
Fig. 39. Comparison of Experimental and Calculated Effective Thermal Conductivities of Al_2O_3 (B45F) Powder in Dry Air at $V_d = 0.49$.
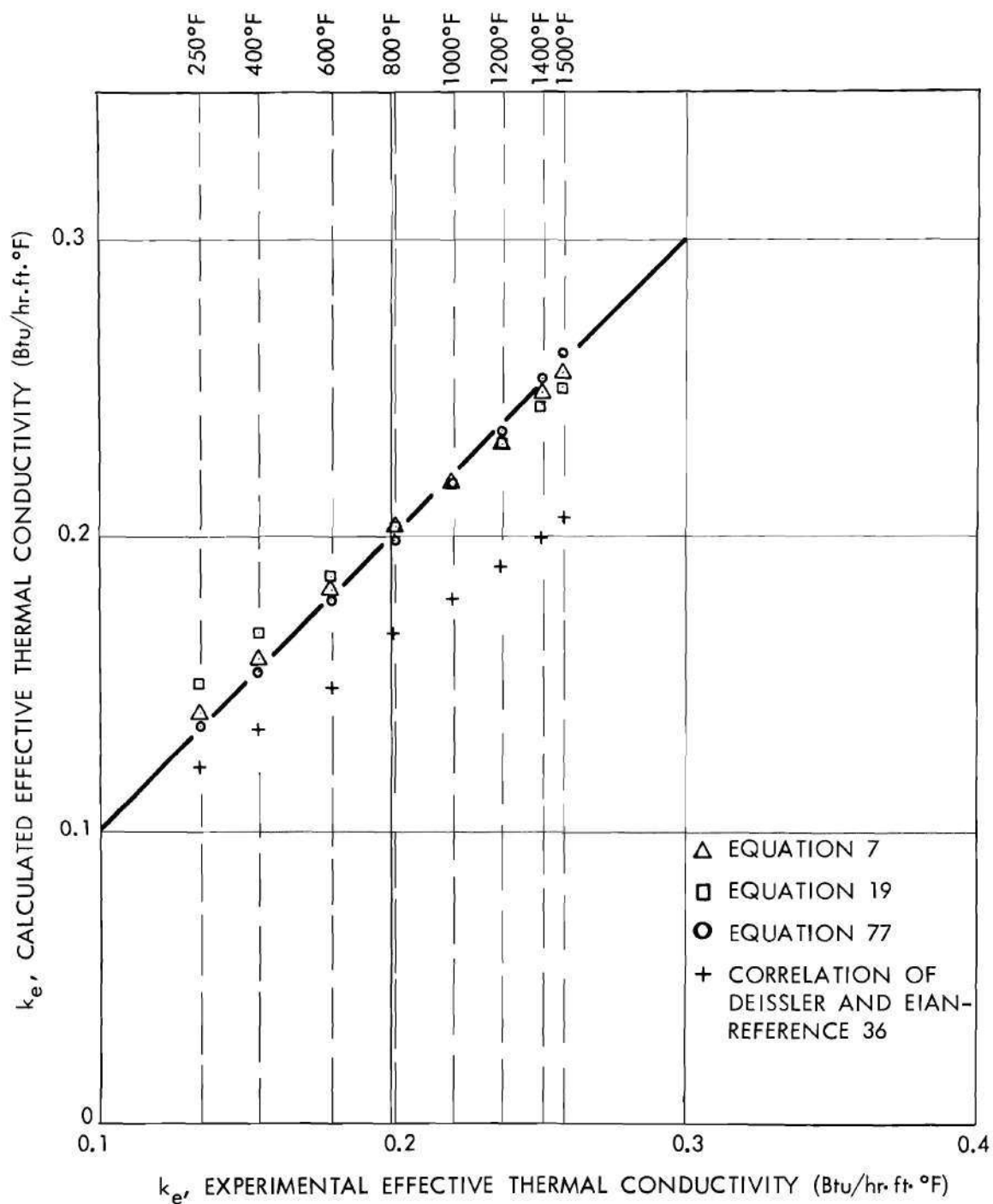
Fig. 40. Comparison of Experimental and Calculated Effective Thermal Conductivities of ZrO_2 (H30F) Powder in Dry Air at V_d = 0.58.

Fig. 41. Comparison of Experimental and Calculated Effective Thermal Conductivities of ZrO_2 (H3OF) Powder in Dry Air at V_d = 0.64.
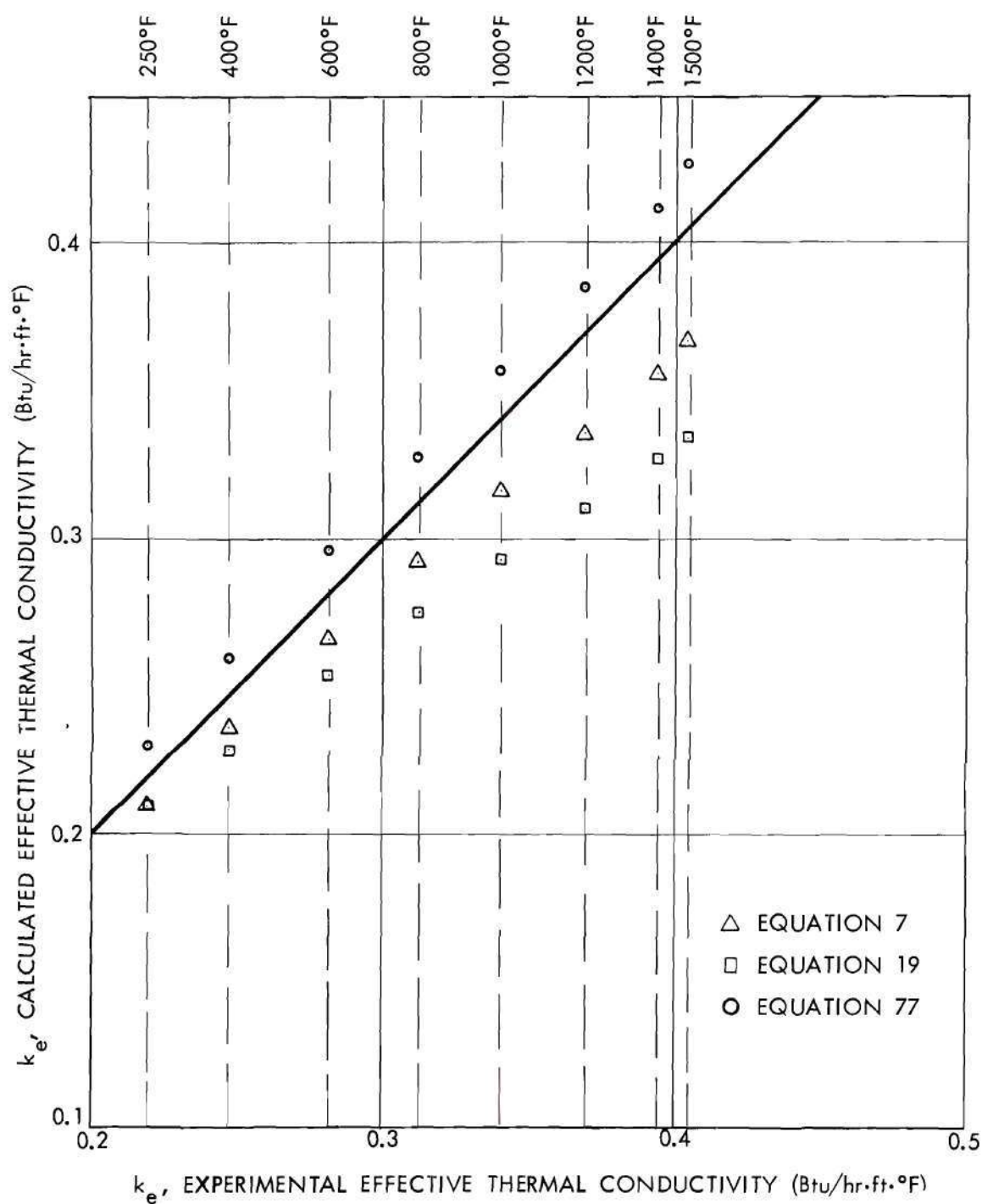
Fig. 42. Comparison of Experimental and Calculated Effective Thermal Conductivities of ZrO_2 (H14F) Powder in Dry Air at V_d = 0.70.

It may be seen that Willhite, Kunii, and Smith's equation with Ω taken as 2/3 gives values for k_e that tend to agree with the experimental values for the magnesia and alumina powders (Figures 33 to 39). The agreement is poorest for the two most densely packed magnesia powders (Figures 35 and 36) and the uniformly sized alumina powder (Figure 39) at the higher temperatures. It may also be seen that the equation does not, and cannot, predict the correct variation of k_e with temperature for the magnesia and alumina powders in this study. For the zirconia powders, the predicted and experimental k_e's are in excellent to good agreement (Figures 40 to 42).

The experimental results of this study were also compared with the correlation (Chapter II) of Deissler and Eian (36). Their correlation gives calculated k_e's for the magnesia and alumina powders that agree fairly well with the experimental k_e's at the lower temperatures (about 200 to 600°F). However, the agreement is poorer than that obtained with the Willhite, Kunii, and Smith equation at the higher temperatures. Typical results are shown in Figures 33 and 35. For the zirconia powders, the Deissler and Eian correlation gives results inferior to those obtained with Fricke's equation or Willhite, Kunii, and Smith's equation. Typical results are shown in Figure 40.

Comparison of Proposed Theory with Experiment

Using the method of calculation illustrated in the preceding chapter, the values of k_e shown in Figures 33 to 38 and 40 to 42 were obtained. The value obtained in the illustration appears as the calculated k_e value (open circle) at 1500°F in Figure 33.

The values of α (Equation 61) used in the calculations are listed in Table 2. No calculations were made for the Al_2O_3 (B45F) powder since a value of α was not available for this powder. The thermal conductivities of dense solid magnesia, alumina, and zirconia were taken from Kingery et al. (86) as mentioned previously. The emissivities of magnesia and alumina were taken from Sully, Brandes, and Waterhouse (89) and the emissivity of zirconia was taken from Olson and Morris (90). The thermal conductivities and Prandtl numbers of air were taken from Glassman and Bonilla (87). The values of γ for air are taken from Hilsenrath et al. (91). The molecular diameter of air as determined from viscosity is taken from Hirschfelder, Curtiss, and Bird (92). The refractive index of air is taken as unity and the thermal accommodation coefficient, from a consideration of measured values (83, 84, and 85), is estimated to be 0.9.

It may be seen that the calculated and experimental k_e's are in excellent agreement in all cases.

To illustrate the calculated contribution of k_r to k_e, values of k_{gsc} and k_r as a function of temperature are listed in Table 5 for one powder—ZrO_2 (H14F). It may be seen that at most ($1500^\circ F$) the calculated radiative contribution to k_e is about 7 per cent if D_s is taken to be the mean particle size and about 3 per cent if D_s is taken to be the median particle size. This powder represents the greatest difference in k_r's (and k_e's) calculated taking D_s to be the mean particle size and to be the median particle size since it has the greatest difference in D_m and $D_{50\%}$ (Table 2). With either value for D_s the calculated k_e's are within the accuracy limits set on the experimental k_e's.

Table 5. Calculated Values of k_{gsc}, k_r, and k_e for a Zirconia Powder[a]

Temperature ($^{\circ}$F)	k_{gsc} (Btu/hr·ft·$^{\circ}$F)		k_r (Btu/hr·ft·$^{\circ}$F)		$k_e = k_{gsc} + k_r$ (Btu/hr·ft·$^{\circ}$F)	
	Mean	Median	Mean	Median	Mean	Median
250	0.228	0.226	0.003	0.001	0.231	0.227
400	0.255	0.253	0.005	0.002	0.260	0.255
600	0.289	0.285	0.008	0.003	0.297	0.288
800	0.317	0.313	0.012	0.004	0.329	0.317
1000	0.341	0.337	0.017	0.005	0.358	0.342
1200	0.363	0.358	0.022	0.007	0.385	0.365
1400	0.384	0.378	0.028	0.009	0.412	0.387
1500	0.395	0.388	0.031	0.010	0.426	0.398

[a] Calculated for ZrO_2 (H14F) powder in air at atmospheric pressure having a volume fraction solid of 0.70 using Equation 77. Mean particle size = 1023 microns and median particle size = 333 microns (Table 2).

These results for k_r and similar results for the other powders lead to the conclusion that radiation is not important to this work because of relatively low temperatures and small inter-particle distance. However, it should be emphasized that heat transfer by radiation was not covered experimentally in this work, and only in a conventional way theoretically.

In passing it should be mentioned that Equation 77 was also derived based on the assumption of linear heat flow. The agreement between calculated and experimental thermal conductivities, using shape factors as determined in Chapter IV, is not as good with the linear heat flow assumption as with the linear isotherms assumption.

Comparison of Selected Previous Experiments with Correlations

The three theoretical expressions above are compared in Figures 43 to 46 with the results of Deissler and Eian (36) on a magnesia powder at 0.58 volume fraction solid in air and in argon and with the results of Eian and Deissler (93) on a different magnesia powder at 0.64 volume fraction solid in air and in argon. The properties of the dense solid and of air used in these calculations are taken from the references mentioned previously. The thermal conductivities, Prandtl numbers, and values of γ for argon are taken from Hilsenrath et al. (91) The molecular diameter of argon, as determined from viscosity, is taken from Hirschfelder, Curtiss, and Bird (92). The refractive index of argon is taken as unity and the thermal accommodation coefficient, from a consideration of measured values (83, 84, and 85), is estimated to be unity. The gas pressure at each temperature (for use in Equation 66) is double that calculated from Deissler and Eian's expression for breakaway pressure. Their expression is
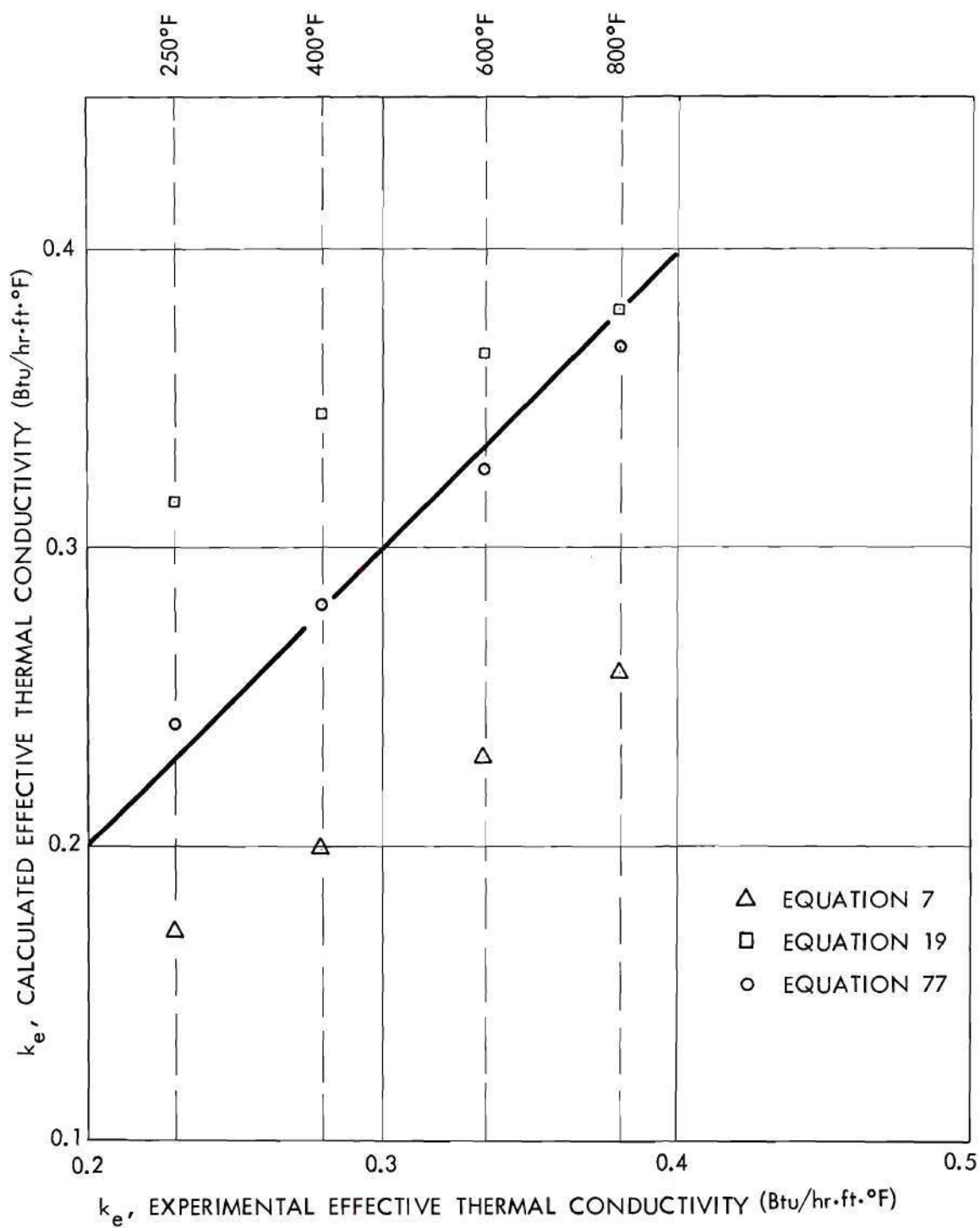
Fig. 43. Comparison of Selected Previous Experimental Results and Calculated Effective Thermal Conductivities of a Magnesia Powder in Dry Air at V_d = 0.58.
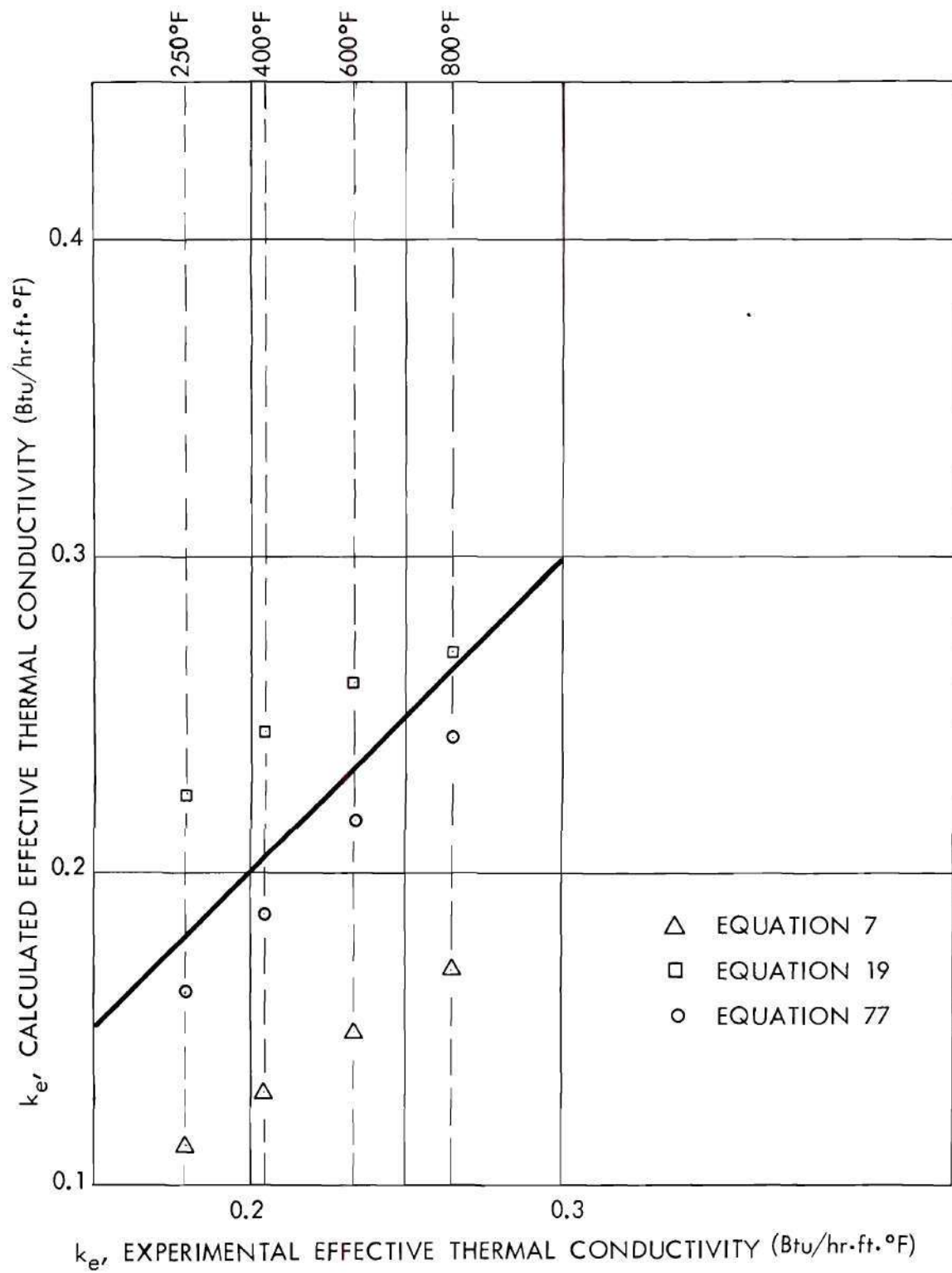
Fig. 44. Comparison of Selected Previous Experimental Results and Calculated Effective Thermal Conductivities of a Magnesia Powder in Argon at $V_d = 0.58$.
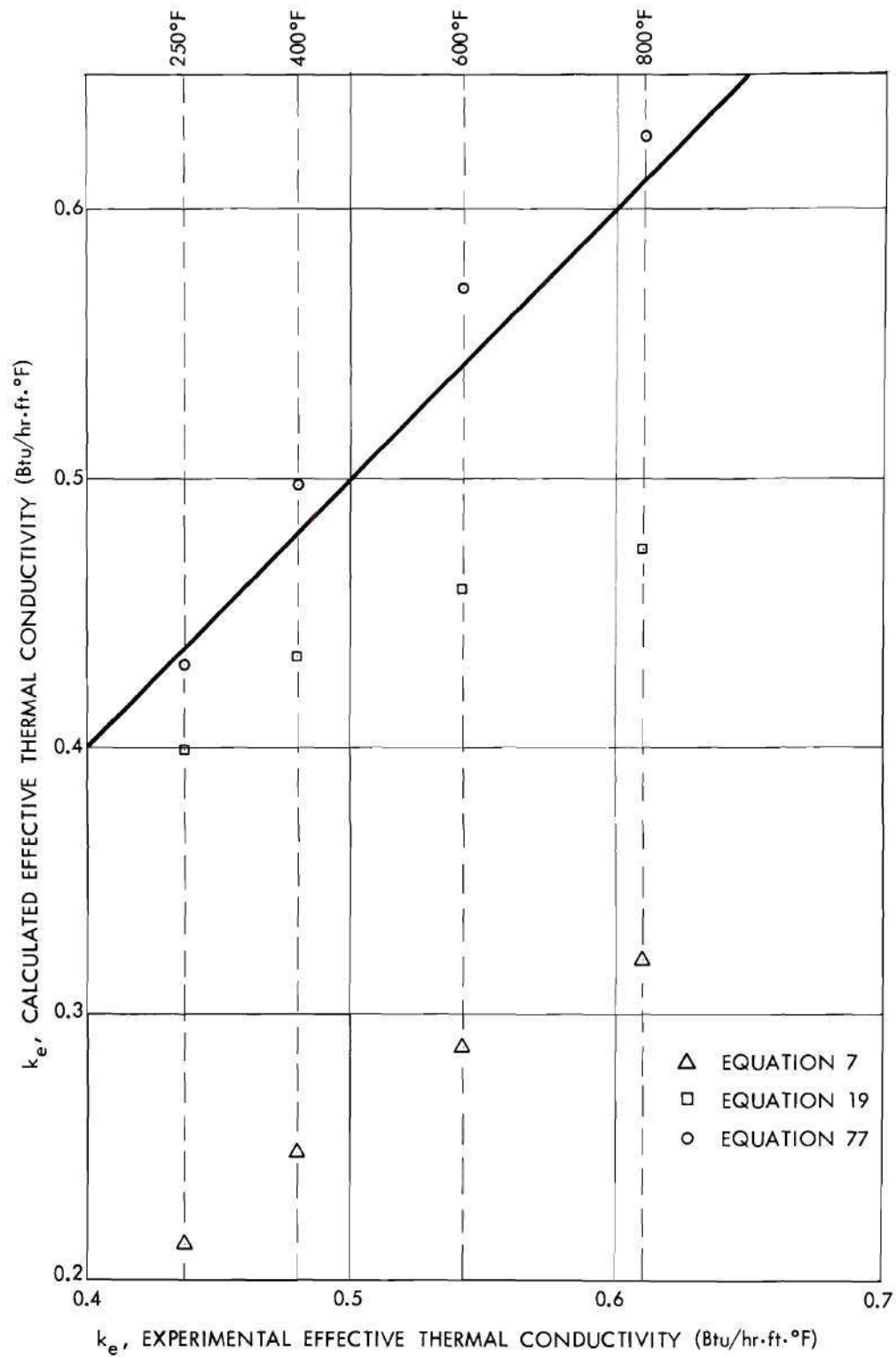
Fig. 45. Comparison of Selected Previous Experimental Results and Calculated Effective Thermal Conductivities of a Magnesia Powder in Dry Air at V_d = 0.64.
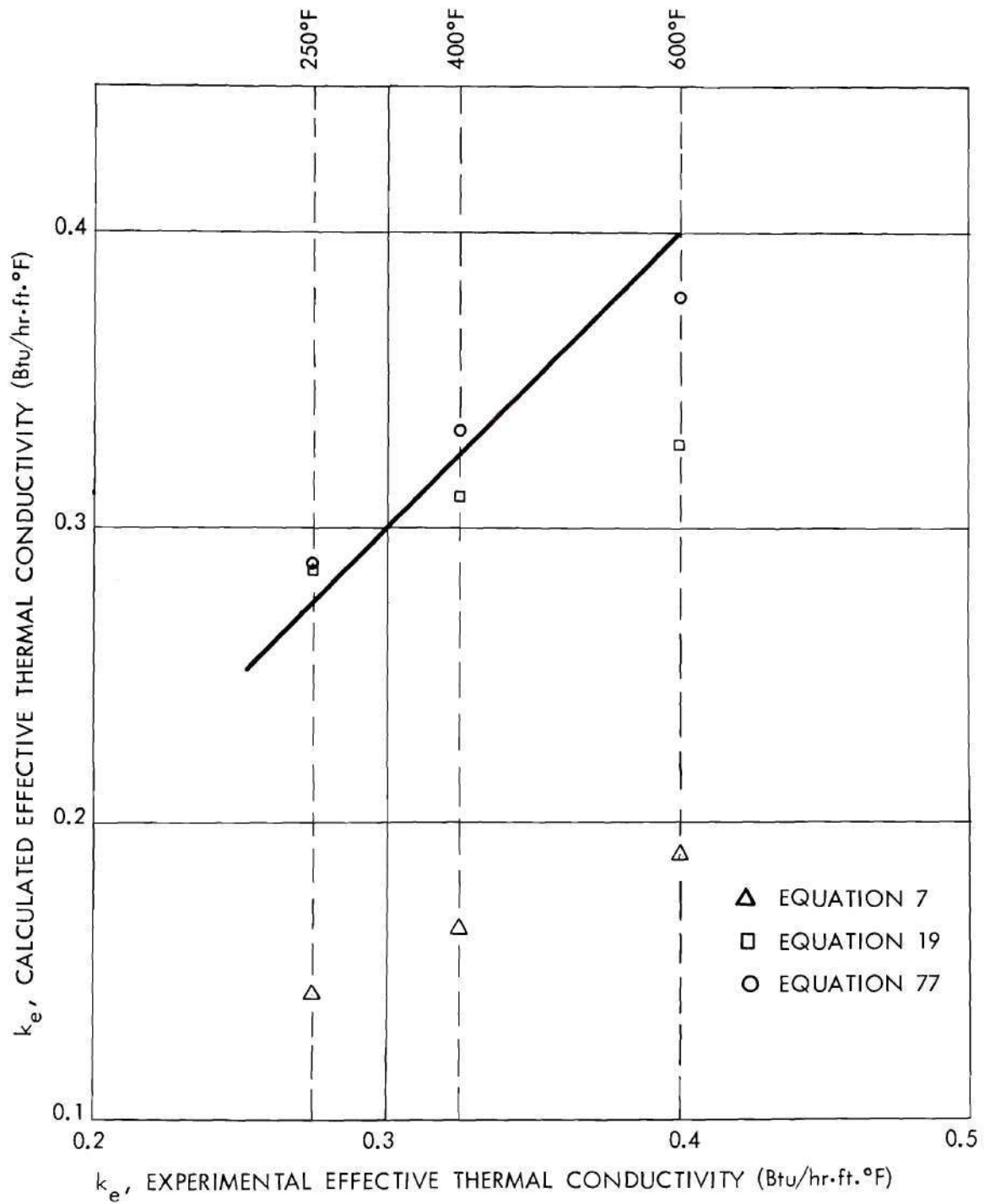
Fig. 46. Comparison of Selected Previous Experimental Results and Calculated Effective Thermal Conductivities of a Magnesia Powder in Argon at $V_d = 0.64$.

$$P_b = 1.77 \times 10^{-21} \; \frac{T}{\emptyset^2 \, D_m} \; , \qquad\qquad (81)$$

where T = temperature in degrees Rankine,

$\emptyset$ = molecular diameter (determined from viscosity) in feet,

D_m = mean particle size (determined by sieving) in feet, and

P_b = breakaway pressure, in pounds per square foot.

The reason for doubling the calculated pressure is that Deissler and Eian as well as Eian and Deissler indicated their pressures were, in all cases, above those given by Equation 81. However, they did not indicate how much above. Thus, the factor of two is to insure that pressures used in the calculations are equal to or greater than the pressures in the previous experiments. Their experiments showed that at pressures above the breakaway pressure the effective thermal conductivities of the powders did not vary with pressure. From the reported screen analyses, the shape factor α is taken to be 0.739 for the powder used by Deissler and Eian and to be 0.728 for the powder used by Eian and Deissler.

The expression of Fricke gives k_e's that are below the 1952 results of Deissler and Eian and considerably below the 1953 results of Eian and Deissler. The expression of Willhite, Kunii, and Smith gives k_e's that tend to agree with the 1952 results of Deissler and Eian. However, the expression gives k_e's that tend to fall away from the 1953 results of Eian and Deissler at the higher temperatures. The theory proposed in this work gives k_e's that are in excellent agreement with the results of both the 1952 and 1953 studies. It should be mentioned that Deissler and Eian as well as Eian and Deissler also

carried out experiments in helium atmosphere. The results of these experiments are not included in the present comparison because of the unavailability of measured values for the accommodation coefficient. Extrapolation or interpretation of available information leads to a value between about 0.3 and 0.7 for the accommodation coefficient. For good agreement between results calculated by Equation 77 and experimental results a value of about 0.15 must be assumed.

CHAPTER XI

CONCLUSIONS

From this investigation of the effective thermal conductivities of magnesia, alumina, and zirconia powders in air at atmospheric pressure from 200°F to 1500°F the following conclusions have been reached:

(1) The steady-state and unsteady-state methods used give results which agree to within about 7 per cent.

(2) For the size of sample and the arrangement of apparatus used, the unsteady-state method offered no time saving over the steady-state method since the time-limiting factor was the heating of the system—sample, sample container, and furnace—to temperature level.

(3) The effective thermal conductivity of a specific powder increases with increasing volume fraction solid until, at values close to the maximum obtainable with the powder, effective thermal conductivity is critically dependent on volume fraction.

(4) The influence of gas conductivity is greater than that of the solid on the effective thermal conductivity of powders, in agreement with most previous investigators.

(5) The effective thermal conductivity for each powder measured increased at a decreasing rate with increasing temperature, following an approximately quadratic temperature dependence.

(6) The effective thermal conductivities of two magnesia powders having different particle-size distributions and points of truncation

but almost the same shape factor, α, were essentially the same at the same volume fraction solid in accord with the theory developed in this work.

(7) The effective thermal conductivity of a magnesia powder was slightly higher than that of an alumina powder with almost the same shape factor, α, and at the same volume fraction solid, in accord with the theory developed in this work.

(8) The presence of a sorbed water film increased the effective thermal conductivity of each powder up to temperatures corresponding to the decomposition temperature of the respective hydroxides.

(9) Mechanical pressure on the particles caused by shrinkage of the sample container upon cooling from high temperatures increased the effective thermal conductivity by factors up to about two.

(10) All the data on effective thermal conductivity for the powders studied can be correlated well by means of a derived equation (Equation 77) which relates effective thermal conductivity to the conductivities and concentrations of the constituent phases as well as to a shape factor.

(11) The extension of Maxwell's equation to ellispoids by Fricke (Equation 7) underestimates the effective thermal conductivity of the magnesia and alumina powders when de Vries' values for semi-principal axes are used but the agreement is excellent for the zirconia powders.

(12) The equation of Willhite, Kunii, and Smith (Equation 19) tends to underestimate the data when used with a constant required by the geometry of the model of 1/2 but agrees fairly well when the constant is taken as 2/3.

(13) By theoretical analysis radiation was determined not to be an important heat transfer mechanism in these powders because of low temperature and small inter-particle distances.

CHAPTER XII

RECOMMENDATIONS

The results of this investigation suggest some interesting areas for further work. These areas include: effect of particle parameters, effect of mechanical pressure, effect of sorbed films, and effect of radiation.

Effect of Particle Parameters

Obviously, for any powder studied, the wider the range of particle parameters; e.g., particle size, particle-size distribution, surface area, the more light will be shed on the influence of each parameter on the effective thermal conductivity of powders. Also, the wider the range of parameters studied, the wider the range of applicability of proposed theoretical expressions which correctly predict k_e.

Powders having known particle sizes, particle-size distributions, etc. should be synthesized or blended so that the influence of these parameters may be investigated systematically. Better control of particle parameters will permit more meaningful intercomparisons between different investigations of heterogeneous systems. Specifically, a powder similar to that used by Eian and Deissler (93), with a small mean particle size, say 40 microns of less, should be investigated at modest pressure (atmospheric or several atmospheres) in gases such as helium or hydrogen. Such studies would demonstrate the interrelation of pressure, temperature, and particle size. A maximum in k_e versus temperature should result,

as observed by Eian and Deissler. It should be emphasized that the experiments of Eian and Deissler were under gas pressures up to about 18 atmospheres so that in theory they should not have observed the maximum which they did observe in fact. Assuming that the accommodation coefficient is fairly constant for a given powder-gas system over the temperature range studied, Equation 77 predicts that for such a system at a pressure of several atmospheres a maximum in a temperature versus effective thermal conductivity plot could exist. Although the bulk conductivity of gases at constant pressure increases with increasing temperature, small inter-particle distances combined with increasing mean free path as temperature increases can lower the apparent conductivity of the gas in the pores (see, for instance, Equation 66). This lowering can be large enough to more than override the increased gas bulk conductivity. By operating under increasing pressure with increasing temperature, Eian and Deissler essentially had a situation wherein the decrease of mean free path with increasing pressure compensated for the increase of mean free path with increasing temperature—assuming that the accommodation coefficient is affected little by temperature and pressure over the range studied.

Powders having, in so far as possible, the same particle size, particle-size distribution, and points of truncation (which implies the same shape factor, α) should be blended from solids with widely different thermal conductivities. For example, an alumina powder having the same particle parameters as the ZrO_2 (H30F) used in this study could be blended. The effective thermal conductivity of these powders measured in the gas at modest pressures and temperatures will permit

better evaluation of the role played by solid conductivity in the conductivity of powders.

Powders of a given material having widely different α's but close to the same mean particle size should be blended. In addition these powders should have $V_{d\ max} - V_{d\ min}$ ranges that overlap so that systems having the same volume fraction solid may be packed with each. For example, the Al_2O_3 (E-98) with a mean particle size of 263 microns used in this study had an α of 0.74. If an alumina powder were blended with particle parameters like the ZrO_2 (H30F), with a mean particle size of 292 microns, it should have an α of 0.85. If these two alumina powders in air at atmospheric pressure were packed to $V_d = 0.58$, Equation 77 predicts that at $800^{\circ}F$, k_e for the one with $\alpha = 0.74$ would be 0.36 Btu/hr·ft·$^{\circ}F$, while for the alumina powder with $\alpha = 0.85$, k_e would be 0.24 Btu/hr·ft·$^{\circ}F$. As has been mentioned previously, one of the principal beliefs propounded by this work is that such a difference in the effective thermal conductivity of apparently similar systems is real, and can be explained by factors such as α.

Effect of Mechanical Pressure

Studies in regions where crushing, coalescence, deformation, etc. of the particles are negligibly small seem desirable to elucidate the effect of mechanical pressure on the effective thermal conductivity of powders. The results of this study suggest that compression of the powder might be used to improve heat transfer rates through the powder. On the other hand, if the powder is being used as an insulator, compression should be avoided. It is worth noting that the effective thermal conductivity of a magnesia powder at $400^{\circ}F$ (Figure 26) was increased

almost 90 per cent after heating to about $1500^{o}F$ and cooling back to the
lower temperature. This effect is here attributed to compression of
the powder by the shrinking metal sample container upon cooling.

Effect of Sorbed Films

Not only water at atmospheric pressure, as observed in this work,
but also films of other sorbed fluids such as carbon dioxide, can prob-
ably enhance the conductivity of powders. In this connection, the
work of Weininger and Schneider (55) on beds of alumina and glass
powders should be noted. They attributed the marked increase in ef-
fective thermal conductivity with increasing carbon dioxide pressure
(about 1 atmosphere to 65 atmospheres) to an increase in gas adsorption.
Results such as these suggest that films might be used to "dope" powders
and improve their effective thermal conductivities. For example, a
powder similar to any of those used in this study, which had been
appropriately treated to remove sorbed films of such fluids as water
and carbon dioxide, could be used as the solid phase for a series of
experiments. Air from which water vapor and carbon dioxide had been
removed could be used as the continuous phase. Carbon dioxide (or
steam) could be added in controlled amounts to the continuous phase.
The effective thermal conductivty, at fixed temperature and pressure,
could be determined as a function of the amount of carbon dioxide added.
Carbon dioxide present as a film could enhance the effective thermal
conductivity of the system. However, carbon dioxide present in the gas
phase should only lower the effective thermal conductivity of the
system, since the thermal conductivity of carbon dioxide (up to about
$1450^{o}F$) is less than the thermal conductivity of dry air.

Effect of Radiation

Powders used in this study were of fairly small particle size so that inter-particle distances were small. Also temperatures were not very high in these studies. Thus, the contribution of radiation to heat transfer through the powders was probably small. Studies with larger particle sizes at higher temperatures with continuous phases of both non-absorbing and absorbing gases, such as water vapor, carbon dioxide, and the Freons will aid in interpreting the radiative contribution to effective thermal conductivity. Radiation is a function of shape but not of length of path. Therefore, when heat transfer by radiation is expressed in terms of an equivalent effective conductivity, and length of pore is introduced as a variable, particle size with all its subtle meanings and implications becomes important. As mentioned several times previously, the effective conductivity ascribed to radiation may vary by factors of 2 or 3 simply because of the technique used to measure "particle size". In addition, from the results of a size measurement, numerous "particle sizes" are possible—the median, the mean, the mode, as well as countless "average" particle sizes. Thus, experimentation is probably the only guide as to how to measure and use particle size in the correct relation to pore length. Effective thermal conductivities of powders with mean particle sizes of several thousand microns should be determined at low pressures (several atmospheres to subatmospheric) and at temperatures of several thousands of degrees Fahrenheit. The radiation contribution to heat transfer for such powders should be large enough so that parametric studies of the radiation term in Equation 77 should lead to a better understanding of the role played by radiation in the overall heat transfer through powders.

APPENDIX I

COMPARISON OF EXACT AND SIMPLIFIED SOLUTIONS TO THE HEAT FLOW EQUATION

Comparison under Certain Limiting Conditions

Austin (1) has given an interesting treatment to the relationship between an exact and a simplified solution to the heat flow equation. From a consideration of his data on alumina and silica bricks, as well as most of the data available to him (year 1939) on refractory solids, he concluded that Russell's simplified solution and Maxwell's exact solution of the heat flow equation yield essentially the same results for any specific system.

He also pointed out that if k_c/k_d is small Maxwell's equation reduces to

$$k_e = k_c \left(\frac{1 + 2\, V_d}{1 - V_d} \right) , \qquad (82)$$

and Russell's equation (a special case of Equation 77) reduces to

$$k_e = k_c \left(\frac{V_d^{2/3}}{V_d^{2/3} - V_d} \right) . \qquad (83)$$

Expressing $V_d^{2/3}$ as $\left[1 - (1 - V_d) \right]^{2/3}$, expanding the binominal, and assuming that the first two terms of the expansion are a reasonably good approximation of the series, Austin showed that Equation 82 is equivalent to Equation 83.

It may easily be shown that for large k_c/k_d, Russell's equation reduces to

$$k_e = k_c \left(\frac{1 - V_d^{2/3}}{1 - V_d^{2/3} + V_d} \right). \tag{84}$$

Expressing $V_d^{2/3}$ as $\left[1 - (1 - V_d) \right]^{2/3}$, expanding the binominal, and, following Austin's lead, assuming that the first two terms of the expansion are a reasonably good approximation of the series, one sees that Equation 84 is equivalent to

$$k_e = k_c \left(\frac{1 - V_d}{1 + 0.5\ V_d} \right). \tag{85}$$

Equation 85 follows from Maxwell's exact solution under the assumption of large k_c/k_d, as Austin has shown.

An objection to Austin's comparison of Equations 82 and 83 and the present comparison of Equations 84 and 85 is that the approximation made by taking the first two terms in the expansion is good only in the range where V_d equals about 0.5 or greater. For example, taking $V_d = 0.2$ it is found that $V_d^{2/3} = 0.34$ and the value of the first two terms in the binominal expansion is 0.47. Whereas, taking $V_d = 0.5$, it is found that $V_d^{2/3} = 0.63$ and the first two terms in the expansion equal 0.67. On the other hand, in the range where V_d equal about 0.5, the system is no longer composed of non-interacting particles so that Maxwell's assumptions are violated, and his equation may not be applicable. Another objection to these comparisons is that Maxwell's equation is based on dispersed spheres, while Russell's equation is based on dispersed cubes. Therefore, unless the shape factor can conclusively be shown to be of no consequence, either in fact, or in the derivation of the equations, the comparisons are suspect. There is considerable

evidence suggesting the importance of the shape factor, so the derivations must be examined for implied shape restrictions which are not actually required for the solutions of the equations. In fact, as has been stated earlier Russell's equation can be obtained from Equation 77 (Chapter IX) without assuming the particles are cubes. The only requirement is that the shape factor α be equal to unity—a requirement that is not necessarily true for random cubes.

Notwithstanding these criticisms, it is significant that under certain conditions an equation based on an exact solution and an equation based on a simplified solution can be shown to be equivalent.

Comparison Using Empirical Shape Factor in Terms of Sphericity

Hamilton and Crosser (88) found that their measured effective thermal conductivities could be correlated using Maxwell's equation in the form

$$k_e = k_c \left[\frac{k_d + (\frac{3}{\psi} - 1) \, k_c - (\frac{3}{\psi} - 1) \, V_d \, (k_c - k_d)}{k_d + (\frac{3}{\psi} - 1) \, k_c + V_d \, (k_c - k_d)} \right]. \qquad (86)$$

Sphericity ψ is defined as the ratio of the surface area of a sphere having a volume equal to that of the particle, to the surface area of the particle itself. They studied systems of aluminum spheres, cylinders, or parallelepipeds and balsa wood disks or cubes dispersed in rubber. Values of V_d ranged from 0.14 to 0.275.

Equation 77 with α expressed (quite arbitrarily) as $3 \, \psi^2$ correlates the data of Hamilton and Crosser as well as their modification of Maxwell's equation above. The purpose of this comparison is not to encourage empiricism but to emphasize the importance of shape factor.

An additional purpose is to show that even for emulsions or dispersions Equation 77 can be made to give essentially the same results as Maxwell's equation in its various forms.

APPENDIX II

ADDITIONAL DIAGRAMS AND PHOTOGRAPHS OF EXPERIMENTAL APPARATUS
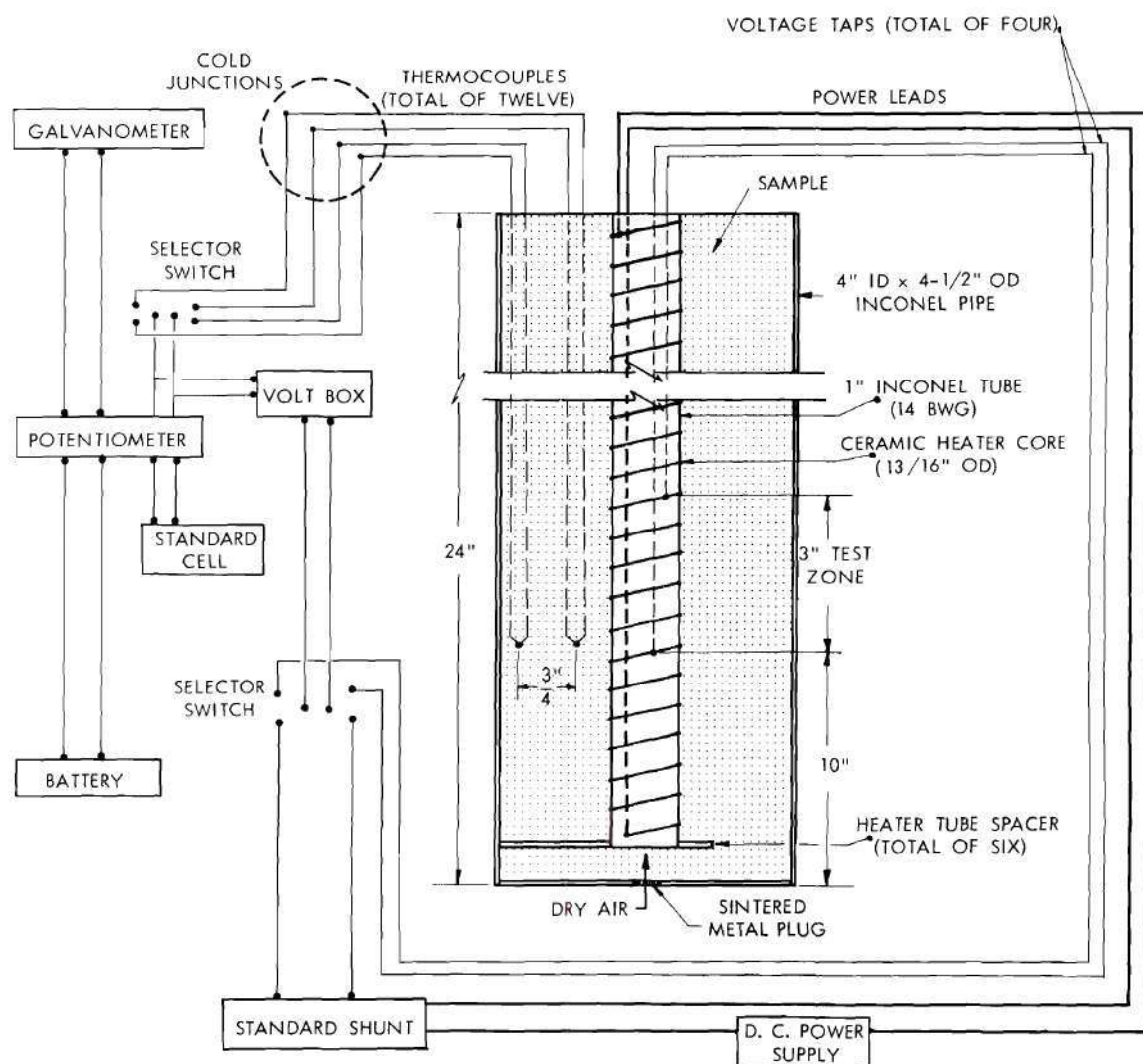
Fig. 47. Schematic Diagram of Principal Components Used to Measure Thermal Conductivity.

1. Power Supplies
2. Recording Potentiometers
3. Furnace Controllers

Fig. 48.   Power Supplies, Furnace Controllers, and Recording Potentiometers.

SPIRAL GROVE IS 0.050"
WIDE AND 0.050" DEEP.
FOUR TURNS PER INCH.

3/8" DIAM HOLE DRILLED
LENGTHWISE THROUGH TUBE

(a)

13/16" DIAM

FOUR 1/16" HOLES DRILLED
INTO CENTER HOLE

7 1/2"
8 1/4"
9 3/4"
10 1/2"

HEATER IS WOUND WITH 25 AWG
PT; POWER LEADS ARE 14 AWG PT;
VOLTMETER LEADS ARE 25 AWG PT

20 1/4"

MATERIAL: LAVA "A"

(b)

14"

CHROMEL-ALUMEL THERMOCOUPLE

17"

12"

30"

1/8" STAINLESS STEEL TUBING

STAINLESS STEEL VOLTAGE TAPS

LAVA "A"

(c)

~ 1/2"

1/8" DIAM

1/8" DIAM

NUT OF 1/2"
STAINLESS STEEL
MALE CONNECTOR

BODY OF 1/2"
STAINLESS STEEL
MALE CONNECTOR

SEAT FOR 1/8"
STAINLESS
STEEL FERRULE

Fig. 49. Schematic Diagrams of Central Heaters for Steady (a) and Unsteady (b)-State
Methods, and Insulating Gland (c) for Unsteady-State Heater.

151

1. Ice bath selector switch.
2. Thermocouple selector switches.
3. Central heater voltage tap selector switch.
4. Central heater current-voltage selector switch.
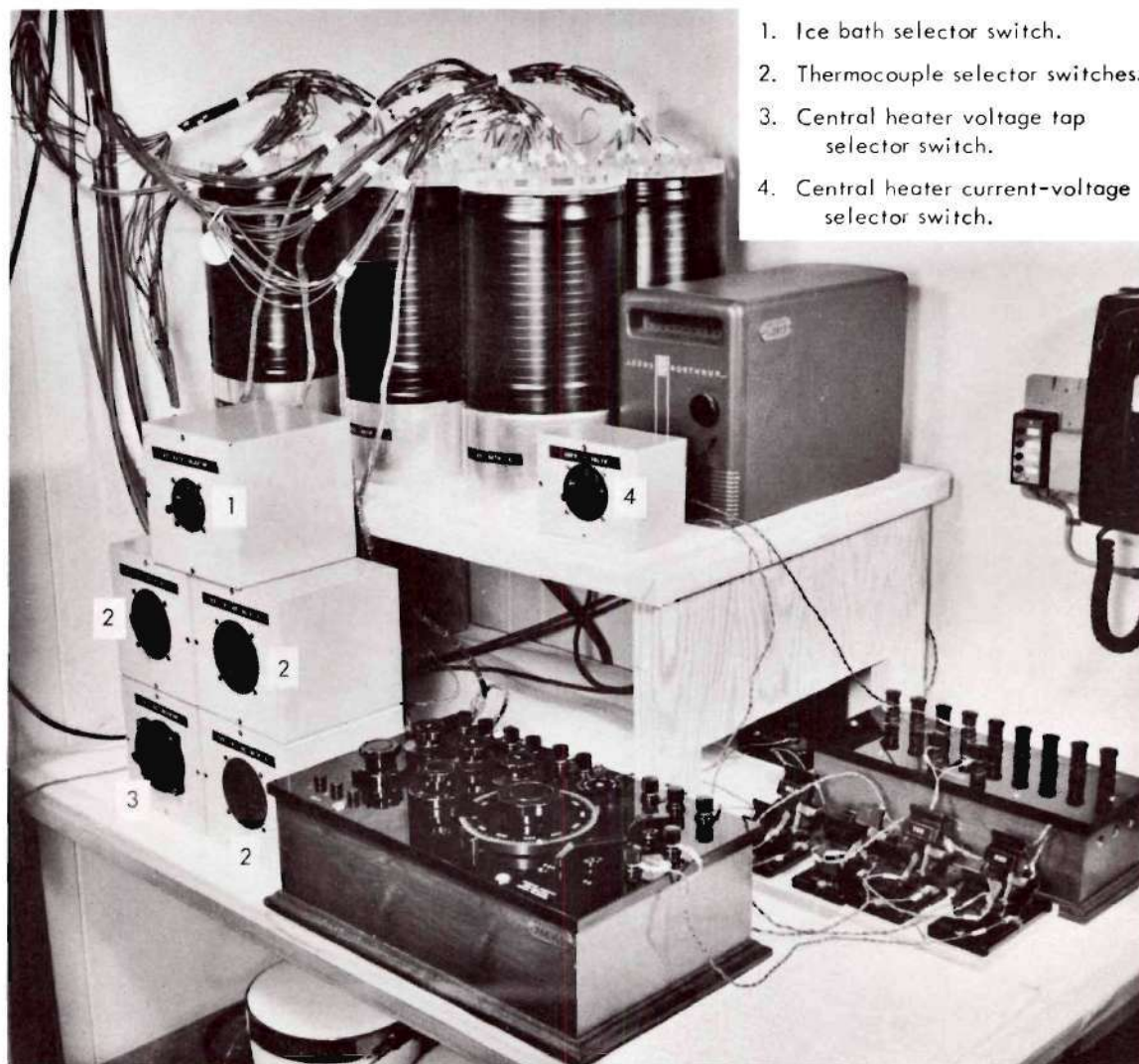
Fig. 50. Temperature and Power Measuring Equipment.

APPENDIX III

SUPPLEMENTARY INFORMATION FOR CHARACTERIZATION OF MATERIAL
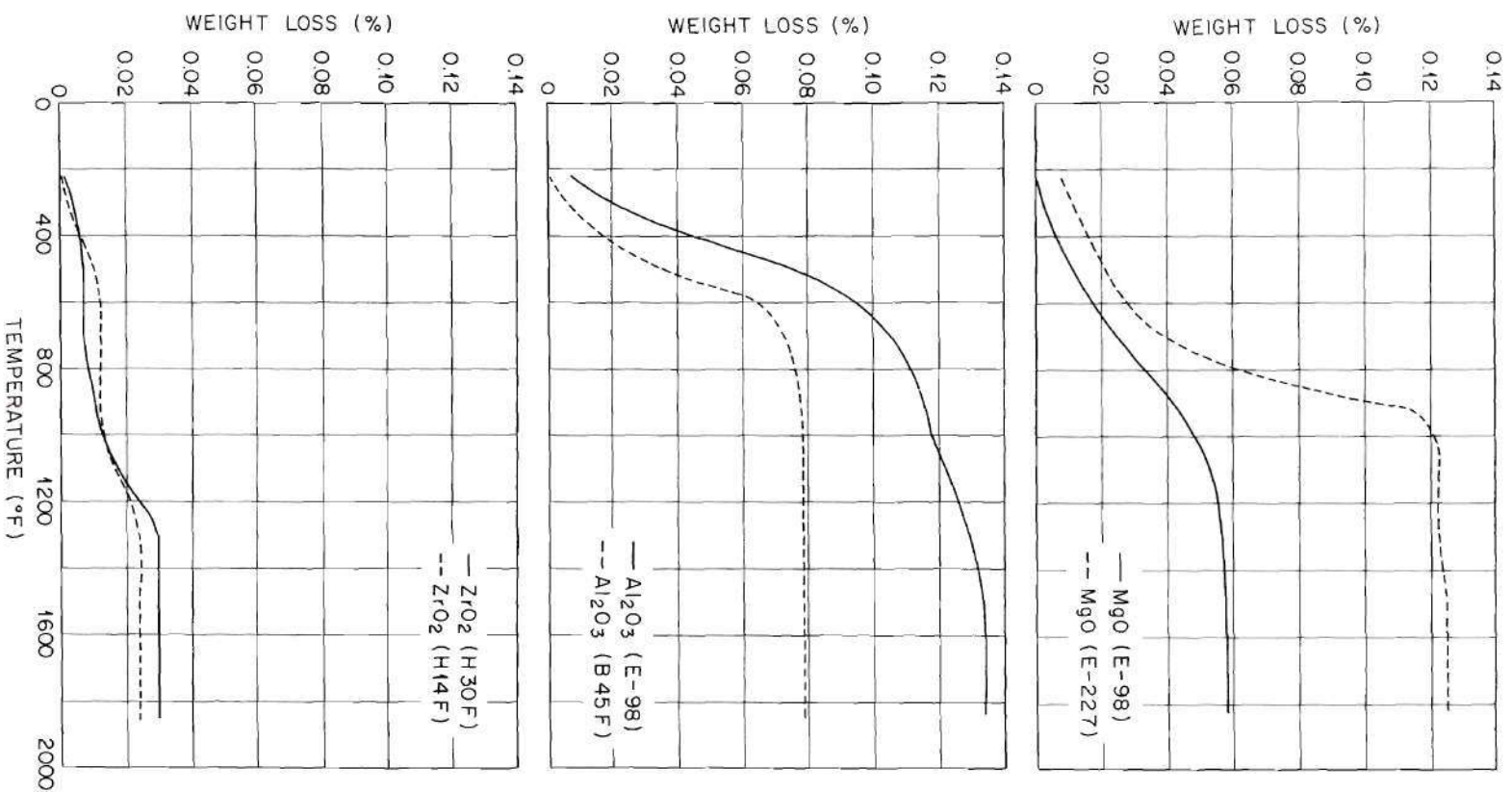
Fig. 51. Thermograms of Magnesia, Alumina, and Zirconia Powders.

154

Table 6. Screen Analyses of Magnesia Powders[a]

Mesh Size (U.S. Standard)	Screen Opening (microns)	Weight Per Cent Retained on Screen[b]	
		MgO (E-98)	MgO (E-227)
25	707		0
30	595	0	0.13
35	500	0.09	0.15
40	420	0.20	4.64
45	354	4.23	20.70
50	297	12.04	12.92
60	250	13.25	11.05
70	210	14.94	7.95
80	177	9.30	7.09
100	149	7.77	7.38
120	125	7.23	4.67
140	105	6.91	5.27
170	88	5.38	4.03
200	74	3.93	3.45
230	63	3.79	2.85
270	53	2.66	1.92
325	44	4.07	2.23
400	37	1.71	1.48
Pan	---	2.50	2.09

[a] Analyses made using 250 gram samples, 8-inch diameter standard full height sieves, and Fisher-Wheeler Sieve Shaker at 900 revolutions per minute for 20 minutes.

[b] Average of four separate determinations—normalized.

Table 7.   Screen Analyses of Alumina Powders[a]

Mesh Size (U.S. Standard)	Screen Opening (microns)	Weight Per Cent Retained on Screen[b]	
		Al_2O_3 (E-98)	Al_2O_3 (B45F)
35	500	0	
40	420	0.12	0
45	354	2.99	0.51
50	297	9.20	0.44
60	250	13.26	4.38
70	210	12.98	88.50
80	177	11.40	5.65
100	149	8.77	
120	125	5.42	
140	105	6.51	
170	88	5.90	
200	74	5.34	
230	63	4.97	
270	53	3.19	
325	44	5.26	
400	37	1.70	
Pan	---	2.99	0.52

[a] Analyses made using 250 gram samples of Al_2O_3 (E-98) and 100 gram samples of Al_2O_3 (B45F), 8-inch diameter standard full height sieves, and Fisher-Wheeler Sieve Shaker at 900 revolutions per minute for 20 minutes.

[b] Average of three separate determinations for Al_2O_3 (E-98) and of two separate determinations for Al_2O_3 (B45F)—normalized.

157

Table 8. Screen Analyses of Zirconia Powders[a]

Mesh Size (U.S. Standard)	Screen Opening (microns)	Weight Per Cent Retained on Screen[b]	
		ZrO_2 (H30F)	ZrO_2 (H14F)
7	2830		0
8	2380		0.43
10	2000		2.42
12	1680		3.59
14	1410		4.40
16	1190		5.19
18	1000		4.66
20	841		4.18
25	707		5.01
30	595	0	4.64
35	500	6.52	5.27
40	420	11.24	5.73
45	354	9.88	5.29
50	297	7.73	4.20
60	250	7.56	4.22
70	210	7.98	4.24
80	177	8.07	4.30
100	149	9.28	5.83
120	125	6.33	3.43
140	105	5.07	3.63
170	88	5.69	1.94
200	74	4.44	2.50
230	63	2.92	2.04
270	53	1.89	1.49
325	44	4.09	5.29
400	37	1.26	5.66
Pan	----	0.12	0.42

[a] Analyses made using 250 gram samples, 8-inch diameter standard full height sieves, and Fisher-Wheeler Sieve Shaker at 900 revolutions per minute for 20 minutes.

[b] Average of four separate determinations—normalized.

Table 9. Sedimentation Analyses of Magnesia, Alumina, and
Zirconia Powders

Powder	Apparent Stokes' Diameter (microns)	Weight Per Cent Less Than Indicated Size
MgO (E-98)	97	12.6
	137	20.9
	168	28.6
	206	47.4
	237	61.5
	375	85.9
MgO (E-227)	68.3	4.3
	96.5	10.0
	136	19.2
	190	45.0
	329	77.0
	465	98.5
Al_2O_3 (E-98)	80	21.7
	139	47.8
	196	62.0
	253	78.4
	310	91.4
Al_2O_3 (B45F)	179	14.0
	196	33.0
	219	56.1
	253	78.3
	310	91.3
ZrO_2 (H30F)	178	15.8
	244	31.7
	343	52.5
	397	62.2
	492	82.9
ZrO_2 (H14F)	114	4.6
	198	16.3
	343	22.5
	532	37.9
	914	52.4
	1075	67.7
	1391	77.8
	1870	89.6

Table 10. Particle-Size Distribution of MgO (E-98) Powder
by Microscopy

Size (microns)	Number of Particles Less Than Indicated Size
21	60
42	167
63	232
84	293
105	332
126	359
147	380
168	397
189	409
210	418
231	423
252	428
273	432
294	435
315	438
336	441
420	448
525	453
630	457
924	460
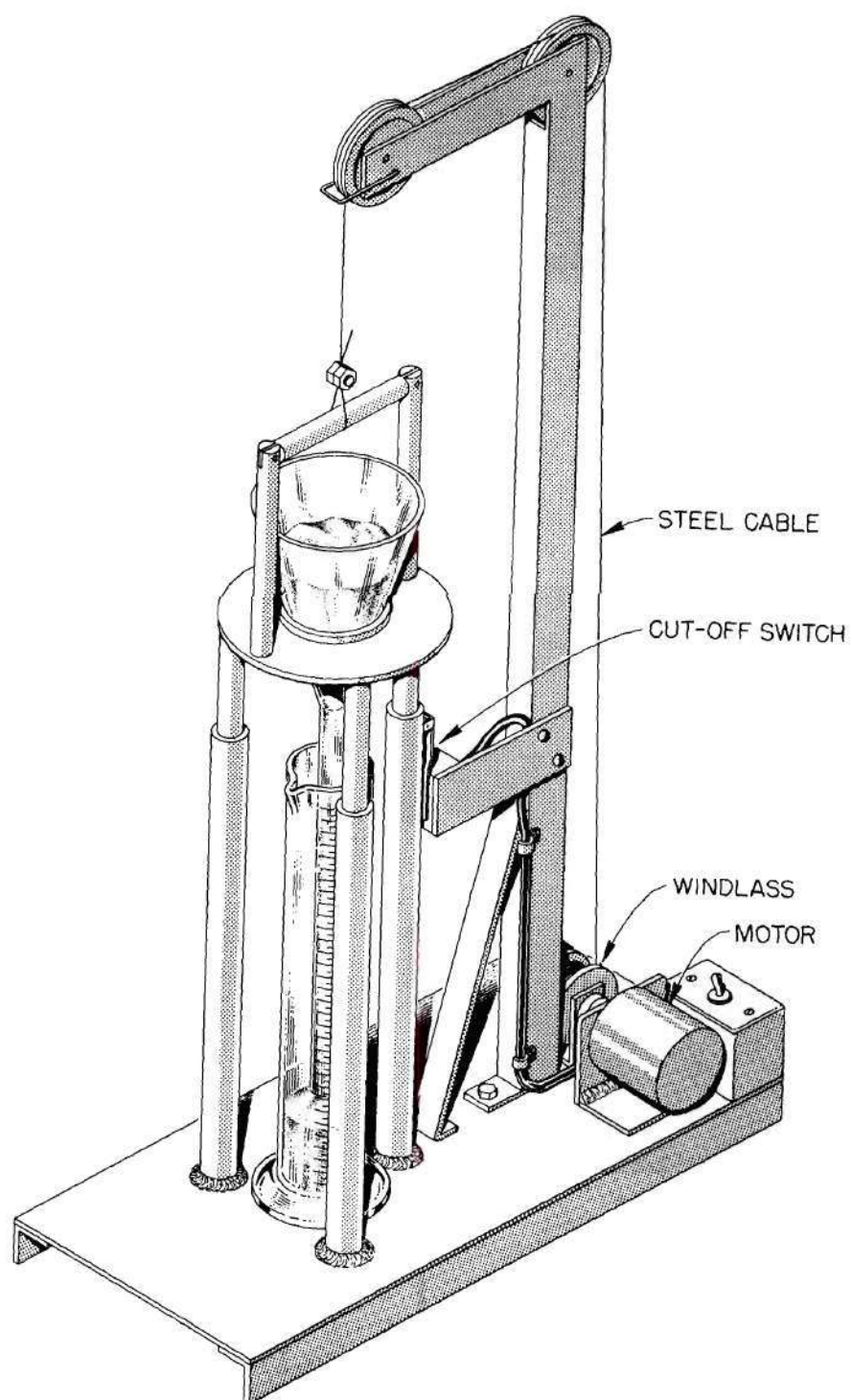
Fig. 52. Apparatus Used to Determine $V_{d\ min}$.
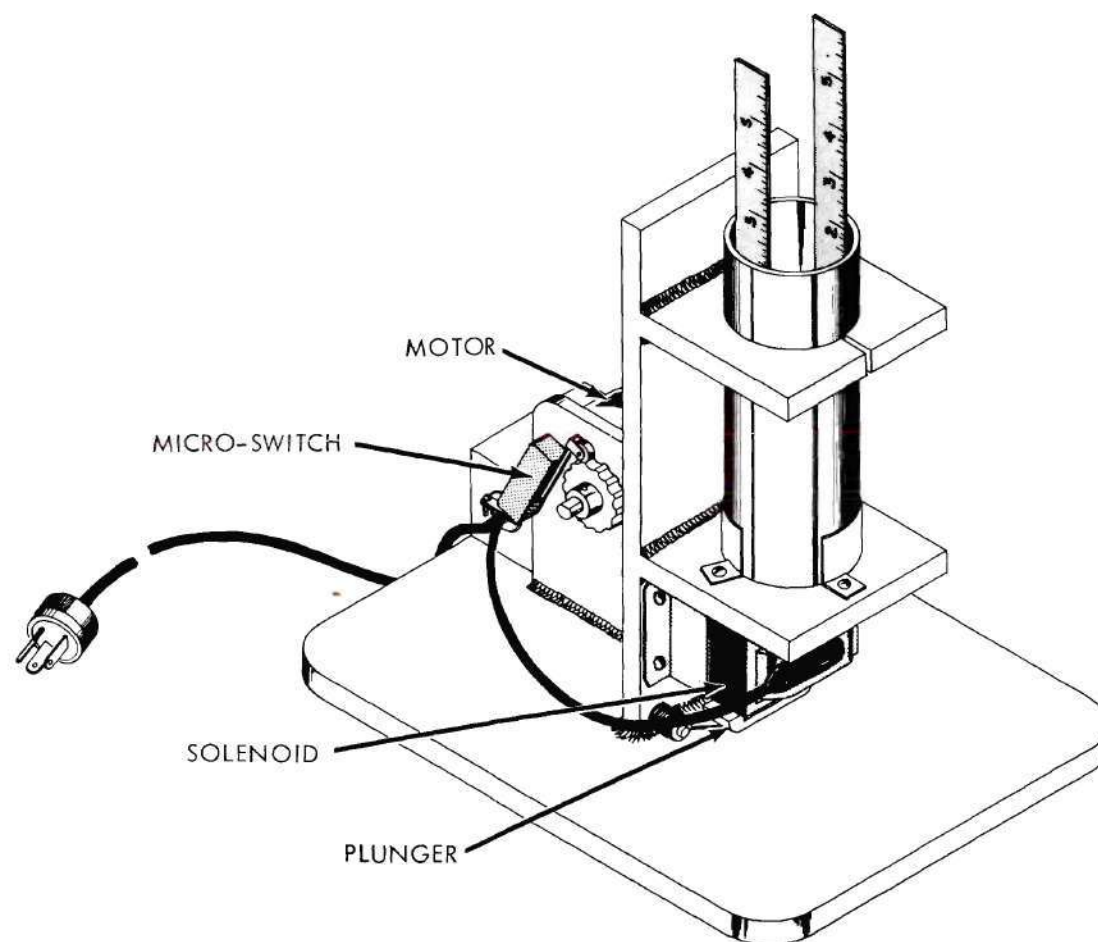
Fig. 53. Apparatus Used to Determine $V_{d\ max}$.

APPENDIX IV

EVALUATION OF k_e FROM EXPERIMENTAL DATA

Sample Calculation Using Steady-State Data

As a specific example of the calculations to evaluate k_e from steady-state data, consider a magnesia powder—MgO (E-98)—in air at atmospheric pressure and having a volume fraction solid of 0.58. The data for this system are given in Appendix IV (Table 12). The expression to be used to calculate k_e is derived from averages of values for k_m.

k_m is given by

$$k_m = \frac{Q}{2\pi L \ (t_1 - t_2)} \ \ln \frac{R_2}{R_1} \ . \tag{34}$$

In particular, consider the data indicated on page 172. For the first pair of thermocouples listed, R_1 = 2.144 centimeters, t_1 = 848.0°F, R_2 = 4.142 centimeters, and t_2 = 815.5°F. The current in the heater was 2.7304 amperes. The voltage drop across the portion of the heater in the test zone (L = 0.25 foot) was 3.1035 volts.

Substituting the above values into the expression for k_m (Equation 34) gives

$$k_m = \frac{(2.7304)(3.1035)(3.4122)}{(2)(3.1416)(0.25)(848.0-815.5)} \ \ln \frac{4.142}{2.144} \ ,$$

where 3.4122 is the conversion factor from absolute watts to Btu per hours, thus

$$k_m = 0.3731 \text{ Btu/hr} \cdot \text{ft} \cdot {}^{\text{o}}\text{F} \; ,$$

at

$$t_{avg} = \frac{848.0 + 815.5}{2} = 831.8{}^{\text{o}}\text{F} \; .$$

Similar calculations give values of k_m and t_{avg} for the other five pairs of thermocouples in the test zone. The effective thermal conductivity, k_e, at temperature, t, is obtained by averaging the six k_m's evaluated as illustrated above. That is,

$$k_e = \frac{0.3731 + 0.4068 + 0.3510 + 0.3960 + 0.3841 + 0.3626}{6}$$

$$k_e = 0.379 \text{ Btu/hr} \cdot \text{ft} \cdot {}^{\text{o}}\text{F},$$

at

$$t = \frac{831.8 + 835.3 + 835.7 + 831.2 + 836.9 + 836.4}{6}$$

$$t = 834.5{}^{\text{o}}\text{F} \; .$$

The values of k_e at t obtained in this manner are tabulated for this system, and all the other systems studied, in Table 11. It is these values of k_e and t which were fitted by least squares to polynomials (Chapter VI).

Sample Calculation Using Unsteady-State Data

As a specific example of the calculations to evaluate k_e from unsteady-state data, consider a magnesia powder—MgO (E-98)—in air at atmospheric pressure having a volume fraction solid of 0.58 and being at a temperature $t_o = 843.5{}^{\text{o}}\text{F}$. The expression to be used to calculate k_e is

$$k_e = \frac{Q}{4\pi L (t_2 - t_1)} \ln \frac{\theta_2}{\theta_1} . \qquad (38)$$

At some time, taken as zero time, power is supplied to the central heater (stainless steel tube) and the temperature of the heater is recorded as a function of time. If temperature rise of the heater, $\Delta t = t - t_o$, is plotted versus time the curve shown in Figure 54 is obtained. From the early linear portion of the curve, at $\theta_1 = 10$ seconds, $(\Delta t)_1 = 64.2°F$ and at $\theta_2 = 100$ seconds, $(\Delta t)_2 = 153.2°F$. The average current in the heater during the first minute was 21.007 amperes and the average voltage drop between potential taps (L = 2 inches) was 0.43151 volt.

Substituting the above values into the expression for k_e under these conditions (Equation 38)

gives

$$k_e = \frac{(21.007)(0.43151)(3.4122)}{4(3.1416)(\frac{2}{12})(153.2-64.2)} \ln \frac{100}{10}$$

or

$$k_e = 0.382 \text{ Btu/hr} \cdot \text{ft} \cdot °F.$$

This is the manner in which all the unsteady-state values of k_e reported in Table 4 were calculated.

As a specific example of the magnitude of the ξ term in Equation 36 (or Equation 39), consider again the data presented in Figure 54 for the MgO (E-98) powder in air at atmospheric pressure having a volume fraction solid of 0.58 at a temperature $t_o = 843.5°F$. Applying Equation 36
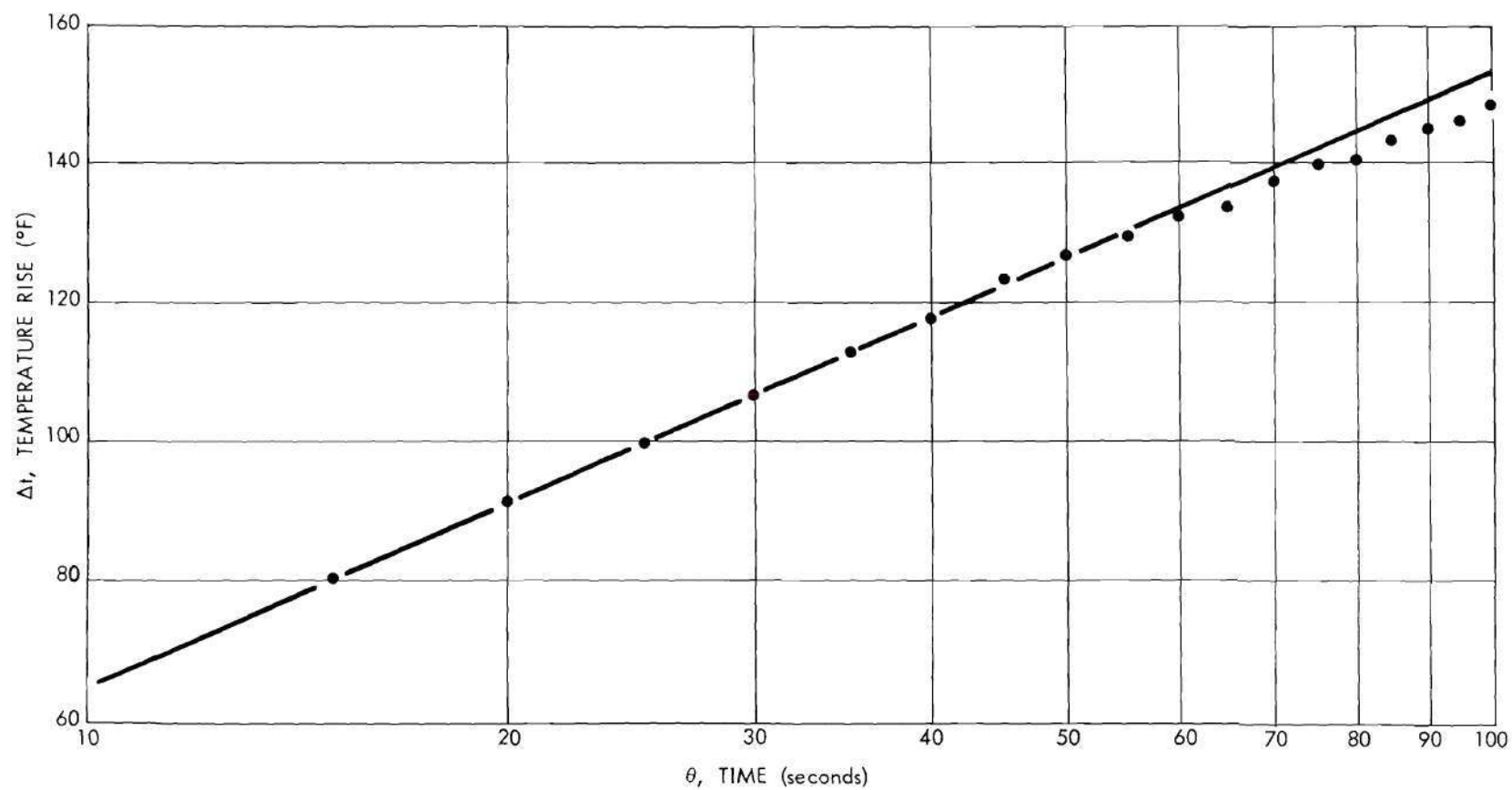
Fig. 54. Log (Time)-Temperature Plot Used to Determine k_e by Unsteady-State Method.

$$t = \frac{Q}{4\pi Lk} \ln \frac{4\tau\theta}{\zeta R^2} + \xi \left(\frac{R^2}{\tau\theta} \right) \tag{36}$$

at temperatures θ_1 and θ_2 and subtracting the results at θ_1 from the results at θ_2 gives

$$\Delta t = \frac{Q}{4\pi Lk} \ln \frac{\theta_2}{\theta_1} + \xi \left[\frac{R^2}{\tau} \left(\frac{1}{\theta_2} - \frac{1}{\theta_1} \right) \right]. \tag{87}$$

The radius of the "probe" heater is 1/16 inch and, as before, the average current in the heater during the first minute was 21.007 amperes and the average voltage drop between potential taps (L = 2 inches) was 0.43151 volt. Taking k_e of the powder as 0.382 Btu/hr·ft·$^\circ$F and τ as 0.018 ft^2/hr at 843.5°F and substituting these values plus the above values into Equation 87 at 20 and 40 seconds gives

$$\Delta t = \frac{(21.007)(0.4315)(3.4122)}{4(3.1416)(\frac{2}{12})(0.382)} \ln \frac{40}{20} + \frac{(\frac{1}{16} \times \frac{1}{12})^2}{0.018} \left[\frac{3600}{40} - \frac{3600}{20} \right],$$

$$\Delta t = 26.78^\circ F - 0.14^\circ F.$$

The approximations which must be made in applying the unsteady-state method more than overshadow the error introduced by neglect of the ξ term above. Therefore, the neglect of this term in the calculations is completely justified.

Table 11. Values of t, k_e, and Corresponding Least-Squares Equations

Powder	V_d	t (^oF)	k_e (Btu/hr·ft·^oF)
MgO (E-98)	0.58	229.6	0.242
		291.0	0.248
		459.4	0.305
		630.3	0.328
		811.8	0.363
		834.5	0.379
		835.3	0.373
		835.9	0.381
		994.6	0.400
		1016.8	0.402
		1017.7	0.390
		1190.6	0.427
		1193.1	0.420
		1370.5	0.446
		1371.2	0.446
		1514.7	0.467
		1517.1	0.464

$$k_e = 0.1788 + 0.2844 \times 10^{-3} t - 0.6444 \times 10^{-7} t^2.$$

Powder	V_d	t (^oF)	k_e (Btu/hr·ft·^oF)
MgO (E-98)	0.61	209.7	0.286
		300.2	0.311
		449.8	0.364
		624.5	0.396
		795.0	0.443
		976.3	0.481
		1152.6	0.505
		1334.6	0.511
		1515.6	0.547

$$k_e = 0.2139 + 0.3634 \times 10^{-3} t - 0.9763 \times 10^{-7} t^2.$$

Table 11. Values of t, k_e, and Corresponding Least-Squares Equations
(Continued)

Powder	V_d	t ($^\circ$F)	k_e (Btu/hr·ft·$^\circ$F)
MgO (E-98)	0.64	205.4	0.387
		322.6	0.408
		562.2	0.498
		660.6	0.534
		823.4	0.578
		828.8	0.587
		1005.3	0.615
		1185.7	0.642
		1361.7	0.674
		1543.3	0.673

$$k_e = 0.2840 + 0.4709 \times 10^{-3} \, t - 1.396 \times 10^{-7} \, t^2.$$

Powder	V_d	t ($^\circ$F)	k_e (Btu/hr·ft·$^\circ$F)
MgO (E-98)	0.65	209.3	0.416
		441.2	0.514
		616.6	0.576
		789.7	0.628
		977.6	0.669
		1151.0	0.681
		1508.5	0.736

$$k_e = 0.3205 + 0.5032 \times 10^{-3} \, t - 1.534 \times 10^{-7} \, t^2.$$

Powder	V_d	t ($^\circ$F)	k_e (Btu/hr·ft·$^\circ$F)
MgO (E-227)	0.61	210.2	0.278
		319.4	0.309
		488.4	0.360
		667.7	0.404
		794.0	0.433
		839.6	0.438
		977.0	0.475
		977.5	0.456

Table 11. Values of t, k_e, and Corresponding Least-Squares Equations
(Continued)

Powder	V_d	t (^{o}F)	k_e (Btu/hr·ft·^{o}F)
MgO (E-227) Continued	0.61	1150.6	0.493
		1150.6	0.500
		1148.9	0.483
		1331.9	0.502
		1333.7	0.521
		1425.9	0.526
		1435.5	0.512
		1510.9	0.545
		1511.0	0.530

$$k_e = 0.2089 + 0.3507 \times 10^{-3} t - 0.9097 \times 10^{-7} t^2.$$

Powder	V_d	t (^{o}F)	k_e (Btu/hr·ft·^{o}F)
Al_2O_3 (E-98)	0.58	220.9	0.238
		300.2	0.250
		471.4	0.298
		616.6	0.327
		802.3	0.356
		982.8	0.383
		1154.8	0.409
		1344.8	0.422
		1526.0	0.436

$$k_e = 0.1740 + 0.2942 \times 10^{-3} t - 0.8070 \times 10^{-7} t^2.$$

Powder	V_d	t (^{o}F)	k_e (Btu/hr·ft·^{o}F)
Al_2O_3 (B45F)	0.49	237.2	0.181
		306.3	0.195
		449.1	0.226
		573.4	0.238
		711.6	0.263
		805.5	0.276
		978.6	0.300

Table 11. Values of t, k_e, and Corresponding Least-Squares Equations
(Continued)

Powder	V_d	t ($^\circ$F)	k_e (Btu/hr·ft·$^\circ$F)
Al$_2$O$_3$ (B45F) Continued	0.49	1160.5	0.311
		1325.4	0.319
		1553.8	0.350

$$k_e = 0.1355 + 0.2129 \times 10^{-3} t - 0.5083 \times 10^{-7} t^2.$$

Powder	V_d	t ($^\circ$F)	k_e (Btu/hr·ft·$^\circ$F)
ZrO$_2$ (H30F)	0.58	190.4	0.124
		472.1	0.168
		663.8	0.189
		840.1	0.205
		1061.7	0.224
		1139.4	0.233
		1200.2	0.239
		1378.5	0.253
		1533.5	0.259

$$k_e = 0.0960 + 0.1622 \times 10^{-3} t - 0.3630 \times 10^{-7} t^2.$$

Powder	V_d	t ($^\circ$F)	k_e (Btu/hr·ft·$^\circ$F)
ZrO$_2$ (H30F)	0.64	227.6	0.166
		312.8	0.178
		672.0	0.231
		848.9	0.252
		1022.6	0.272
		1197.7	0.286
		1382.8	0.302
		1567.0	0.321

$$k_e = 0.1283 + 0.1728 \times 10^{-3} t - 0.3274 \times 10^{-7} t^2.$$

Table 11. Values of t, k_e, and Corresponding Least-Squares Equations
(Continued)

Powder	V_d	t ($^{\circ}$F)	k_e (Btu/hr·ft·$^{\circ}$F)
ZrO$_2$ (H14F)	0.70	226.6	0.218
		300.1	0.225
		654.6	0.293
		837.4	0.322
		1009.1	0.343
		1184.3	0.370
		1371.0	0.390
		1552.2	0.411

$$k_e = 0.1692 + 0.2102 \times 10^{-3} t - 0.3530 \times 10^{-7} t^2.$$

Table 12. Values of k_m Calculated from Different Thermocouple Pairs for Powder at V_d = 0.58. MgO (E-98)

k_m ($\frac{Btu}{hr\cdot ft\cdot ^\circ F}$)	t_{avg} ($^\circ F$)	t_1 ($^\circ F$)	t_2 ($^\circ F$)	Δt ($^\circ F$)	R_2 (cm.)	R_1 (cm.)	y (in.)	L (ft.)	AMPS	VOLTS
0.3972	1015.0	1032.7	997.2	35.5	4.142	2.144	14.0	0.2500	2.8358	3.4785
0.4336	1018.4	1035.6	1001.1	34.5	4.248	2.114	13.2	0.2500	2.8358	3.4785
0.3784	1018.0	1037.5	998.4	39.1	4.288	2.149	12.5	0.2500	2.8358	3.4785
0.4138	1012.3	1029.9	994.7	35.1	4.162	2.122	12.5	0.2500	2.8358	3.4785
0.4100	1018.9	1036.9	1000.9	36.0	4.265	2.142	11.7	0.2500	2.8358	3.4785
0.3847	1017.9	1036.4	999.5	36.9	4.200	2.166	11.0	0.2500	2.8358	3.4785
0.3668	835.0	852.3	817.7	34.6	4.142	2.144	14.0	0.2500	2.8632	3.1043
0.3953	836.8	853.9	819.8	34.1	4.248	2.114	13.2	0.2500	2.8632	3.1043
0.3486	835.9	855.0	816.7	38.2	4.288	2.149	12.5	0.2500	2.8632	3.1043
0.3953	831.9	848.4	815.5	32.9	4.162	2.122	12.5	0.2500	2.8632	3.1043
0.3721	836.7	854.6	818.9	35.7	4.265	2.142	11.7	0.2500	2.8632	3.1043
0.3619	835.6	853.3	818.0	35.3	4.200	2.166	11.0	0.2500	2.8632	3.1043
0.3747	834.2	850.8	817.7	33.2	4.142	2.144	14.0	0.2500	2.8042	3.0992
0.4090	837.3	853.4	821.2	32.2	4.248	2.114	13.2	0.2500	2.8042	3.0992
0.3539	836.7	855.1	818.3	36.8	4.288	2.149	12.5	0.2500	2.8042	3.0992
0.3971	832.4	848.4	816.4	32.0	4.162	2.122	12.5	0.2500	2.8042	3.0992
0.3883	837.6	854.4	820.9	33.5	4.265	2.142	11.7	0.2500	2.8042	3.0992
0.3643	837.0	854.1	819.8	34.3	4.200	2.166	11.0	0.2500	2.8042	3.0992
0.3731	831.8	848.0	815.5	32.5	4.142	2.144	14.0	0.2500	2.7304	3.1035
0.4068	835.3	851.0	819.9	31.6	4.248	2.114	13.2	0.2500	2.7304	3.1035
0.3510	835.7	853.8	817.6	36.2	4.288	2.149	12.5	0.2500	2.7304	3.1035
0.3960	831.2	846.8	815.5	31.3	4.162	2.122	12.5	0.2500	2.7304	3.1035
0.3841	836.9	853.4	820.4	33.0	4.265	2.142	11.7	0.2500	2.7304	3.1035
0.3626	836.4	853.2	819.6	33.6	4.200	2.166	11.0	0.2500	2.7304	3.1035
0.2586	228.6	242.6	214.5	28.2	4.198	2.134	14.0	0.2500	2.5488	1.9452
0.2369	229.3	244.8	213.8	31.1	4.222	2.130	13.2	0.2500	2.5488	1.9452
0.2358	231.5	247.2	215.8	31.3	4.248	2.139	12.5	0.2500	2.5488	1.9452
0.2462	228.8	242.8	214.9	27.9	4.238	2.238	12.5	0.2500	2.5488	1.9452
0.2127	232.0	249.3	214.7	34.6	4.305	2.175	11.7	0.2500	2.5488	1.9452
0.2591	227.2	241.2	213.2	28.0	4.310	2.196	11.0	0.2500	2.5488	1.9452
0.3827	1016.9	1035.3	998.6	36.7	4.142	2.144	14.0	0.2500	2.8286	3.4731
0.4223	1019.5	1037.1	1001.9	35.2	4.248	2.114	13.2	0.2500	2.8286	3.4731
0.3663	1018.8	1038.9	998.7	40.2	4.288	2.149	12.5	0.2500	2.8286	3.4731
0.3986	1013.2	1031.3	995.2	36.0	4.162	2.122	12.5	0.2500	2.8286	3.4731
0.3958	1019.4	1038.0	1000.8	37.1	4.265	2.142	11.7	0.2500	2.8286	3.4731
0.3733	1018.5	1037.4	999.6	37.8	4.200	2.166	11.0	0.2500	2.8286	3.4731

DATA USED IN ILLUSTRATIVE EXAMPLE

Table 12. Values of k_m Calculated from Different Thermocouple Pairs for Powder at $V_d = 0.58$. MgO (E-98) (Continued)

k_m ($\frac{Btu}{hr \cdot ft \cdot °F}$)	t_{avg} (°F)	t_1 (°F)	t_2 (°F)	Δt (°F)	R_2 (cm.)	R_1 (cm.)	y (in.)	L (ft.)	AMPS	VOLTS
0.4545	1516.2	1531.5	1501.0	30.5	4.142	2.144	14.0	0.2500	2.4942	3.8861
0.5131	1521.1	1535.4	1506.8	28.6	4.248	2.114	13.2	0.2500	2.4942	3.8861
0.4733	1520.9	1536.2	1505.5	30.7	4.288	2.149	12.5	0.2500	2.4942	3.8861
0.4134	1509.3	1526.4	1492.2	34.2	4.162	2.122	12.5	0.2500	2.4942	3.8861
0.4891	1519.5	1534.3	1504.6	29.6	4.265	2.142	11.7	0.2500	2.4942	3.8861
0.4378	1515.6	1531.5	1499.7	31.8	4.200	2.166	11.0	0.2500	2.4942	3.8861
0.4611	1513.8	1529.0	1498.7	30.3	4.142	2.144	14.0	0.2500	2.5104	3.8901
0.5241	1518.7	1532.8	1504.6	28.2	4.248	2.114	13.2	0.2500	2.5104	3.8901
0.4782	1518.4	1533.7	1503.1	30.6	4.288	2.149	12.5	0.2500	2.5104	3.8901
0.4133	1506.9	1524.2	1489.6	34.6	4.162	2.122	12.5	0.2500	2.5104	3.8901
0.4901	1516.9	1531.8	1502.0	29.8	4.265	2.142	11.7	0.2500	2.5104	3.8901
0.4352	1513.5	1529.6	1497.4	32.3	4.200	2.166	11.0	0.2500	2.5104	3.8901
0.4428	1372.7	1389.7	1355.7	34.1	4.142	2.144	14.0	0.2500	2.7068	3.8987
0.4908	1375.5	1391.8	1359.2	32.6	4.248	2.114	13.2	0.2500	2.7068	3.8987
0.4455	1374.4	1392.2	1356.7	35.5	4.288	2.149	12.5	0.2500	2.7068	3.8987
0.4173	1364.4	1382.9	1345.9	37.0	4.162	2.122	12.5	0.2500	2.7068	3.8987
0.4638	1372.3	1389.3	1355.3	34.0	4.265	2.142	11.7	0.2500	2.7068	3.8987
0.4137	1368.0	1386.3	1349.6	36.7	4.200	2.166	11.0	0.2500	2.7068	3.8987
0.4431	1373.3	1390.4	1356.2	34.2	4.142	2.144	14.0	0.2500	2.7108	3.9070
0.4907	1375.5	1391.9	1359.2	32.7	4.248	2.114	13.2	0.2500	2.7108	3.9070
0.4473	1373.9	1391.6	1356.1	35.5	4.288	2.149	12.5	0.2500	2.7108	3.9070
0.4183	1363.6	1382.1	1345.1	37.0	4.162	2.122	12.5	0.2500	2.7108	3.9070
0.4599	1370.9	1388.1	1353.6	34.4	4.265	2.142	11.7	0.2500	2.7108	3.9070
0.4162	1365.7	1384.0	1347.4	36.6	4.200	2.166	11.0	0.2500	2.7108	3.9070
0.4129	1190.7	1206.8	1174.7	32.1	4.142	2.144	14.0	0.2500	2.6814	3.4570
0.4574	1194.7	1210.1	1179.4	30.7	4.248	2.114	13.2	0.2500	2.6814	3.4570
0.4124	1195.0	1211.9	1178.1	33.7	4.288	2.149	12.5	0.2500	2.6814	3.4570
0.4049	1187.6	1204.3	1170.8	33.5	4.162	2.122	12.5	0.2500	2.6814	3.4570
0.4384	1195.4	1211.2	1179.6	31.6	4.265	2.142	11.7	0.2500	2.6814	3.4570
0.3925	1195.1	1212.1	1178.1	34.0	4.200	2.166	11.0	0.2500	2.6814	3.4570
0.4215	1190.5	1206.8	1174.2	32.6	4.142	2.144	14.0	0.2500	2.7746	3.4664
0.4732	1193.3	1208.7	1177.9	30.8	4.248	2.114	13.2	0.2500	2.7746	3.4664
0.4169	1192.9	1210.2	1175.5	34.6	4.288	2.149	12.5	0.2500	2.7746	3.4664
0.4097	1185.1	1202.2	1167.9	34.3	4.162	2.122	12.5	0.2500	2.7746	3.4664
0.4415	1192.1	1208.4	1175.8	32.6	4.265	2.142	11.7	0.2500	2.7746	3.4664
0.3963	1190.0	1207.4	1172.5	34.9	4.200	2.166	11.0	0.2500	2.7746	3.4664

Table 12. Values of k_m Calculated from Different Thermocouple Pairs for Powder at $V_d = 0.58$. MgO (E-98)
(Continued)

k_m $\left(\dfrac{Btu}{hr \cdot ft \cdot {}^\circ F}\right)$	t_{avg} (°F)	t_1 (°F)	t_2 (°F)	Δt (°F)	R_2 (cm.)	R_1 (cm.)	y (in.)	L (ft.)	AMPS	VOLTS
0.2617	290.7	308.6	272.9	35.7	4.198	2.134	14.0	0.2500	2.7762	2.2907
0.2412	291.3	310.8	271.8	39.1	4.222	2.130	13.2	0.2500	2.7762	2.2907
0.2437	293.6	313.0	274.1	38.9	4.248	2.139	12.5	0.2500	2.7762	2.2907
0.2499	290.1	307.8	272.5	35.3	4.238	2.238	12.5	0.2500	2.7762	2.2907
0.2236	293.1	314.2	272.1	42.2	4.305	2.175	11.7	0.2500	2.7762	2.2907
0.2689	287.0	304.3	269.6	34.6	4.310	2.196	11.0	0.2500	2.7762	2.2907
0.3084	458.9	477.5	440.2	37.3	4.198	2.134	14.0	0.2500	2.9692	2.6344
0.2967	460.0	479.6	440.4	39.2	4.222	2.130	13.2	0.2500	2.9692	2.6344
0.3042	462.1	481.2	442.9	38.3	4.248	2.139	12.5	0.2500	2.9692	2.6344
0.2974	458.8	477.0	440.6	36.5	4.238	2.238	12.5	0.2500	2.9692	2.6344
0.2833	461.4	481.9	440.9	40.9	4.305	2.175	11.7	0.2500	2.9692	2.6344
0.3410	455.3	472.1	438.5	33.6	4.310	2.196	11.0	0.2500	2.9692	2.6344
0.3175	630.3	650.4	610.3	40.0	4.198	2.134	14.0	0.2500	2.8512	3.0329
0.3172	631.9	652.1	611.6	40.5	4.222	2.130	13.2	0.2500	2.8512	3.0329
0.3290	633.2	652.8	613.6	39.2	4.248	2.139	12.5	0.2500	2.8512	3.0329
0.3121	629.7	648.9	610.5	38.4	4.238	2.238	12.5	0.2500	2.8512	3.0329
0.3108	631.6	652.3	611.0	41.2	4.305	2.175	11.7	0.2500	2.8512	3.0329
0.3790	625.3	642.0	608.6	33.4	4.310	2.196	11.0	0.2500	2.8512	3.0329
0.3522	993.3	1012.9	973.8	39.1	4.198	2.134	14.0	0.2500	2.7424	3.4189
0.3795	996.5	1014.9	978.2	36.7	4.222	2.130	13.2	0.2500	2.7424	3.4189
0.4197	998.1	1014.7	981.4	33.3	4.248	2.139	12.5	0.2500	2.7424	3.4189
0.3647	994.0	1011.8	976.1	35.6	4.238	2.238	12.5	0.2500	2.7424	3.4189
0.3957	995.8	1013.3	978.2	35.1	4.305	2.175	11.7	0.2500	2.7424	3.4189
0.4856	989.6	1003.8	975.5	28.3	4.310	2.196	11.0	0.2500	2.7424	3.4189
0.3345	809.4	827.9	790.8	37.1	4.198	2.134	14.0	0.2500	2.7524	3.0679
0.3518	812.8	830.7	795.0	35.7	4.222	2.130	13.2	0.2500	2.7524	3.0679
0.3735	814.6	831.5	797.8	33.7	4.248	2.139	12.5	0.2500	2.7524	3.0679
0.3366	811.4	828.8	794.0	34.8	4.238	2.238	12.5	0.2500	2.7524	3.0679
0.3498	814.0	831.8	796.1	35.8	4.305	2.175	11.7	0.2500	2.7524	3.0679
0.4323	808.6	822.9	794.3	28.6	4.310	2.196	11.0	0.2500	2.7524	3.0679

BIBLIOGRAPHY

1. Austin, J. B., "Factors Influencing the Thermal Conductivity of Nonmetallic Materials," American Society for Testing Materials Symposium on Thermal Insulating Materials, Philadelphia, 1939, pp. 3-67.

2. Kingery, W. D., Journal of the American Ceramic Society, 38, 251-255 (1955).

3. Barrett, L. R., Transactions of the British Ceramic Society, 48, 235-262 (1949).

4. Kingery, W. D. and McQuarrie, M. C., Journal of the American Ceramic Society, 37, 67-72 (1954).

5. Powers, A. E., Fundamentals of Thermal Conductivity at High Temperatures, Knolls Atomic Power Laboratory, KAPL-2143 (April 7, 1961).

6. Carslaw, H. S. and Jaeger, J. C., Conduction of Heat in Solids, 2nd ed., Oxford University Press, London, 1959, p. 26.

7. Jakob, M., Heat Transfer, Vol. 1, John Wiley and Sons, Inc., New York, 1949.

8. Carslaw, H. S. and Jaeger, J. C., Conduction of Heat in Solids, 2nd ed., Oxford University Press, London, 1959.

9. Kingery, W. D., Property Measurements at High Temperatures, John Wiley and Sons, Inc., New York, 1959.

10. Ross, A. M., A Literature Survey on the Measurement of Thermal Conductivity of Several Solids Including Uranium Dioxide, Atomic Energy of Canada Limited, CRFD-762 (March 1958).

11. Woodside, W., Heating, Piping, and Air Conditioning, 30, 163-170 (1958).

12. Powell, R. W., Research (London), 7, 492-501 (1954).

13. Adams, M., Journal of the American Ceramic Society, 37, 74-79 (1954).

14. Kingery, W. D., Journal of the American Ceramic Society, 37, 88-90 (1954).

15. Lichtenecker, K., Physikalische Zeitschrift, 27, 115-158 (1926).

16. Woodside, W. and Messmer, J. H., _Journal of Applied Physics_, 32, 1688-1699 (1961).

17. Powers, A. E., _Conductivity in Aggregates_, Knolls Atomic Power Laboratory, KAPL-2145 (March 6, 1961).

18. Babanov, A. A., _Soviet Physics—Technical Physics_, 2, 476-484 (1957).

19. Gorring, R. L. and Churchill, S. W., _Chemical Engineering Progress_, 57, 53-59 (1961).

20. Laubitz, M. J., _Canadian Journal of Physics_, 37, 798-808 (1959).

21. Maxwell, J. C., _A Treatise on Electricity and Magnetism_, Vol. 1, 3rd ed., Oxford University Press, London, 1892, p. 440.

22. Rayleigh, Lord, _The Philosophical Magazine_, 34, 481-502 (1892).

23. Burgers, H. C., _Physikalische Zeitschrift_, 20, 73-75 (1919).

24. Fricke, H., _The Physical Review_, 24, 575-587 (1924).

25. Bruggeman, D. A. G., _Annalen der Physik_, 24, 636-679 (1935).

26. Meredith, R. E. and Tobias, C. W., _Journal of Applied Physics_, 31, 1270-1273 (1960).

27. Meredith, R. E. and Tobias, C. W., _Journal of the Electrochemical Society_, 108, 286-290 (1961).

28. de Vries, D. A., _Mededelingen van de Landbouwhogeschool te Wageningen/Nederland_, 52, (1), 1-73 (1952).

29. Lichtenecker, K., _Physikalische Zeitschrift_, 25, 169-181 (1924).

30. Lichtenecker, K., _Physikalische Zeitschrift_, 25, 193-204 (1924).

31. son Frey, G. S., _Zeitschrift fur Electrochemie_, 38, 260-274 (1932).

32. Tsao, G. T.-N., _Industrial and Engineering Chemistry_, 53, 395-397 (1961).

33. Schumann, T. E. W. and Voss, V., _Fuel in Science and Practice_, 13, 249-256 (1934).

34. Wilhelm, R. H., Johnson, W. C., Wynkoop, R., and Collier, D. W., _Chemical Engineering Progress_, 44, 105-116 (1948).

35. Preston, F. W., _Mechanism of Heat Transfer in Unconsolidated Porous Media at Low Flow Rates_, Ph.D. Thesis, The Pennsylvania State University, 1957.

36. Deissler, R. G. and Eian, C. S., Investigation of Effective Thermal Conductivities of Powders, National Advisory Committee for Aeronautics, NACA RM E52C05 (June 24, 1952).

37. Willhite, G. P., Kunii, D., and Smith, J. M., A. I. Ch. E. Journal (American Institute of Chemical Engineers), 8, 340-345 (1962).

38. Kunii, D. and Smith, J. M., A. I. Ch. E. Journal, 6, 71-78 (1960).

39. Yagi, S. and Kunii, D., A. I. Ch. E. Journal, 3, 373-381 (1957).

40. Smith, W. O., Foote, P. D., and Busang, P. F., The Physical Review, 34, 1271-1274 (1929).

41. Kannuluik, W. G. and Martin, L. H., Proceedings of the Royal Society (London), A 141, 144-158 (1933).

42. Kimura, M., Chemical Engineering (Tokyo), 21, 473-480 (1957).

43. Kling, G., Forschung auf dem Gebiete des Ingenieurwesens, 9, 28-34 (1938).

44. Waddams, A. L., Journal of the Society of Chemical Industry (London), 63, 337-340 (1944).

45. Masamune, S. and Smith, J. M., Industrial and Engineering Chemistry Fundamentals, 2, 136-143 (1963).

46. Russell, H. W., Journal of the American Ceramic Society, 18, 1-5 (1935).

47. Topper, L., Industrial and Engineering Chemistry, 47, 1377-1379 (1955).

48. Webb, J., Nature, 177, 989 (1956).

49. Woodside, W., Canadian Journal of Physics, 36, 815-823 (1958).

50. Shimokawa, J., Deionization Processes with Ion Exchange and with Electromigration, Japan Atomic Energy Research Institute, JAERI 1038 (June 30, 1962).

51. Deissler, R. G. and Boegli, J. S., Transactions of the American Society of Mechanical Engineers, 80, 1417-1425 (1958).

52. Warren, J. E. and Messmer, J. H., Industrial and Engineering Chemistry Fundamentals, 1, 222-223 (1962).

53. Schleiermacher, A., Annalen der Physik und Chemie, 34, 623-643 (1888).

54. Kingery, W. D., Property Measurements at High Temperatures, John Wiley and Sons, Inc., New York, 1959, p. 105.

55. Weininger, J. L. and Schneider, W. G., Industrial and Engineering Chemistry, 43, 1229-1233 (1951).

56. Lentz, C. P., Canadian Journal of Technology, 30, 153-166 (1952).

57. Blackwell, J. H., Journal of Applied Physics, 25, 137-144 (1954).

58. Hooper, F. C. and Lepper, F. R., Heating, Piping, and Air Conditioning, 22, 129-135 (1950).

59. Woodside, W. and Messmer, J. H., Journal of Geophysical Research, 65, 3481-3485 (1960).

60. DeNee, P. B., The Thermal Conductivity of Granular Material at Low Temperature, Ph.D. Thesis, Lehigh University, 1963.

61. Carslaw, H. S. and Jaeger, J. C., Conduction of Heat in Solids, 2nd ed., Oxford University Press, London, 1959, p. 345.

62. Schotte, W., A. I. Ch. E. Journal, 6, 63-67 (1960).

63. DallaValle, J. M., Micromeritics, 2nd ed., Pitman Publishing Corporation, New York, 1948.

64. Orr, C. and DallaValle, J. M., Fine Particle Measurement, The MacMillan Company, New York, 1959.

65. Herdan, G., Small Particle Statistics, 2nd ed., Academic Press Inc., New York, 1960.

66. Herdan, G., Small Particle Statistics, 2nd ed., Academic Press Inc., New York, 1960, p. 84.

67. Hald, A., Statistical Theory with Engineering Applications, John Wiley and Sons, Inc., New York, 1952, p. 144.

68. Kendall, M. G. and Stuart, A., The Advanced Theory of Statistics, Vol. 2, Hafner Publishing Company, New York, 1961, p. 522.

69. DallaValle, J. M., Micromeritics, 2nd ed., Pitman Publishing Corporation, New York, 1948, p. 123.

70. Herdan, G., Small Particle Statistics, 2nd ed., Academic Press Inc., New York, 1960, p. 181.

71. Gregg, S. J., The Surface Chemistry of Solids, 2nd ed., Chapman and Hall Ltd., London, 1961, p. 232.

72. Carslaw, H. S. and Jaeger, J. C., Conduction of Heat in Solids, 2nd ed., Oxford University Press, London, 1959, p. 339.

73. Smoluchowski, M., _Polaka Akademija Umiejetnoschi Krakow Bulletin International_, A, 129-153 (1910).

74. Aberdeen, J. and Laby, T. H., _Proceedings of the Royal Society (London)_, A 113, 459-477 (1926).

75. Kunii, D. and Smith, J. M., _A. I. Ch. E. Journal_, 7, 29-34 (1961).

76. Mischke, R. A. and Smith, J. M., _Industrial and Engineering Chemistry Fundamentals_, 1, 288-292 (1962).

77. Hill, F. B. and Wilhelm, R. H., _A. I. Ch. E. Journal_, 5, 486-496 (1959).

78. Argo, W. B. and Smith, J. M., _Chemical Engineering Progress_, 49, 443-451 (1953).

79. Chen, J. C. and Churchill, S. W., _A. I. Ch. E. Journal_, 9, 35-41 (1963).

80. Kennard, E. H., _Kinetic Theory of Gases_, McGraw-Hill Book Company, Inc., New York, 1938, p. 311.

81. Kennard, E. H., _Kinetic Theory of Gases_, McGraw-Hill Book Company, Inc., New York, 1938, p. 315.

82. Kennard, E. H., _Kinetic Theory of Gases_, McGraw-Hill Book Company, Inc., New York, 1938, p. 314.

83. Grilly, E. R., Taylor, W. J., and Johnston, H. L., _The Journal of Chemical Physics_, 14, 435-440 (1946).

84. Eggleton, A. E. J. and Tompkins, F. C., _Transactions of the Faraday Society_, 48, 738-749 (1952).

85. Eckert, E. R. G. and Drake, R. M., _Heat and Mass Transfer_, McGraw-Hill Book Company, Inc., New York, 1959, p. 282.

86. Kingery, W. D., Francl, J., Coble, R. L., and Vasilos, T., _Journal of the American Ceramic Society_, 37, 107-110 (1954).

87. Glassman, I. and Bonilla, C. F., _Chemical Engineering Progress Symposium Series_, 49, No. 5, 153-162 (1953).

88. Hamilton, R. L. and Crosser, O. K., _Industrial and Engineering Chemistry Fundamentals_, 1, 187-191 (1962).

89. Sully, A. H., Brandes, E. A., and Waterhouse, R. B., _British Journal of Applied Physics_, 3, 97-101 (1952).

90. Olson, O. H. and Morris, J. C., Determination of Emissivity and Re-flectivity Data on Aircraft Structural Materials, Part III. Techniques for Measurement of Total Normal Emissivity, Normal Spectral Emissivity at 0.665 Microns, Solar Absorptivity, and Presentation of Results, Wright Air Development Center, WADC TR 56-222, Pt. III (April 1960).

91. Hilsenrath, J., Beckett, C. W., Benedict, W. S., Fano, L., Hoge, H. J., Masi, J. F., Nuttall, R. L., Touloukian, Y. S., and Woolley, H. W., Tables of Thermodynamic and Transport Properties of Air, Argon, Carbon Dioxide, Carbon Monoxide, Hydrogen, Nitrogen, Oxygen, and Steam, Pergamon Press, New York, 1960.

92. Hirschfelder, J. O., Curtiss, C. F., and Bird, R. B., Molecular Theory of Gases and Liquids, John Wiley and Sons, Inc., New York, 1954, p. 552.

93. Eian, C. S. and Deissler, R. G., Effective Thermal Conductivities of Magnesium Oxide, Stainless Steel, and Uranium Oxide Powders in Various Gases, National Advisory Committee for Aeronautics, NACA RM E53G03 (October 29, 1953).

VITA

Herschel Willcox Godbee was born in Hinesville, Georgia on March 4, 1928. He was educated in the elementary schools of Savannah, Georgia and was graduated from Savannah High School in June, 1946. The following September he entered the Georgia Institute of Technology and was graduated with the degree of Bachelor of Science in Chemical Engineering in June, 1952. From August, 1952 until May, 1954, he served as a lieutenant in the Ordnance Corps of the United States Army. He entered the Graduate Division of Georgia Institute of Technology in June, 1954. In June, 1958, he joined the Chemical Technology Division of the Oak Ridge National Laboratory, continuing graduate studies on a part-time basis.

Mr. Godbee is married to the former Doris Ann Grider and has three sons, John Douglas, Dan Clark, and Benton Arthur.

He is a member of Tau Beta Pi and Sigma Xi.

He is author or co-author of several Oak Ridge National Laboratory technical reports. Among these are the following:

H. W. Godbee and J. T. Roberts, "Survey on the Measurement of Thermal Conductivity of Solids Produced by Evaporation and Calcination of Synthetic Fuel Reprocessing Solutions," ORNL-2769 (August 10, 1959).

H. W. Godbee, "Characterization of Solid Products of Pot Calcination," ORNL-CF-60-9-47 (September 1960).

H. W. Godbee and J. T. Roberts, "Laboratory Development of a Pot Calcination Process for Converting Liquid Wastes to Solids," ORNL-2986 (August 30, 1961).

In addition, he is co-author of the following publication:
H. W. Godbee and W. E. Clark, "Use of Phosphite and Hypophosphite to Fix
Ruthenium from High-Activity Wastes in Solid Media," Industrial and
Engineering Chemistry Product Research and Development, 2, 157-162
(1963).